Induction of ileal permeability and alterations in metabolome in the gut–liver axis induced by 12α-hydroxylated bile acids in rats

（ラットにおける 12α 水酸化胆汁酸による回腸透過性の誘導と腸肝軸における代謝物の変動）

Hokkaido University, Graduate School of Agriculture
Division of Frontiers in Biosciences, Doctor Course

Hongxia Liu
劉 洪霞

Abstract

A high-fat diet is associated with and may contribute to the prevalence of a series of gut–liver diseases and metabolic disorders. Bile acids (BAs) are cholesterol catabolites. Both the level and composition of BAs are regulated by the amount of dietary fat. 12α-hydroxylated (12αOH) BAs are selectively increased under the condition of a high-fat diet and may influence hepatic steatosis and gut barrier dysfunction. High-fat diet raises the fecal output of deoxycholic acid (DCA), which disrupts epithelial integrity. An increase in fecal DCA level implies the accumulation of primary 12αOH BAs in the enterohepatic circulation. However, the potential role of abundant primary 12αOH BAs in gut barrier dysfunction has not been studied yet. In addition, dietary supplementation of cholic acid (CA) at a level that does not disturb 7α-dehydroxylation in the large intestine induces hepatic steatosis without obesity in rats. The underlying mechanism by which 12αOH BAs induce gut barrier dysfunction and hepatic steatosis has not been fully clarified. The purposes of this study were to investigate the role of primary 12αOH BAs in gut barrier impairment and the effect of 12αOH BAs on metabolic alterations in hepatic steatosis induced by the dietary CA supplementation.

To examine the role of primary 12αOH BAs in gut barrier impairment, rats were fed a CA-supplemented diet (0.5 g/kg diet). The CA diet increased the 12αOH BA concentrations in the small and large intestine, accompanied by gut barrier impairment. Based on the luminal 12αOH BA concentrations, *ex vivo* gut leakiness was determined. DCA increased permeability in the large intestine, whereas taurocholic acid (TCA) increased the ileal permeability, but not jejunal permeability. A Rho kinase inhibitor attenuated TCA-induced ileal permeability. Administration of vancomycin that abolishes secondary BA production did not influence the gut leakiness induced by the CA diet. Changes in the gut permeation marker in the tail vein blood suggested that the major site of the CA-induced leakiness was small intestine. The CA diet enhanced the phosphorylation of myosin light chain 2 and reduced claudin expressions in the rat ileal epithelia. Such alteration of the expression of barrier function-related genes was not clearly observed in the large intestine. These observations suggest a primary event in

12αOH BA-induced gut leakiness is the TCA-induced ileal barrier dysfunction.

Next, to investigate the gut–liver metabolic responses to 12αOH BAs, rats were fed the CA-supplemented diet. After 12 weeks of the dietary CA intervention, the hepatic lipid accumulation was greater in the CA-fed rats than in control without an increase in dietary energy absorption. Untargeted metabolomics suggested marked differences in the fecal metabolome between the CA-fed rats and control, which was characterized by depletion of fatty acids and enrichment of amino acids and amines. Moreover, an alteration of molecules in redox-related pathways was observed in liver metabolomics in the CA-fed rats. The CA diet tended to reduce hepatic concentration of nicotinamide adenine dinucleotide and enhanced poly(ADP-ribosyl)ation of peroxisome proliferator-activated receptor α (PPARα), which suggests that the activation of poly(ADP-ribose) polymerase 1 impaired PPARα signaling in the liver of the CA-fed rats. The ingestion of the CA diet increased the sedoheptulose-7-phosphate level and enhanced glucose-6-phosphate dehydrogenase activity in the liver, suggesting promotion of the pentose phosphate pathway that contributes to an increase in reduced nicotinamide adenine dinucleotide phosphate in the liver. Integrated analysis of the gut–liver metabolomics revealed that DCA produced in the large intestine is the major mediator in these metabolic alterations.

Overall, this study demonstrated the significance of TCA in proximal gut leakiness, and alterations in metabolites induced by DCA in the gut–liver axis contributed to the enhancement of liver lipid accumulation. These results provide a novel perspective on how 12αOH BAs regulate the pathophysiology of the gut–liver axis.

List of abbreviations

7oDCA	7-oxodeoxycholic acid
12αOH	12α-hydroxylated
12oLCA	12-oxolithocholic acid
AAA	aromatic amino acid
Acox1	acyl-CoA oxidase 1
ASBT	apical sodium-dependent bile acid transporter
ATP	adenosine triphosphate
BA	bile acid
BCAA	branched-chain amino acid
BSH	bile salt hydrolases
CA	cholic acid
Cd36	cluster of differentiation 36
CDCA	chenodeoxycholic acid
cDNA	complementary deoxyribonucleic acid
Cld	claudin
CHRM2	M2 muscarinic acetylcholine receptor
Co-IP	co-immunoprecipitation
Cpt1a	carnitine palmitoyltransferase 1A
Cr	chromium
Ct	control
CYP27A1	sterol 27-hydroxylase
CYP7A1	cholesterol 7α-hydroxylase
CYP7B1	oxysterol 7α-hydroxylase
CYP8B1	sterol 12α-hydroxylase
DCA	deoxycholic acid
DSS	dextran sulfate sodium
EDTA	ethylenediaminetetraacetic acid
Fatp4	fatty acid transport protein 4

List of abbreviations (Cont.)

FD4	fluorescein-isothiocyanate-dextran 4 kDa
FFA	free fatty acid
FoxO1	forkhead box O1
FXR	farnesoid X receptor
G6PD	glucose-6-phosphate dehydrogenase
Glud	glutamate dehydrogenase
Gpx	GSH peroxidase
GSH	glutathione
GSSG	glutathione disulfide
Gstk1	GSH S-transferase κ1
IB	immunoblotting
IBABP	ileal BA-binding protein
IBD	inflammatory bowel disease
Idh1	mitochondrial isocitrate dehydrogenase
Idh2	cytosolic isocitrate dehydrogenase
IgA	immunoglobulin A
MAFLD	metabolic dysfunction-associated fatty liver disease
MCA	muricholic acid
MDA	malondialdehyde
Me3	mitochondrial malic enzyme
MLC2	myosin light chain 2
MUC2	mucin 2
NAD^+	nicotinamide adenine dinucleotide
NADPH	nicotinamide adenine dinucleotide phosphate
NAFL	nonalcoholic fatty liver
NAFLD	nonalcoholic fatty liver disease
Nampt	nicotinamide phosphoribosyltransferase
NASH	non-alcoholic steatohepatitis

List of abbreviations (Cont.)

Nnt	nicotinamide nucleotide transhydrogenase
NOX	NADPH oxidase
OPLS-DA	orthogonal partial least squares discriminant analysis
OSTα/β	heterodimeric organic solute transporter alpha/beta
PAR	poly(ADP-ribose)
PARP1	poly(ADP-ribose) polymerase 1
PGC1α	peroxisome-proliferator-activated receptor γ coactivator 1α
PPARα	peroxisome proliferator-activated receptor α
PPP	pentose phosphate pathway
REG	regenerating islet-derived
Rplp0	ribosomal protein lateral stalk subunit P0
qPCR	quantitative PCR
S-7-P	sedoheptulose 7-phosphate
Sirt1	sirtuin 1
Srebp1	sterol regulatory element-binding protein 1
TβMCA	tauro-β-MCA
TCA	taurocholic acid
TDCA	taurodeoxycholic acid
TEER	transepithelial electrical resistance
TG	triglyceride
TGR5/GPBAR1	G protein-coupled bile acid receptor 1
UCA	ursocholic acid
VCM	vancomycin
VIP	variable importance in projection
VLDL	very-low-density lipoprotein

List of tables

List of figures

Contents

Chapter 1 General introduction

Hepatic steatosis

Non-alcoholic fatty liver disease (NAFLD) refers to a series of liver diseases that are independent of alcohol consumption, ranging from nonalcoholic fatty liver (NAFL) to non-alcoholic steatohepatitis (NASH). NAFL is defined as the presence of ≥ 5% hepatic steatosis with or without mild inflammation and is slowly progressive (Chalasani et al., 2018). NASH is characterized by the presence of hepatocellular injury in the form of hepatocyte ballooning and is a more active form of the disease that can progress to cirrhosis and fibrosis, and even liver cancer (Powell et al., 2021). Although less than 10% of NAFLD patients eventually develop liver cancer (Powell et al., 2021), there is a large population of NAFLD. It is reported to affect about a quarter of the world's population (Younossi et al., 2016). Also, NAFLD is closely linked to other metabolic comorbidities such as obesity, diabetes mellitus, dyslipidemia, and hypertension (Younossi et al., 2016). Thus, the prevalence of the disease is an increasing burden for society. In 2020, an international expert group has put forward the concept of metabolic dysfunction-associated fatty liver disease (MAFLD) to positively incorporate criteria for diagnosis (Eslam et al., 2020; Fouad et al., 2020). The diagnosis of MAFLD is based on the presence of steatosis together with one of the three metabolic risks, including overweight/obesity, diabetes mellitus, and evidence of metabolic dysregulation (Eslam et al., 2020).

A comprehensive understanding of the complex pathogenesis of MAFLD still remains limited. The substrate overload may explain the metabolic mechanisms leading to hepatic steatosis. Excess energy substrates (primarily carbohydrates and fatty acids) are supplied to the liver, which exceeds the hepatic capacity to oxidize them to CO_2 or re-esterify to triglyceride (TG) and export as very-low-density lipoprotein (VLDL) (Friedman et al., 2018). The sources of fatty acids in the liver are considered mainly including the following: 1) Delivery of excess peripheral fatty acids induced by insulin resistance to the liver (Lomonaco et al., 2012); 2) Endogenous synthesis of fatty acids from excess dietary components (usually carbohydrates) (Donnelly et al., 2005) or other

energy substrates (such as acetic acid of microbial origin) (Zhao et al., 2020); 3) Excess dietary lipids (Lindeboom et al., 2015). These factors contribute to lipid accumulation in the liver and may serve as substrates for the generation of lipotoxic lipids that induce endoplasmic reticulum stress, oxidative stress, inflammasome activation, and hepatocellular injury (Friedman et al., 2018; Neuschwander-Tetri, 2010). There is no approved therapy for MAFLD until now (Powell et al., 2021). Nevertheless, there is enormous evidence that diet and lifestyle modifications can be protective against the development of hepatic steatosis and disease progression (Hydes et al., 2020).

Leaky gut

The theory of the gut–liver axis describes the complex interaction among the liver, gastrointestinal tract, and gut microbes (Albillos et al., 2020). There is increasing evidence that molecules of liver origin affect intestinal microbiota composition and gut barrier integrity, and in turn, intestinal factors regulate hepatic bile acid (BA) synthesis and glucose and lipid metabolism (Thaiss et al., 2018). The gastrointestinal tract is responsible for digestive, absorptive, metabolic, and immune functions. An impaired gut barrier leads to a portal influx of gut microbial products or even gut microbes *per se* to the systemic circulation and liver (Mouries et al., 2019; Thaiss et al., 2018), which implies a relationship between the gut barrier dysfunction and the occurrence of liver diseases and other metabolic disorders. Indeed, there is evidence that suggests an impaired intestinal epithelial barrier in subjects with NAFLD (Miele et al., 2009).

The gut barrier contains multiple functional structures, including mucus, epithelial cells, immune cells, and a gut-vascular barrier (Camilleri, 2019). The mucus layer covers the intestinal epithelia and prevents bacterial adhesion. It is mainly composed of mucins secreted by the goblet cell (Vancamelbeke and Vermeire, 2017). Antibodies especially immunoglobulin A (IgA) secreted by the plasma cell and antibacterial peptides secreted by the Paneth cell are also important elements of the mucus layer (Vancamelbeke and Vermeire, 2017). Studies have shown that changes in the thickness and composition of the mucus layer are associated with impaired barrier function (Johansson et al., 2008). In addition, tight junction proteins seal the paracellular spaces

between epithelial cells (Camilleri, 2019). There is a large body of evidence demonstrating the association between the expression of tight junction proteins and gut permeability (Gupta et al., 2020; Otani et al., 2019). Moreover, immune cells that are located in the gut-associated lymphoid tissue interact with microbiota and other antigens, which play an important role in gut barrier function (Kayama et al., 2020). Further, emerging evidence identifies a gut-vascular barrier that restricts the translocation of microbiota into the bloodstream (Spadoni et al., 2015). Disruption of the gut-vascular barrier is recognized as an early event in experimental NASH development, while prevention of the gut-vascular barrier disruption protects against NASH development (Mouries et al., 2019). It is of great interest to identify gut microbial-derived metabolites that are associated with the onset and development of gut–liver diseases and to investigate the underlying mechanisms.

BA synthesis, transport, and microbial BA transformation

BAs are liver-derived catabolites of cholesterol and are further modified by gut microbes. In the liver, BAs synthesized via either the classical or the alternative pathways are referred to as primary BAs. Cholic acid (CA) is synthesized via the classical pathway that requires the key enzymes cholesterol 7α-hydroxylase (CYP7A1) and sterol 12α-hydroxylase (CYP8B1) (Chiang, 2009). Due to the presence of 12α-hydroxyl on the steroid skeleton, CA-derived BAs are also known as 12α-hydroxylated (12αOH) BAs. On the other hand, chenodeoxycholic acid (CDCA) is synthesized through the alternative pathway that is mediated by sterol 27-hydroxylase (CYP27A1) and oxysterol 7α-hydroxylase (CYP7B1) (Chiang, 2009). In rodents, CDCA is further 6-hydroxylated into muricholic acids (MCAs) (Takahashi et al., 2016). These BAs are thereafter conjugated to glycine or taurine in the liver and released into the small intestine to facilitate dietary lipids absorption (de Aguiar Vallim et al., 2013). In the terminal ileum, most BAs are actively reabsorbed by the specific BA transporter called apical sodium-dependent bile acid transporter (ASBT) and return to the liver through portal circulation (Ticho et al., 2019). These processes constitute the enterohepatic circulation of BA molecules. A proportion of BAs escape ileal reabsorption and enter

the large intestine where they undergo microbial transformation. The first step is deconjugation. Taurine and glycine are removed under the action of bile salt hydrolases (BSH). The next step forms the secondary BAs through various modifications on the hydroxyl groups, usually involving dehydroxylation, oxidation, and epimerization (Ridlon et al., 2006). The hepatic synthetic pathways and microbial modifications contribute to the diverse hydrophobicity, cytotoxicity, and receptor affinity of different BA molecules (Araki et al., 2003). For example, deoxycholic acid (DCA) is highly hydrophobic and is an agonist of G protein-coupled bile acid receptor 1 (TGR5/GPBAR1) (Kawamata et al., 2003). CDCA is a potent agonist of farnesoid X receptor (FXR) (Lew et al., 2004), whereas tauro-β-MCA (TβMCA) is an antagonist of FXR (Sayin et al., 2013).

Alteration of BA metabolism is frequently observed in gut–liver axis diseases

Increasing evidence has shown that BAs exhibit a variety of biological effects that are related to gut–liver diseases. Exposure to some BA species induces acute increases in epithelial permeability *in vitro* in Caco-2 monolayers (Raimondi et al., 2008). DCA, a secondary 12αOH BA, has long been attracting researchers' interest as it increases with ingestion of dietary fat (Stenman et al., 2012), and its hydrophobic feature is related to the disruption of epithelial integrity (Stenman et al., 2013). Recent studies suggest that DCA activates macrophages and drives colonic inflammation via the M2 muscarinic acetylcholine receptor (CHRM2) (L. Wang et al., 2020). The disruptive effect of DCA on gut barrier function also involves the suppression of FXR activity (Dermadi et al., 2017) and the induction of oxidative stress (Z. Wang et al., 2020).

BA composition is also altered in fatty liver disease and other metabolic disorders, suggesting BAs for disease pathogenesis. The levels of 12αOH BA species in the serum and feces are high in NAFLD patients (Mouzaki et al., 2016; Sang et al., 2021; Smirnova et al., 2022). BA receptors have been implicated. A study shows that FXR signaling is suppressed in the liver of NAFLD patients, possibly due to the decrease in FXR agonistic CDCA (Jiao et al., 2018). FXR activation has been reported to protect against NAFLD via inhibition of lipogenesis in the liver and intestinal lipid uptake

(Clifford et al., 2021). In addition, the proportion of 12αOH BAs in the serum is high in unhealthy subjects with high body mass index (Wei et al., 2020). Animal studies have shown that 12αOH BAs may contribute to obesity susceptibility via the downregulation of glucagon-like peptide 1 in the ileum and uncoupling protein-1 in brown adipose tissue (Wei et al., 2020). Also, a higher ratio of 12αOH/non-12 BAs is associated with lower insulin sensitivity and higher plasma TGs (Haeusler et al., 2013). Mechanistically, the insulin/Akt-mediated nuclear exclusion of FoxO1 inhibits the transcription of *Cyp8b1*, which is a target gene of FoxO1 (Haeusler et al., 2012). Thus, the impaired insulin/Akt signaling in insulin resistance may result in more active FoxO1/*Cyp8b1* and excess 12αOH BAs synthesis. Altogether, these features of BAs have placed BAs especially 12αOH BAs as the critical focus in gut–liver disease-related research.

Objectives of this study

An increase in the fecal output of DCA under the condition of overnutrition may reflect the accumulation of primary 12αOH BAs in the gastrointestinal tract in order to emulsify the increased levels of dietary lipids. Indeed, in a previous study in which rats were fed a high-fat diet, taurocholic acid (TCA), a taurine-conjugated primary 12αOH BA, was the most abundant BA observed in the enterohepatic circulation (Yoshitsugu et al., 2019). The effect of primary 12αOH BAs on gut barrier function has not yet been elucidated. Thus, the objective of Chapter 2 was to investigate the effect of primary 12αOH BAs on gut permeability.

Previous studies suggest that 12αOH BAs are selectively increased in rats fed a high-fat diet (Hori et al., 2020). Dietary supplementation of CA in rats reveals a causal link between 12αOH BAs and hepatic steatosis (Lee et al., 2020). The rats develop simple hepatic steatosis by the CA diet, despite the fact that no symptoms of obesity and deterioration of glucose tolerance are found. An important question is how metabolically gut, microbes, and liver respond to 12αOH BAs. Thus, Chapter 3 aimed to investigate the changes in the metabolome of the gut–liver axis under the CA diet feeding and their contribution to liver lipid metabolism.

Chapter 2 Taurocholic acid induces leakiness in the distal small intestine in rats

Abstract

A high-fat diet increases 12αOH BAs secretion in rats, and secondary BAs are responsible for the leaky gut. This study aimed to examine the role of primary 12αOH BAs in gut barrier impairment in rats using dietary CA supplementation (0.5 g/kg diet). The CA diet increased the concentrations of 12αOH BAs including TCA and DCA in the small and large intestine, respectively, accompanied by gut barrier impairment. Based on the luminal 12αOH BAs concentrations, *ex vivo* gut leakiness was determined. DCA increased permeability in the large intestine, whereas TCA increased the ileal permeability, but not jejunal permeability. A Rho kinase inhibitor attenuated TCA-induced ileal permeability. Administration of vancomycin, which abolishes secondary BAs, did not influence the gut leakiness induced by the CA diet. Changes in the gut permeation marker in the tail vein blood suggested the possibility that the CA-induced leakiness occurred in the small intestine. The CA diet enhanced the phosphorylation of myosin light chain 2 and reduced claudin expressions in the rat ileal epithelia. Reductions in barrier function-related genes were observed in the ileum, but not in the colon of the CA-fed rats. Overall, the present study demonstrated the significance of TCA in proximal gut leakiness.

2.1 Introduction

The gut contributes to nutrient absorption and prevents the translocation of toxic molecules. Excess food consumption, such as the intake of a high-fat diet, impairs the gut barrier, which is closely associated with the occurrence of fatty liver disease, obesity, type 2 diabetes mellitus, and colorectal cancer (Chopyk and Grakoui, 2020; Khan et al., 2021). Several factors driven by a high-fat diet may influence intestinal barrier properties, such as excess saturated fatty acids, gut dysbiosis, and alteration of BA metabolism (Rohr et al., 2020).

BAs are amphipathic molecules that play a role in hydrophobic nutrient absorption (Hofmann and Hagey, 2014) and act as signaling molecules (Chen et al., 2019; Jia et al., 2018). Primary BAs are produced by the liver via two distinct pathways. One is the classical pathway, in which 12αOH BAs, such as CA, are synthesized, and the other is an alternative pathway, in which non-12αOH BAs, such as CDCA, are formed (Chiang and Ferrell, 2018). In the large intestine, microbes modify hydroxyl groups on the steroid ring and produce various types of secondary BAs with diverse chemical characteristics (Griffiths and Sjovall, 2010). Most BAs are reabsorbed at the distal ileum, while the others are excreted in the feces. Higher levels of BAs circulate in enterohepatic tissues than in the peripheral blood (Hofmann and Hagey, 2014). The level and balance of BA compositions play a role in intestinal barrier function, and dietary factors modulate these (Hegyi et al., 2018; Rohr et al., 2020). The increased expression levels of hepatic BA synthesis genes, including cholesterol 7α-hydroxylase and sterol 12α-hydroxylase, under a high-fat diet elevate 12αOH BA concentrations in enterohepatic circulation and feces (Hori et al., 2020; Yoshitsugu et al., 2019). The microbial *baiB* gene is involved in 7α-dehydroxylation, which is responsible for the production of DCA, a secondary 12αOH BA, in the large intestine (Ridlon et al., 2006). A high level of DCA induces leaky gut *in vivo* and in isolated gut tissues (Stenman et al., 2013). These observations suggest the significance of secondary 12αOH BAs in the leaky gut under high-fat diets.

However, it is unclear whether primary 12αOH BAs participate in intestinal barrier dysfunction. The concentration of BAs in the rat small intestine is about 10 times higher than that in the large intestine under normal conditions, and the level becomes much higher under a high-fat diet (Yoshitsugu et al., 2019). TCA, a taurine-conjugated primary 12αOH BA, constitutes over 50% of the total BAs in the rat small intestine (Yoshitsugu et al., 2019). This suggests that the small intestinal mucosa is exposed to high levels of primary 12αOH BAs in the body. In the previous study, dietary CA supplementation that mimics the BA environment under high-fat diets in rats was used to clarify the involvement of 12αOH BAs in the leaky gut (Lee et al., 2020; Lee et al., 2016). It was observed that the CA diet enhances the *in vivo* gut permeability. In the

present study, the role of primary 12αOH BAs in gut barrier dysfunction in both *in vivo* and *ex vivo* models was investigated.

2.2 Materials and methods

2.2.1 Animal models and sample collection

Animal experiments were approved by the Institutional Animal Care and Use Committee of the National Corporation Hokkaido University (approval numbers 17–0119 and 19–0161), and all animals were maintained in accordance with the Hokkaido University Manual for Implementing Animal Experimentation. Unless otherwise stated, WKAH rats (3-week-old male; Japan SLC, Shizuoka, Japan) were used. Diets were prepared based on the AIN-93G formulation (Reeves et al., 1993), as shown in Table 2-1. Rats were housed individually in wire-bottomed cages under controlled temperature (22 ± 2 °C), humidity (55 ± 5%), and light cycle (12:12 h), with food and water available *ad libitum*. The body weight and food consumption of each rat were measured every two days.

2.2.2 Dietary CA supplementation for 13 weeks (Study 1)

After acclimation, the rats were randomly divided into two groups (n = 10 each) and fed either the control (Ct) or CA-supplemented diet at 0.5 g/kg diet for 13 weeks. Every 2 weeks from week 0 to 12, the rats were orally administered chromium (III) chloride hexahydrate ($CrCl_3 \cdot 6H_2O$, Wako Pure Chemical Industries, Osaka, Japan) solution with ethylenediaminetetraacetic acid (EDTA) 2Na (Dojindo, Kumamoto, Japan), and urine was collected for 24 h. Fecal samples were collected for 24 h for BA analysis every 2 weeks from weeks 0 to 12. In addition, food deprivation for 16 h was carried out every 2 weeks from week 1 to 11, and the data on body weight, food intake, and blood parameters have already been reported (Yoshitsugu et al., 2021). At the end of the test period, the animals were sacrificed by exsanguination under anesthesia with pentobarbital sodium salt (50 mg/kg body weight; Kyoritsu Seiyaku Corporation). Intestinal contents were collected for the BA analysis. Urine was stored at 4 °C and analyzed within a week. All other samples were stored at −80 °C until analysis.

2.2.3 Dietary CA supplementation for 13 weeks (Study 2)

In a separate experiment in which the rats were fed the same diet (Ct or CA) for 13 weeks without food deprivation (n = 7 for Ct; n = 8 for CA), mucosal scrapings were collected from the ileum and colon after sacrifice as described in section 2.2.2 to determine the BA composition and mucosal gene expression.

2.2.4 Dietary CA supplementation in combination with vancomycin (VCM) treatment for 6 weeks

VCM was used to suppress secondary BA production via 7α-hydroxylation in gram-positive bacteria (Vrieze et al., 2014). Rats were randomly assigned to four groups (n = 8 each) and fed either a Ct or CA diet in combination with VCM (200 mg/L in drinking water) for 6 weeks. Some of the data, including body weight and food intake other than gut permeability, has been published previously (Hori et al., 2021). The rats were administered Cr-EDTA at the end of the experimental period, and urine was collected for 24 h. Fecal samples were collected 24 h before dissection. Portal blood was collected using syringes containing heparin (final concentration of 50 IU/mL blood; Ajinomoto, Tokyo, Japan) and aprotinin (final concentration of 500 kallikrein inhibitor units (kIU)/mL blood; Wako) under anesthesia with pentobarbital sodium salt (50 mg/kg body weight). Intestinal contents were collected immediately after sacrifice by exsanguination. BA composition was measured in the portal plasma, gut contents (ileum and cecum), and feces.

2.2.5 *In vivo* gut permeability with Cr-EDTA

Cr-EDTA is a non-absorbable gut permeability marker excreted in urine without being degraded in the body as previously described (Suzuki and Hara, 2010). Cr-EDTA complex was prepared by boiling a mixture of 100 mL of a 266 mmol/L $CrCl_3 \cdot 6H_2O$ solution and 150 mL of a 198 mmol/L EDTA·2Na solution for 1 h according to Binnerts et al. (1968). After cooling, excess EDTA was neutralized with 2 mL of 1 mol/L calcium chloride, with pH adjusted to 7 in a total volume of 300 mL. The rats were orally administered a Cr-EDTA solution at 0.5 mL/kg body weight. The urine was collected for 24 h after administration by placing a steel sieve mesh and a plastic container under the rat cage. 20 mL of 0.05% w/v sodium azide was added to the plastic container in advance. The collected urine sample was then diluted to 100 mL with deionized water.

4.25 mL of diluted urine sample was digested with 0.25 mL of 70% perchloric acid and 0.5 mL of 2 g/L ammonium chloride at room temperature for 1 h and centrifuged at 3000 × *g* for 10 min at 4 °C. The amount of urinary Cr was determined using a polarized Zeeman atomic absorption spectrophotometer (Z-5310; Hitachi High-Technologies Corporation, Tokyo, Japan). Cr excretion was calculated as the percentage of urinary Cr in the administered amount to evaluate the *in vivo* gut leakiness.

2.2.6 *In vivo* gut permeability with fluorescein-isothiocyanate-dextran 4 kDa (FD4)

Changes in the blood FD4 concentration were assessed after oral gavage to estimate the responsible permeation site in the gut. Rats were fed the Ct (n = 8) or CA (n = 7) diet for 7 weeks to acclimatize them to each dietary condition. Rats were deprived of food for 4 h and then orally administered FD4 at 300 mg/kg body weight (100 mg/mL in saline; Sigma-Aldrich, NSW, Australia). Tail vein blood was collected every 30 min for 4 h. The plasma FD4 concentrations were measured by fluorometric determination at 485 nm for excitation and 535 nm for emission (Infinite M200, Tecan, Grodig, Austria).

2.2.7 *Ex vivo* gut permeability in Ussing chamber

Fresh segments (jejunum, ileum, cecum, and colon) were dissected from Wistar/ST male rats (7 weeks old; Japan SLC) after exsanguination under anesthesia. Luminal contents were rinsed with Hanks' balanced salt solution (HBSS). Segments (1.5 cm) were opened along the mesenteric border and gently pinned on the block of the Navicyte Ussing chamber system (0.64 cm^2 pore size; Warner Instruments, MA, USA). Both the mucosal and basolateral surfaces were immediately immersed in 1 mL of HBSS and equilibrated for 10 min. The system was bubbled with O_2, and the temperature was maintained at 37 °C throughout the incubation period. Lucifer yellow (Sigma-Aldrich) was added to the mucosal buffer (final concentration of 0.075 μmol/L) in combination with different concentrations of selected BAs and inhibitors, as described below. Jejunal and ileal segments were challenged with TCA at 12.5 or 50 mmol/L. The cecal segments were challenged with 5 mmol/L CA or DCA. Colonic tissues were challenged with 10 mmol/L CA or DCA. In addition, the ileal samples were challenged with 50 mmol/L TCA in the presence or absence of 100 μmol/L of Rho

kinase inhibitor Y-27632 (Wako). The ileal segments were challenged with 40 mmol/L of TCA in the presence or absence of 100 μmol/L methoctramine (Sigma-Aldrich), an CHRM2 antagonist. Intestinal transepithelial electrical resistance (TEER) was measured with a Millicell ERS-2 Volt-Ohm meter (Millipore, Bedford, MA) every 10 min during incubation. After 60 min of incubation, the serosal buffer was collected, and the lucifer yellow concentration was determined at 430 nm for excitation and 530 nm for emission (Infinite M200). Lucifer yellow permeability was calculated as a percentage of the permeated amount relative to the amount added to the mucosal buffer.

2.2.8 BA analysis

BA composition was analyzed based on previously reported methods (Hagio et al., 2011, 2009; Lee et al., 2019). Briefly, samples, including feces, gut contents, gut mucosa, and plasma, were lyophilized, followed by ethanol extraction and evaporation. The extracts were then dissolved in methanol and purified using an HLB cartridge (Waters, Milford, MA, USA). The BA extracts were analyzed by ultra-performance liquid chromatography (UPLC)/mass spectrometry (MS). Acquity UPLC with Quattro Premier XE quadrupole tandem MS (Waters) was used for the data in Study 1 (Hagio et al., 2011, 2009). Dionex UltiMate 3000 UPLC with Orbitrap MS (Thermo Fisher Scientific, San Jose, USA) was used for the data in the other studies due to instrument updates (Lee et al., 2019). Nordeoxycholic acid (23-nor-5β-cholanic acid-3α,12α-diol) was used as an internal standard to calculate the individual BA concentrations. The classification and structural information of the BAs analyzed in this study are presented in Table 2-2.

2.2.9 Postprandial BA circulation

Wistar/ST male rats (7 weeks old; Japan SLC; n = 8) were fed a Ct diet in a time-restricted manner (feeding period between 10:00 and 13:00) for a week. A laparotomy was performed under anesthesia with pentobarbital sodium salt for portal vein cannulation, as previously described (Hira et al., 2009). Rats were then allowed to recover for 4 days in the time-restricted feeding. On the day of sample collection, both portal and tail vein blood was collected before (0 min as baseline) and after (3, 6, and

9 h) initiation of the feeding period. Total plasma BA levels were measured using the Total Bile Acid Test (Wako). This experiment was done by Ayana Sakaguchi.

2.2.10 Real-time quantitative PCR (RT-qPCR)

Briefly, total RNA was extracted from ileal or colonic mucosa samples using an RNeasy Mini Kit (Qiagen, Hilden, Germany). The cDNA templates were synthesized from 1 μg of RNA using a qPCR RT master mix with gDNA remover (Toyobo, Osaka, Japan). RT-qPCR was conducted on an Mx3000P real-time PCR system (Stratagene, La Jolla, CA, USA) based on the SYBR Green method using TB Green Premix Ex Taq II (Takara, Shiga, Japan). The primers used in this study are listed in Table 2-3. The relative mRNA expression levels were calculated using the standard curve method. The ribosomal protein lateral stalk subunit P0 (Rplp0) was used as the reference gene.

2.2.11 Western blotting

Briefly, 50 mg of wet ileal mucosa samples were homogenized in 500 μL of the radioimmunoprecipitation assay lysis buffer with a protease inhibitor cocktail (Nacalai Tesque, Kyoto, Japan). The lysate was incubated for 30 min at 4 °C, followed by centrifugation at 12,000 × *g* for 15 min. Protein concentration was determination by a BCA assay (Takara). Then, 50 μL of extracts were denatured in 10 μL of SDS-PAGE loading buffer (6% w/v SDS, 10% 2-mercaptoehtanol, 22% glycerol, 0.15% w/v bromophenol blue, and 0.18 mol/L Tris-HCl pH 6.8) at 100 °C for 10 minutes. An aliquot of protein extract (30–50 μg) was run on 12.5% gels that were prepared as shown in Table 2-4. Then, separated proteins were transferred to a polyvinylidene fluoride (PVDF) membrane with semi-dry transfer cells (Bio-Rad, Hercules, CA). The membranes were blocked with 5% bovine serum albumin, followed by overnight incubation with primary antibodies at 4 °C. The primary antibodies used in this study are shown in Table 2-5. The membranes were then incubated for 1 h with horseradish peroxidase-conjugated secondary antibody (1:5000, 7074; Cell Signaling, Berkeley, CA). The signals were visualized using Chemi-Lumi One Super (Nacalai Tesque) and detected with LumiVision PRO 400EX (Aisin, Aichi, Japan). β-actin expression was used as a loading control for normalization. Quantification was performed using the ImageJ 1.53a software.

2.2.12 Statistical analysis

Data are expressed as the mean ± standard error of the mean (SEM) unless otherwise indicated. Statistical analyses were performed using JMP Pro 15 (SAS Institute Inc., Cary, NC, USA). The unpaired Student's *t*-test was used to perform two-group comparisons. In the case of multiple comparisons (data in Figures 2-2C and 2-5B), Dunnett's test was used. For data on urinary Cr (Figure 2-1C) and FD4 in plasma (Figure 2-5A), repeated measures analysis of variance (ANOVA) was carried out (CA, time, and the interaction). Two-way ANOVA was used to compare the data from more than two independent groups with two variables (data in Figures 2-2E, 2-3, 2-4A, 2-5A, and 2-6E). When there was an interaction in the two-way ANOVA (CA × time or CA × VCM), a post-hoc test was applied (Student's *t*-test or Tukey-Kramer). Pearson's correlation analysis was used to analyze the relationships between different variables. Statistical significance was set at $P < 0.05$.

Table 2-1 Diet compositions

Ingredient (g/kg diet)	Ct	CA
Dextrin [a]	529.5	529.5
Casein [b]	200	200
Sucrose [c]	100	100
Soybean oil [d]	70	70
Cellulose [e]	50	50
Mineral mixture [f]	35	35
Vitamin mixture [f]	10	10
L-Cystine [g]	3	3
Choline hydrogen tartrate [g]	2.5	2.5
Cholic acid [g]	-	0.5

Ct, control diet; CA, cholic acid supplemented diet.

[a] TK-16, Matsutani Chemical Industry Co., Ltd., Hyogo, Japan.

[b] NZMP Acid Casein, Fonterra Co-Operative Group Limited, Auckland, New Zealand.

[c] Nippon Beet Sugar Manufacturing Co.,Ltd., Tokyo, Japan.

[d] J-Oil Mills, Inc., Tokyo, Japan.

[e] Crystalline cellulose, Ceolus PH-102, Asahi Kasei Corp., Tokyo, Japan.

[f] Mineral and vitamin mixtures were prepared according to the AIN-93G formulation.

[g] Fujifilm Wako Pure Chemical Corporation, Osaka, Japan.

Table 2-2 12αOH and non-12αOH BAs analyzed in the experiments

Systemic name	Trivial name	Abbreviation
Primary 12αOH BAs		
5β-cholanic acid-3α,7α,12α-triol	cholic acid	CA
5β-cholanic acid-3α,7α,12α-triol-*N*-(2-sulfoethyl)-amide	taurocholic acid	TCA
5β-cholanic acid-3α,7α,12α-triol-*N*-(carboxymethyl)-amide	glycocholic acid	GCA
Secondary 12αOH BAs		
5β-cholanic acid-3α,12α-diol	deoxycholic acid	DCA
5β-cholanic acid-3α,12α-diol-*N*-(2-sulfoethyl)-amide	taurodeoxycholic acid	TDCA
5β-cholanic acid 3α,12α-diol-*N*-(carboxymethyl)-amide	glycodeoxycholic acid	GDCA
5β-cholanic acid-3α,7β,12α-triol	ursocholic acid	UCA
5β-cholanic acid-3α,12α-diol-7-one	7-oxo-deoxycholic acid	7oDCA
5β-cholanic acid-3α-ol-12-one	12-oxo-lithocholic acid	12oLCA
5β-cholanic acid-12α-ol-3-one	–	3o12α
Primary non-12αOH BAs		
5β-cholanic acid-3α,7α-diol	chenodeoxycholic acid	CDCA
5β-cholanic acid-3α,6α,7α-triol	hyocholic acid	HCA
5β-cholanic acid-3α,6β,7α-triol	α-muricholic acid	αMCA
5β-cholanic acid-3α,6β,7β-triol	β-muricholic acid	βMCA
5β-cholanic acid-3α,7α-diol-*N*-(2-sulfoethyl)-amide	taurochenodeoxycholic acid	TCDCA
5β-cholanic acid-3α,7α-diol-*N*-(carboxymethyl)-amide	glycochenodeoxycholic acid	GCDCA
5β-cholanic acid-3α,6β,7α-triol-*N*-(2-sulfoethyl)-amide	tauro-α-muricholic acid	TαMCA
5β-cholanic acid-3α,6β,7β-triol-*N*-(2-sulfoethyl)-amide	tauro-β-muricholic acid	TβMCA
Secondary non-12αOH BAs		
5β-cholanic acid-3α,6α,7β-triol	ω-muricholic acid	ωMCA
5β-cholanic acid-3α,6α,7β-triol-*N*-(2-sulfoethyl)-amide	tauro-ω-muricholic acid	TωMCA
5β-cholanic acid-3α,7β-diol	ursodeoxycholic acid	UDCA
5β-cholanic acid-3α,7β-diol-*N*-(2-sulfoethyl)-amide	tauroursodeoxycholic acid	TUDCA
5β-cholanic acid-3α,7β-diol-*N*-(carboxymethyl)-amide	glycoursodeoxycholic acid	GUDCA
5β-cholanic acid-3α-ol	lithocholic acid	LCA
5β-cholanic acid-3α-ol-*N*-(2-sulfoethyl)-amide	taurolithocholic acid	TLCA
5β-cholanic acid-3α-ol-*N*-(carboxymethyl)-amide	glycolithocholic acid	GLCA
5β-cholanic acid-3α-ol-7-one	7-oxo-lithocholic acid	7oLCA
5β-cholanic acid-3α,6α-diol	hyodeoxycholic acid	HDCA
5β-cholanic acid-3α,6α-diol-*N*-(2-sulfoethyl)-amide	taurohyodeoxycholic acid	THDCA
5β-cholanic acid-3α, 6α-diol-*N*-(carboxymethyl)-amide	glycohyodeoxycholic acid	GHDCA

All bile acid standards analyzed in this study were obtained from Steraloids, Inc. (Newport, RI, USA), except for UCA, which was obtained from Toronto Research Chemicals (Toronto, Ontario, Canada).

Table 2-3 qPCR primer sequences

Gene	Forward primer (5' to 3')	Reverse primer (5' to 3')
Rplp0	GGCAAGAACACCATGATGCG	GTGATGCCCAAAGCTTGGAA
Cld1	TGGGGACAACATCGTGACTG	CCCCAGCAGGATGCCAATTA
Cld2	TGCTCACCTCAGGGAAATCG	TCTTGGCTTTGGGCTGTTGA
Cld3	GAGTGCTTTTCCTGTTGGCG	TTGGTGGGTGCGTACTTCTC
Ocln	CCAACGGCAAAGTGAATGGC	AGTCATCCACGGACAAGGTC
Jama	GCAGATGCCAAGAAAACCCG	GTTCTGTGCCTCGCAGTAGT
Zo1	GACACCCACTCTTCCAGAACC	GCTAGTCGCAAACCCACACT
Ctnnb	GCTGAAGGTGCTGTCTGTCT	CCTTCCATCCCTTCCTGCTT
Reg3b	AGTCATGTCCTGGATGCTGCT	GGTATCTGAAACAGGGCATAGC
Reg3g	GGGCTCCATGATCCAACACT	CCCACAGTGACTTCCAGAGAC
Lyz2	TCTCCTAGTTCTGGGGTTCCTC	GGGTTGTAGTTTCTGGCTTGTG
Muc2	GCCAGGAGATTACCAATGACTG	GCAAGGCAGGTCTTTACACATC
Asbt	GGTGACATGGACCTCAGTGTT	GTAGGGGATCACAATCGTTCCT
Ibabp	CCTTCACCGGCAAATACGA	CGTCCCCTTTCAATCACATCT
Osta	CCTCATACTTACCAGGAAGAAGCTAC	CCATCAGGAATGAGAAACAGGC
Ostb	TATTCCATCCTGGTTCTGGCAGT	CGTTGTCTTGTGGCTGCTTCTT
Tnfa	TTCTCATTCCTGCTCGTGGC	AACTGATGAGAGGGAGCCCA
Il1b	TGGCAACTGTCCCTGAACTC	ACACTGCCTTCCTGAAGCTC
Fxr	CATGTTCCTTCGTTCAGCGG	GAGCGTACTCTTCCTGGGTC
Vdr	TGTGTGGACATCGGCATGAT	TCAGCGTAGGTGGGGTCATA
Car	AAGGCTTTTTCAGACGAACAG	AGGGCTTCTGCTGACAGTATC
Pxr	CGGCTACCTGCGGTGTTTC	GGTAGTTCCAGATGCTGCCG
Gpbar1	CTCATCGTCATCGCCAACCT	CCAAGTGGAGAAGGAGGCAG
Chrm2	TGTCAGCAATGCCTCCGTTA	GGTCCGCTTAACTGGGTAGG
S1pr2	AGACTCTACCTGTCCCGTCC	AGTACCTCCCTCCGAAGGTC

Table 2-4 Formulation of SDS-PAGE gel

	Separating gel					Stacking gel
	6%	7.5%	10%	12.5%	15%	4%
30% acrylamide	3.75	4.73	6.23	7.8	9.38	1.3
Milli Q	10.28	9.3	7.8	6.23	4.65	6
1.5 M Tris-HCl pH 8.8	4.5	4.5	4.5	4.5	4.5	2.5
10% SDS	0.18	0.18	0.18	0.18	0.18	0.1
10% APS	0.1	0.1	0.1	0.1	0.1	0.06
TEMED	0.01	0.01	0.01	0.01	0.01	0.02

Unit: mL.

Table 2-5 Primary antibodies for western blotting

Name	Abbreviation	Dilution	Catalog No.	Manufacturer
myosin light chain 2	MLC2	1:1000	8505	Cell Signaling
phospho-myosin light chain 2 Ser19	pMLC2S	1:1000	3671	Cell Signaling
phospho-myosin light chain 2 Thr18/Ser19	pMLC2TS	1:1000	3674	Cell Signaling
claudin 1	CLD1	1:1000	71-7800	Invitrogen
claudin 2	CLD2	1:1000	51-6100	Invitrogen
jam-a	JAMA	1:1000	36-1700	Invitrogen
occludin	OCLN	1:5000	ab167161	Abcam
apical sodium-dependent BA transporter	ASBT	1:1000	bs-23146R	Bioss
β-actin	β-actin	1:5000	4970S	Cell Signaling

2.3 Results

2.3.1 Fecal BA composition and gut permeability in CA-fed rats

Changes in fecal BA and *in vivo* gut permeability during the experimental period of 13 weeks were investigated. CA feeding dramatically elevated the concentration of 12αOH BA species and had a moderate effect on non-12 BAs (Figure 2-1A, B). Among 12αOH BAs, CA, 7oDCA, and UCA transiently increased in the first 6 weeks, whereas DCA and 12oLCA increased progressively during the test period. Notably, urinary Cr excretion significantly increased in response to the CA diet (Figure 2-1C). The fecal DCA output can be interesting, which is linked to colonic barrier dysfunction (Stenman et al., 2013). An increase in gut permeability was observed in the CA-fed rats at week 2, regardless of a subtle increase in fecal DCA concentration. The fecal DCA concentration at week 10 was 3-fold higher than that at week 2 in the CA-fed rats, while the change in gut permeability was almost stable throughout the experimental period. The correlation between fecal BA levels and gut permeability was further analyzed. The total BA concentration was associated with gut permeability during the experimental period (Figure 2-1D). The ratio of 12αOH/non-12 BAs, but not secondary/primary BAs, was associated with changes in gut permeability. Among 12αOH BAs, it was found that CA, 7oDCA, and UCA showed a strong positive correlation with gut permeability in the early phase and DCA and 12oLCA in the latter phase (Figure 2-1E).

2.3.2 BAs responsible for gut permeability depending on the site of the intestine

BA composition was different among the sites of the intestine and the CA diet altered that (Figure 2-2A). A high concentration of BAs, mainly TCA, was observed in the jejunal and ileal contents compared to the large intestinal contents. Moreover, accumulation of TCA was also observed in the ileal mucosa (Figure 2-2B). It was hypothesized that such a high level of TCA accumulation in the ileum may influence gut permeability and examined the effect in Ussing chamber. A selective increase in ileal permeability was observed at a concentration of 50 mmol/L (Figure 2-2C). The concentration was nearly the same as that observed in the small intestinal contents of rats fed a CA diet or a high-fat diet (Yoshitsugu et al., 2019). On the other hand, DCA

increased cecal and colonic permeability at doses corresponding to the luminal concentrations of the rats on a CA diet (Figure 2-2D), although the effect was much more moderate than that of TCA on the ileum. Rho GTPases play a role in the regulation of cytoskeletal dynamics and paracellular permeability (Schlegel et al., 2011). Both TCA and the Rho kinase inhibitor Y-27632 had a significant effect on permeability (Figure 2-2E). Notably, in the presence of Y-27632, TCA did not increase permeability.

2.3.3 Role of primary 12αOH BAs in *in vivo* gut permeability

Then, an attempt was made to verify the effect of primary 12αOH BAs on CA-induced gut permeability *in vivo*. The suppression of secondary BA production in the ileal contents, cecal contents, and feces of rats administered VCM was confirmed (Figure 2-3A). The major BA was TCA in the ileal contents of CA-fed rats regardless of the VCM treatment (Figure 2-3B). In contrast, DCA was almost undetectable at each site in the VCM-treated rats, although DCA was abundant in cecal contents and feces in rats without VCM treatment (Figure 2-3B-E). A high cecal and fecal concentration of CA was observed in rats fed the CA+VCM diet. These results confirmed that VCM treatment suppressed the 7α-dehydroxylation of CA in the large intestine.

Interestingly, the degree of gut permeability in the CA+VCM group was almost comparable to that in the CA group, and no effect was observed with VCM treatment on the CA-induced leaky gut (Figure 2-4A). The 12αOH BAs in portal plasma were closely correlated with gut permeability (Figure 2-4B), and the highest correlation was observed between portal TCA concentration and gut permeability ($r = 0.7388$, $P < 0.0001$; Figure 2-4C). On the other hand, significant correlations were also found between cecal and fecal primary 12αOH BAs and gut permeability (Figure 2-4B), which may be due to the remaining CA in the cecal contents and feces of the CA+VCM-fed rats. The effect of CA on permeability in isolated cecal and colonic tissues was measured in Ussing chamber experiment, but no significant influence was observed (Figure 2-4D, E).

2.3.4 Estimation of the responsive site of the leaky gut in the CA-fed rats

To estimate the site of gut leakage in CA-fed rats, another permeability test using FD4 was introduced. A transient increase was observed in tail vein plasma FD4

concentration as expected, and the peak value was approximately twice that in the CA-fed rats as compared to that in Ct-fed rats (Figure 2-5A). The peak times were 71 ± 5 and 90 ± 13 min in Ct-and CA-fed rats, respectively.

Postprandial changes in total BAs in the plasma of the tail vein and portal blood were measured in rats (Figure 2-5B). The total BA in portal plasma was > 100 μmol/L and was stable regardless of meal feeding. On the other hand, total BA concentration in tail vein plasma was transiently increased in response to meal feeding, and the maximum level was approximately 10 μmol/L.

2.3.5 Alteration of gene expression associated with mucosal barrier in the gut mucosa of the CA-fed rats

The expression of intercellular junction proteins in the ileal and colonic mucosa of CA-fed rats was analyzed. Both the mRNA and protein levels of claudin 1 (CLD1) and claudin 2 (CLD2) were significantly downregulated in the ileum of CA-fed rats (Figure 2-6A, D). It was also found that increased phosphorylation of myosin light chain 2 (MLC2) (Figure 2-6D), which is a central physiological modulator involved in perijunctional actomyosin contraction and tight junction regulation (Jin and Blikslager, 2020). In addition to the tight junctions that serve as the mechanical barrier, the mRNA expression of antibacterial defense that relates to the chemical barrier was determined. The expression levels of antimicrobial-regenerating islet-derived (REG)-3 lectins, including *Reg3b* and *Reg3g*, were suppressed in the ileal mucosa of CA-fed rats (Figure 2-6A). The mRNA expression of mucin 2 (*Muc2*), which encodes the primary component of mucus, was also decreased in the ileal mucosa. There was no difference in the colon following CA feeding (Figure 2-6B). Additionally, there was no increase in mRNA levels of tumor necrosis factor-α and interleukin 1β in the ileal and colonic mucosa of CA-fed rats (Figure 2-6C). Such changes in gene expression were observed mainly in the ileal mucosa but not in the colonic mucosa.

BAs activate various BA receptors in the regulation of metabolism, immunity, and inflammation (Jia et al., 2018), and BA receptors may be involved in the leaky gut caused by CA supplementation. In the ileal mucosa, the expression level of *Fxr* was significantly decreased in CA-fed rats compared to that in the Ct rats, while no

differences were observed in the other BA receptors (Figure 2-6A). In the colonic mucosa, where the BA composition was different from that in the ileum, the CA diet slightly enhanced the *Chrm2* expression (Figure 2-6B). CHRM2 has emerged as a receptor of conjugated BAs (Raufman et al., 2003), however, inhibition of this receptor had no obvious effect on gut permeability in response to TCA in the Usssing chamber (Figure 2-6E). Moreover, a reduction in the mRNA and protein levels of ASBT was found in the ileum of the CA-fed rats (Figure 2-6A, D). A subtle increase was found in mRNA expressions of *Asbt* and ileal BA-binding protein (*Ibabp*) in the colon upon CA diet (Figure 2-6B). Interestingly, single regression analysis revealed positive correlations between ileal levels of *Fxr* and those of *Reg3b*, *Muc2*, and *Asbt* (Figure 2-6F).

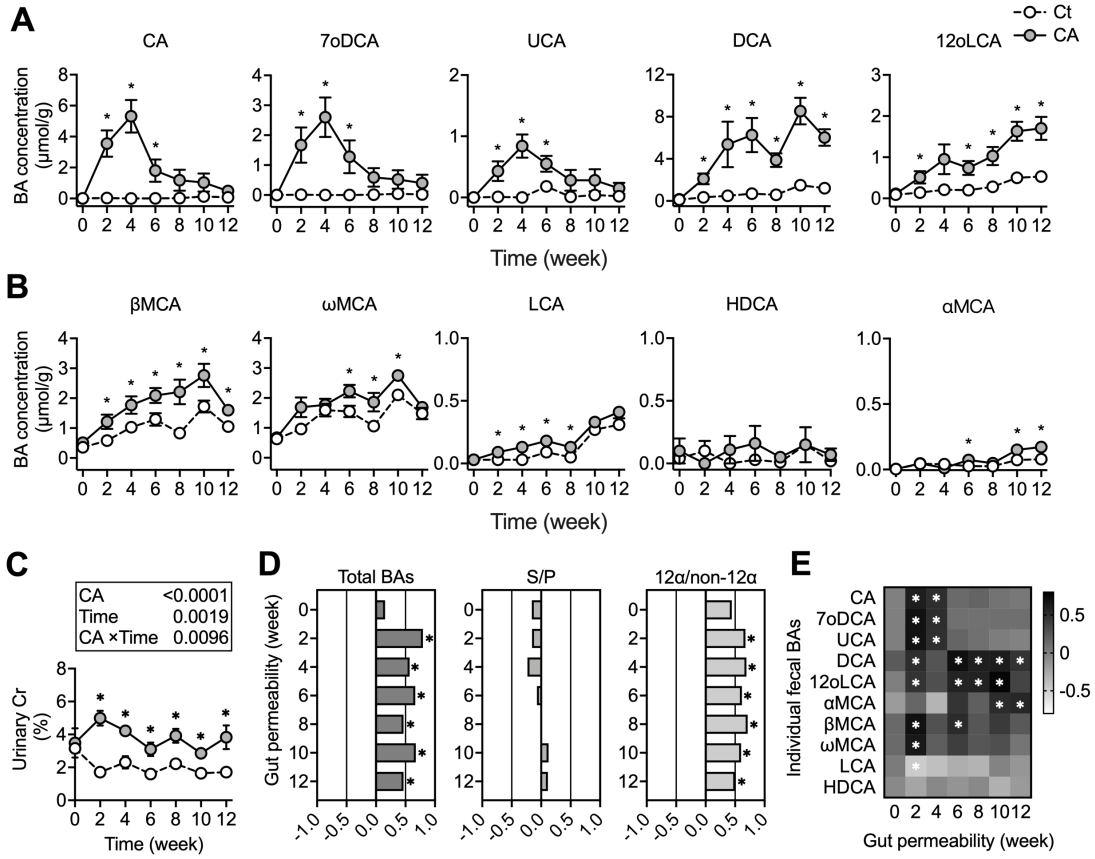

Figure 2-1 Changes in the bile acid (BA) profiles and gut permeability in WKAH rats fed with either a control (Ct) or cholic acid (CA)-supplemented diet (Study 1; n = 10, n refers to the number of animals in the *in vivo* studies). Changes in fecal levels of 12α-hydroxylated BAs (**A**) and non-12α-hydroxylated BAs (**B**) over time. BAs with average concentrations greater than 0.01 μmol/g are shown. Asterisks indicate the significant difference in the values between groups at each time point ($P < 0.05$, Student's *t*-test). (**C**) Changes in the urinary chromium (Cr) excretion as an indicator of gut permeability. The *P* values of repeated measures analysis of variance (ANOVA) are shown in the inset. Asterisks indicate the significant difference in the values between groups at each time point ($P < 0.05$, Student's *t*-test). (**D**) Correlations between gut permeability and the three factors of fecal BA profiles, including total BA, secondary/primary (S/P) ratio, and 12α-hydroxylated (12α)/non-12α ratio, at different time points. Asterisks indicate significance ($P < 0.05$, multivariate correlation analysis). (**E**) Heatmap of correlation coefficients between individual fecal BAs and gut permeability at different time points. The gradient colors represent the positive (blue) or negative (yellow) correlation. Asterisks indicate significance ($P < 0.05$, multivariate correlation analysis).

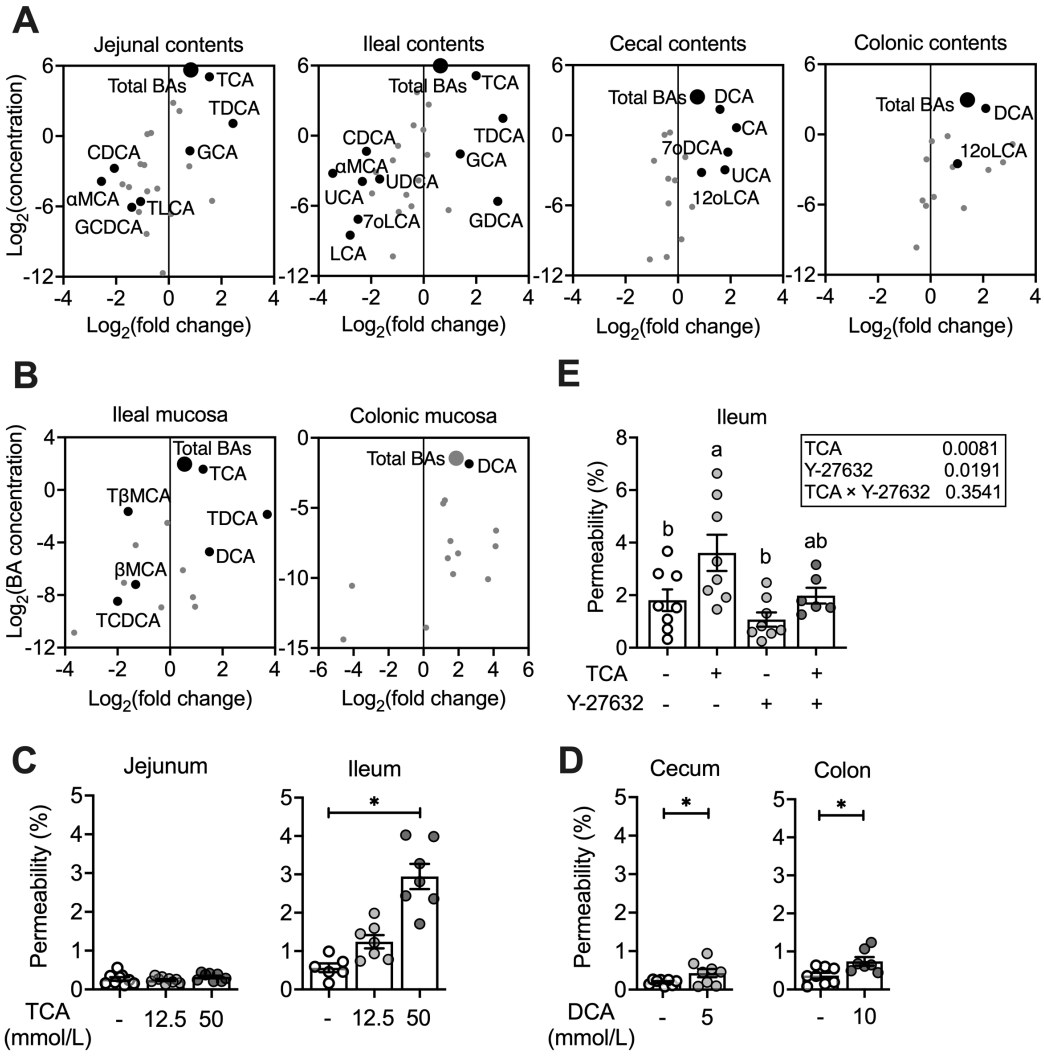

Figure 2-2 Intestinal BA metabolism in the CA-fed rats and *ex vivo* permeability of intestinal tissues in response to taurocholic acid (TCA) or deoxycholic acid (DCA) in Ussing chamber. Alteration of BA metabolism at week 13 in the intestinal contents **(A)** and mucosa **(B)** of the CA-fed rats (Study 1). Each dot represents individual BA species. Fold change in BA concentration (μmol/g) in the CA-fed rats compared to that in Ct is shown on the x-axis as $\log_2$ values. Black dots represent significantly changed BAs. Grey dots indicate no significance in the values (Student's *t*-test, n = 10). **(C)** Percentages of lucifer yellow were detected in the serosal buffer after the incubation of jejunal (n = 8–9) or ileal (n = 6–7) segments with TCA (0, 12.5, or 50 mmol/L). Asterisk indicates the significance ($P < 0.05$, Dunnett's test). **(D)** Percentages of lucifer yellow were detected in the serosal buffer after the incubation of cecal (n = 8) and colonic (n = 7–8) segments with DCA (5 or 10 mmol/L). Asterisk indicates the significance ($P < 0.05$, Student's *t*-test). **(E)** Percentages of lucifer yellow were detected in the serosal buffer after the incubation of ileal segments (n = 6–8) with TCA (50 mmol/L) in the presence or absence of Rho kinase inhibitor (Y-27632, 100 μmol/L). Two-way ANOVA with a Tukey post-test were performed. *P*-values in two-way ANOVA are shown in the inset. Different alphabets (lowercase) represent significance by Tukey-Kramer's test ($P < 0.05$).

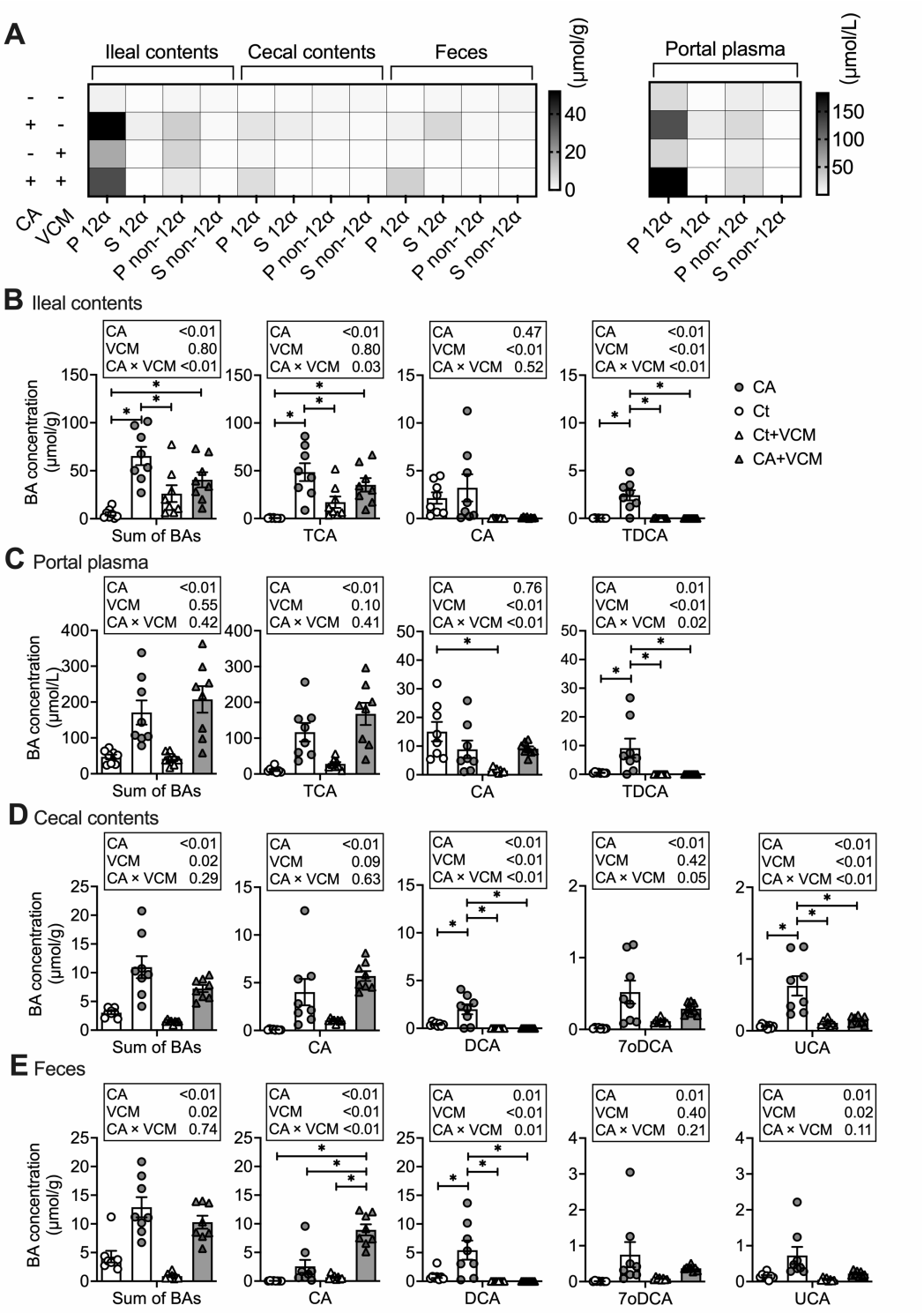

Figure 2-3 Abrogation of secondary BAs with vancomycin (VCM). Samples were collected from the WKAH rats fed with either the Ct or CA diet in combination with VCM in drinking water for 6 weeks (n = 8). (**A**) Heatmap of 12αOH and non-12αOH BA concentrations in ileal contents, cecal contents, feces, and portal plasma (P, primary; S, secondary; n = 8). Concentrations of the sum of BAs and major 12αOH BAs in the ileal contents (**B**), portal plasma (**C**), cecal contents (**D**), and feces (**E**). *P*-values of two-way analysis of variance (ANOVA) were presented in the insets. Asterisks indicate the significance ($P < 0.05$, Tukey-Kramer's test).

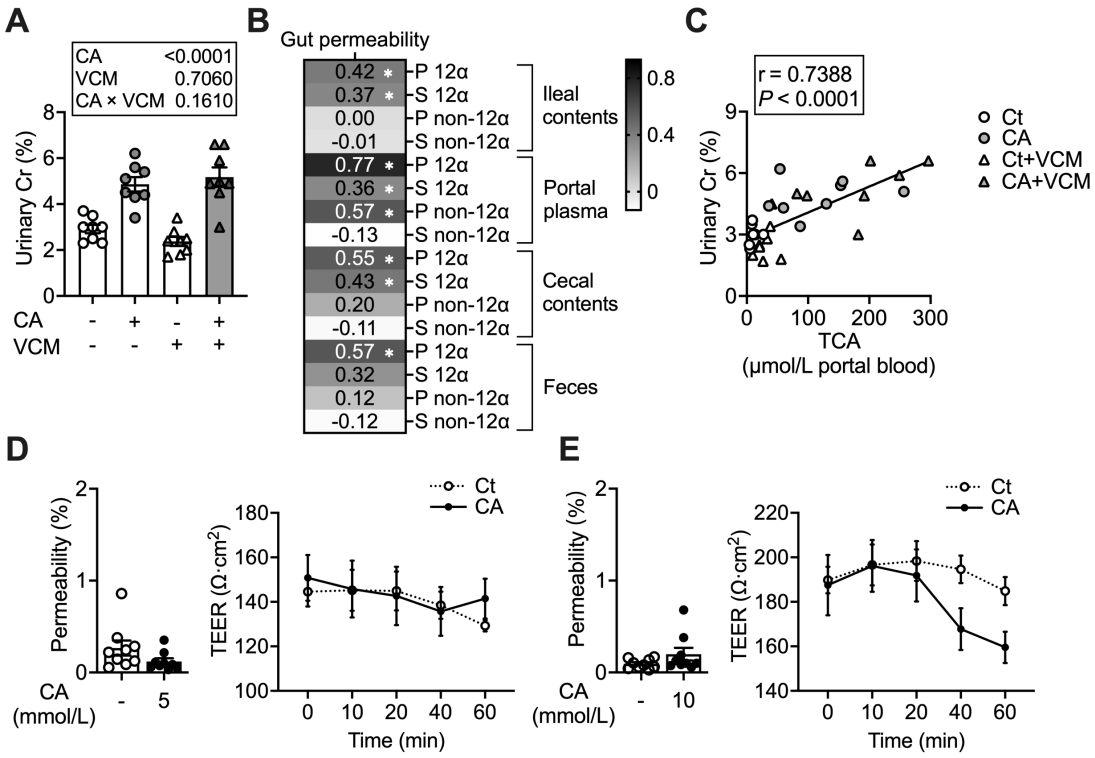

Figure 2-4 Abrogation of secondary BAs did not affect CA diet-induced gut permeability. Samples were collected from the WKAH rats fed with either the Ct or CA diet in combination with VCM in drinking water for 6 weeks (n = 8). (**A**) *In vivo* gut permeability test. *P*-values of two-way ANOVA are shown in the inset. (**B**) Heatmap of correlation coefficients between gut permeability and BA classifications in different sites. The coefficient values are shown in the panel. Asterisks indicate significance ($P < 0.05$, multivariate correlation analysis). (**C**) Pearson's correlation between portal TCA concentration and *in vivo* gut permeability. The coefficient values and *P*-values are shown in the inset. Cecal (**D**) and colonic (**E**) permeability and changes in TEER over time in response to CA exposure in Ussing chamber (n = 9). Percentages of lucifer yellow were detected in the serosal buffer after incubation of cecal or colonic tissues with CA (5 or 10 mmol/L, respectively).

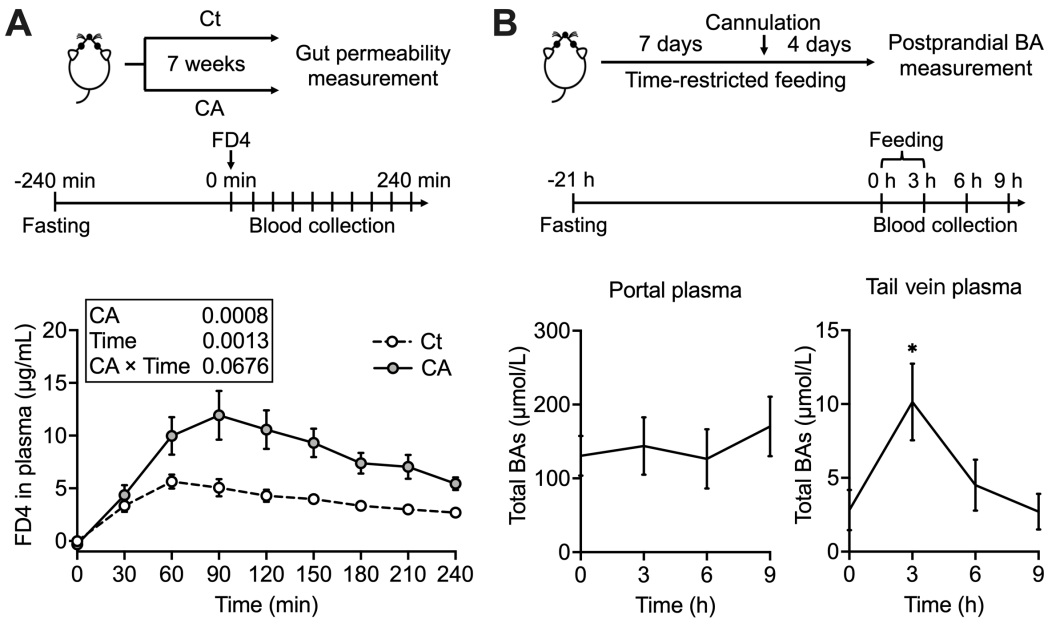

Figure 2-5 Estimation of the leakage site in the gut based on the appearance of the plasma permeation marker. (**A**) Changes in the plasma fluorescein-isothiocyanate-dextran 4 kDa (FD4) concentration over time. FD4 (300 mg/kg) was orally administered with gavage in the WKAH rats fed either the Ct or CA diet (n = 7–8). *P*-values of repeated measures ANOVA are shown in the inset. (**B**) Postprandial changes of total BA concentrations in the tail vein and portal plasma in Wistar/ST rats (n = 8). This experiment was done by Ayana Sakaguchi. The experimental schedule is shown in the inset. Asterisks show a significant difference from time 0 ($P < 0.05$, Dunnett's test).

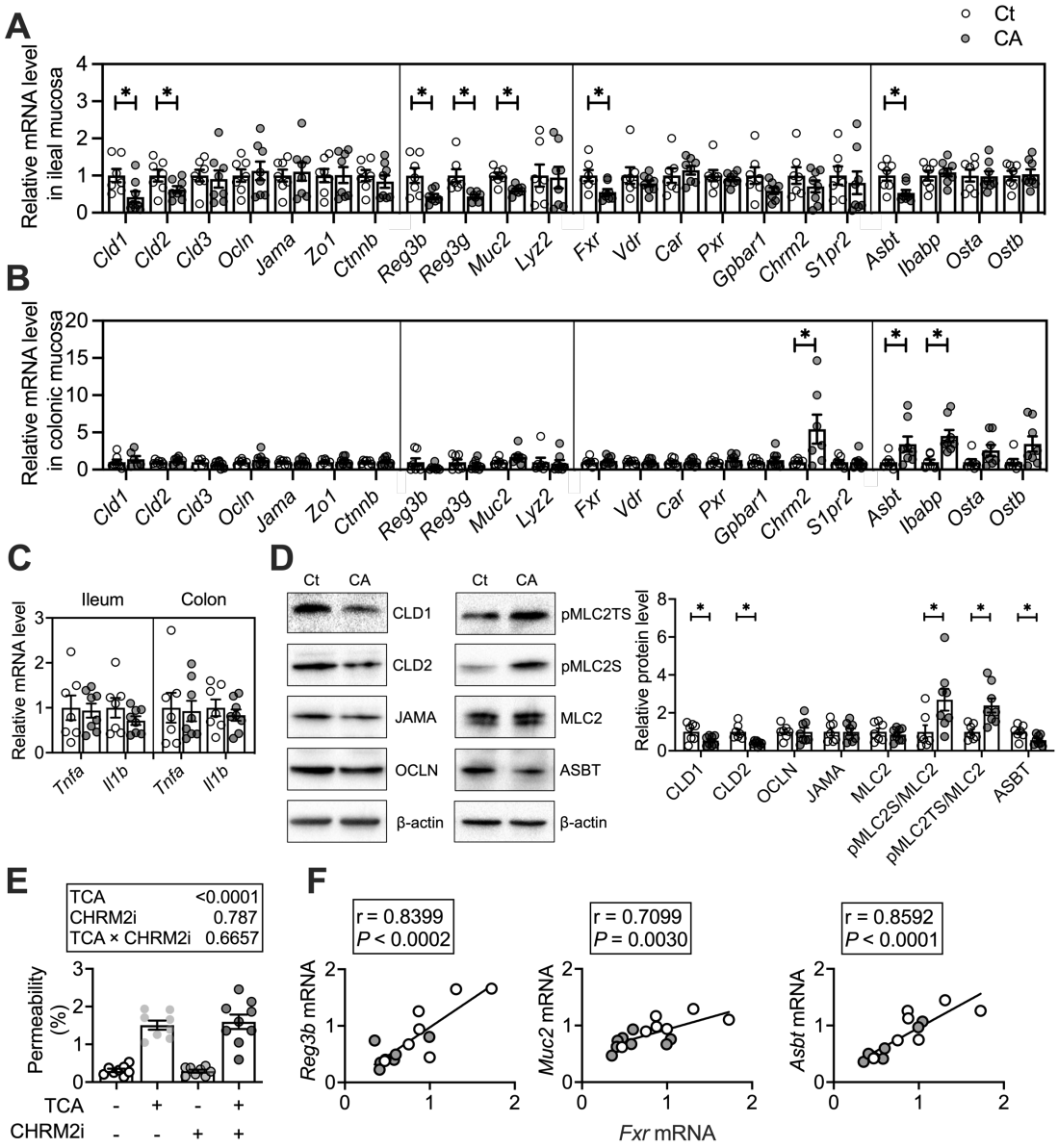

Figure 2-6 Expression levels of genes responsible for the gut barrier and BA metabolism in rats fed the Ct or CA diet for 13 weeks (Study 2; n = 7–8). (A) Transcript levels of genes encoding tight junction proteins, antimicrobial peptides, BA receptors, and BA transporters in the ileal mucosa. Asterisks indicate the significant difference between the groups ($P < 0.05$, Student's *t*-test). **(B)** Transcript levels in the colonic mucosa. (**C**) Transcript levels of genes encoding proinflammatory cytokines. **(D)** Representative western blotting images of the tight junction proteins, myosin light chain 2 (MLC2), phospho-myosin light chain 2 Ser19 (pMLC2S), phospho-myosin light chain 2 Thr18/Ser19 (pMLC2TS), and ASBT. Western blotting analysis was performed in 7–8 independent experiments. (**E**) Effects of TCA and inhibition of M2 muscarinic acetylcholine receptor (Chrm2) on ileal permeability *ex vivo* in Ussing chamber (n = 8–9). *P*-values in two-way ANOVA are shown in the inset. **(F)** Pearson's correlation of the ileal levels of the *Fxr* with those of the *Reg3b*, *Muc2*, and *Asbt*. The coefficient values and *P*-values are shown in the inset.

2.4 Discussion

The effect of secondary BAs on gut permeability has attracted researchers for a long time, as secondary BAs are one of the factors responsible for leaky gut (Stenman et al., 2013). Previously, it was found a selective increase in primary 12αOH BAs in the enterohepatic circulation upon high-fat diet feeding (Hori et al., 2020; Yoshitsugu et al., 2019), and the level of primary BAs in the small intestine is quite high compared to that of secondary BAs in the large intestine. Thus, the role of primary 12αOH BAs in the leaky gut and the site of leakiness were examined. The present study demonstrated the following: 1) increase in TCA concentration in enterohepatic circulation associated with *in vivo* gut permeability, 2) TCA-induced ileum-specific leakiness, 3) abrogation of secondary BAs did not alter the CA diet-induced leaky gut *in vivo*, and 4) alteration in gene expression that is related to gut permeability frequently observed in the ileum. Additionally, almost no change in the genes was observed in the colon, although accumulation of DCA was observed in the large intestinal contents and colonic mucosa. These results provide new insights into the role of primary 12αOH BAs in inducing a leaky gut.

The effect of primary BAs on intestinal permeability has been neglected because of their low hydrophobicity and cytotoxicity in intestinal epithelial cell lines compared to secondary BAs (Araki et al., 2003). In the present study, the CA diet-induced leaky gut was observed in week 2, where no sufficient conversion was found from CA to DCA (Figure 2-1). Therefore, it was hypothesized that primary 12αOH BAs are inducers of leaky gut. A study showed that CA enhances permeability in Caco-2 monolayers, although its effect is moderate in comparison with CDCA and DCA (Raimondi et al., 2008). Considering the important distinctions in the BA composition and concentration between the small and large intestines, it is necessary to compare the effects of BAs on different intestinal sites at a reasonable physiologic dose depending on the site of the intestine. In this study, the influence of ileal TCA was more apparent than that of colonic DCA in gut leakiness in *ex vivo* experiments (Figure 2-2). Although VCM treatment increased the proportion of CA in the colonic contents, exposure of isolated colon tissue to CA in the Ussing chamber was less effective (Figure 2-4). In addition, the selective

effect of TCA on the permeability in the ileum rather than in the jejunum could be due to the fact that the ileum is the site for reabsorbing conjugated BAs. Ileal internalization of excessive TCA may alter cell signals, leading to modulation of cellular contraction. The absence of ASBT expression in the jejunum (Bijvelds et al., 2005) restricts TCA incorporation in the jejunal mucosa, which can explain site differences in the effect of TCA on the mucosal permeability. The present study demonstrates that the influence of TCA on ileal permeability is much stronger than that of DCA in the colon in terms of gut leakiness.

BA metabolism in the rats fed the CA diet resembles those found in the rats fed a high-fat diet (Yoshitsugu et al., 2019), in which predominance of TCA and DCA is observed in the small and large intestines, respectively. It has been reported that mice fed a 0.2% DCA diet develop colitis (Bernstein et al., 2006). The CA diet induced a leaky gut without any implications for intestinal inflammation (Figure 2-6). Although DCA was abundant in the large intestine of CA diet-fed rats, alterations in barrier function-related genes were only observed in the ileum rather than in the colon (Figure 2-6). It is considered that a higher concentration of DCA (at millimolar levels) is required in the *in vivo* studies to trigger intestinal barrier dysfunction with local inflammation (Stenman et al., 2013; L. Wang et al., 2020). The present study indicates that a high level of TCA evokes epithelial paracellular permeability and barrier dysfunction in the ileum, even under conditions in which DCA-induced colonic abnormalities have not yet been identified.

A significant increase of FD4 in the tail venous plasma was observed under CA diet feeding and the peak time was at 90 ± 13 min (Figure 2-5). A report showed that the mean transit time of liquid meal is about 100 min to the small intestine, whereas the mean cecal arrival time is approximately 200 min in rats (Quini et al., 2012), which suggests that FD4 leakage under the CA diet feeding occurs mainly in the proximal intestine. TCA, which is reabsorbed from the distal ileum, is a dominant BA in either the portal or peripheral circulation under a high-fat diet in rats (Yoshitsugu et al., 2019; Hori et al. 2020). An interesting question to pursue is whether TCA challenges the ileal mucosa only postprandially or continuously. BA concentration was nearly 10 times

higher in portal blood than in peripheral circulation, even under fasting conditions in rats (Figure 2-5). This is in line with previous human and porcine studies, which also showed a high baseline flux of BA in the portal vein (Angelin et al., 1982; Eggink et al., 2018). This underscores intestinal BA absorption even in the fasting state. In addition, a transient rise in postprandial BA levels in the portal vein could be ascribed to increased hepatic BA output in response to feeding (Angelin et al., 1982). These results indicate a stable and high flow of enterohepatic BA circulation in rats, regardless of food intake, suggesting that epithelial cells of the distal small intestine are continuously exposed to high levels of TCA.

Phosphorylation of MLC2 regulated by Rho kinase leads to actomyosin contraction, which increases paracellular permeability by regulating intercellular junctions (Jin and Blikslager, 2020). Claudins are highly expressed in the rat small intestine and constitute tight junction strands connected with zonula occludens 1 (Markov et al., 2010). Claudins are thought to be responsible for restricting the paracellular passage of electrolytes and small molecules (Otani et al., 2019). In this study, the TCA-induced *ex vivo* ileal permeability was alleviated by the Rho kinase inhibitor (Figure 2-2). Exposure to TCA of the ileal mucosa led to the enhancement of MLC2 phosphorylation and reduction in claudins (Figure 2-6). Similarly, a recent study shows that MLC2 phosphorylation mediates DCA-induced permeabilization in Caco-2 cells (Z. Wang et al., 2020). These observations suggest that the MLC2 phosphorylation plays a role in the enhancement of intestinal permeability induced by 12αOH BAs. Such MLC2 phosphorylation may lead to cellular contraction, and a reduction in claudin expression may open the paracellular pathway via modulation of the tight junction.

Notably, the reduced expressions of *Reg3b* and *Muc2* were positively correlated with reduced *Fxr* gene expression (Figure 2-6). FXR is expressed mainly in the ileum (Inagaki et al., 2006) and plays a role in enterohepatic BA circulation and gut immunity. Similarly, FXR dysfunction is found to be associated with a selective increase in FD4 permeability in the ileum (Verbeke et al., 2015). Under the condition of CA-supplementation in the present study, TCA might be the major BA that is incorporated in the mucosa via ASBT. In a recent study, TCA is reported to be an FXR antagonist

that inhibits CDCA-induced expressions of *Fxr* and *Fgf15* mRNA and the antagonistic effect of TCA is comparable to that of TβMCA (Tveter et al., 2020). In the present study, the increase in TCA concentration in the ileal mucosa might suppress FXR activity. It is likely that FXR dysfunction mediates transcriptional regulation of *Reg3b* and *Muc2* in a TCA-abundant condition.

In addition, the expression of ASBT decreased in the ileum upon CA diet feeding (Figure 2-6). The reduction in ASBT could have played an adaptive function in restricting BA influx in the ileum to keep the BA enterohepatic circulation within a physiologic range. And yet, the higher portal level of BAs observed in the CA group (Figure 2-3) was not consistent with the reduced ASBT, which suggests that some TCA may traverse through the ileal mucosa via the paracellular pathway when there is a leaky gut.

Alterations of 12αOH BAs in metabolic disorders are reported in humans as follows: 1) an increase in plasma 12αOH BAs accompanied by the symptoms of insulin resistance (Haeusler et al., 2013), 2) marked increases in hepatic levels of TCA and TDCA in NAFLD patients (Lake et al., 2013), and 3) an increase in the fecal level of CA in NAFLD patients (Mouzaki et al., 2016). Those suggest alterations of 12αOH BAs in human metabolic dysfunctions. Although a substantial proportion of muricholic acids is observed in rodents (Takahashi et al., 2016), those are CDCA derivatives and non-12αOH BAs. On the other hand, the significance of 12αOH BAs in liver lipid accumulation is also confirmed in several rodent experiments (Lee et al., 2020; Hori et al., 2020), and close similarity is observed in the positive relationship between 12αOH BAs and liver lipid accumulation in those rodent studies and human studies. Although CA-supplementation to diet seems artificial, the CA-supplementation level is carefully considered in rats in terms of 12αOH BA metabolism (Islam et al., 2011) that is frequently observed in rats fed a high-fat diet (Yoshitsugu et al., 2019). Therefore, this is a reasonable model to reproduce the 12αOH BAs-abundant condition (Lee et al., 2020) that reflects BA metabolism in human metabolic dysfunctions (Haeusler et al., 2013).

Finally, there are some potential limitations to be discussed. Due to limited

information on enterohepatic BA circulation in humans, especially during postprandial conditions, we are therefore unable to investigate and compare the postprandial 12αOH BA levels and their impact on ileal permeability between rodents and humans. For example, a report that shows postprandial changes in humans with a comparison between systemic and portal blood is published in the early 1980s (Angelin et al., 1982), but the method for BA measurement was GC-MS which could not determine BA conjugates due to the deconjugation in the derivatization step for GC measurement. A recent study demonstrates a high level of portal BAs than peripheral BAs in obese subjects (Eggink et al. 2018), and the BA concentration is almost comparable with that in the rats fed a high-fat diet (Hori et al., 2020), but no information is included on the postprandial changes in the BA composition and the relationship between 12αOH BAs and gut permeability. It is interesting to evaluate such relationship, especially in the small intestine in humans in the future.

2.5 Conclusion

In conclusion, an increase in primary 12αOH BAs in the small intestine plays a key role in high-fat diet-induced gut barrier impairment. Excessive and stable flow of TCA in the enterohepatic circulation is a possible inducer of ileal leakiness, which can be partially explained by the phosphorylation of MLC2 and the downregulation of claudins. This predominance of TCA also leads to a reduction in *Fxr* expression, which correlates with the reduction in antimicrobial peptide genes in the ileum. These results highlight the significant role of TCA in gut leakiness, especially in the ileum.

Chapter 3 Alterations in the liver and fecal metabolome in cholic acid-induced hepatic steatosis in rats

Abstract

12α-Hydroxylated (12αOH) BAs are selectively increased with high-fat diet intake. Dietary supplementation of cholic acid (CA) in rats is a possible strategy to reveal a causal link between 12αOH BAs and hepatic steatosis. The present study aimed to investigate the mechanism underlying the impact of 12αOH BAs on hepatic steatosis from a metabolic perspective. Male WKAH rats were fed either a control (Ct) diet or a CA-supplemented diet at 0.5 g/kg. After the 12-week intervention, the CA diet elevated 12αOH BAs levels in the gut–liver axis. The CA-fed rats showed greater hepatic lipid accumulation compared with the Ct group regardless of no difference in dietary energy balance. Untargeted metabolomics suggested marked differences in the fecal metabolome in rats subjected to the CA diet compared to Ct, characterized by depletion of fatty acids and enrichment in amino acids and amines. Moreover, liver metabolome differed upon CA diet, featured as an alteration in redox-related pathways. The CA diet elevated nicotinamide adenine dinucleotide (NAD^+) consumption due to the activation of poly(ADP-ribose) polymerase 1 (PARP1), resulting in impaired peroxisome proliferator-activated receptor α (PPARα) signaling in the liver. We also observed that the CA diet promoted the pentose phosphate pathway that generates reducing equivalents. Integrated analysis of the gut–liver metabolomic data found a role of deoxycholic acid (DCA) and its liver counterpart in mediating these metabolic alterations. These observations suggest that alterations in metabolites induced by 12αOH BAs in the gut–liver axis contribute to the enhancement of liver lipid accumulation.

3.1 Introduction

Patients suffer from NAFLD, or its new concept MAFLD, are up to a quarter of the global population over the past decades and is commonly observed with other metabolic

syndromes, such as type 2 diabetes and obesity (Powell et al., 2021). The high prevalence of hepatic steatosis is considered largely due to unhealthy dietary patterns and lifestyles (Powell et al., 2021). Increased energy intake, particularly high dietary fat intake enhances lipid accumulation into the liver (Westerbacka et al., 2005). The crosstalk among gut microbiota, its metabolites, and the liver might also contribute to liver lipid accumulation (Li et al., 2022).

BA metabolism is intricately regulated by the host, diet, and gut microbiota. They are currently receiving great interest as signaling molecules regulating a wide range of gut–liver diseases (Fuchs and Trauner, 2022). BAs can be classified into 12αOH and non-12OH BAs based on the presence or absence of the hydroxyl on position 12 of the steroid skeleton. Recently, it has been found that the BA concentration in the portal circulation is nearly 10 times higher than that in the systemic circulation (Liu et al., 2022), suggesting that the enterohepatic tissues are under a much higher BA load than the rest of the tissues and organs. Moreover, selective increase in 12αOH BAs in rats under high-fat diets associates with hepatic TG levels closely (Hori et al., 2020; Yoshitsugu et al., 2019). Such enrichment in 12αOH BAs is also frequently observed in humans with metabolic diseases (Haeusler et al., 2016, 2013), particularly NAFLD (Smirnova et al., 2022). Further, dietary supplementation of CA at a dose that does not disturb secondary BA production in the gut induces gut dysbiosis, leaky gut, and simple hepatic steatosis in rats, despite no symptoms of obesity and deterioration of oral glucose tolerance (Lee et al., 2020; Liu et al., 2022). These studies suggest 12αOH BAs as critical players in the onset of hepatic steatosis under overnutrition. However, it is unclear how 12αOH BAs affect the metabolism in the gut–liver axis. In addition, it has been documented that some hydrophobic BAs elevate cellular oxidants *in vitro* (Sokol et al., 1995; Z. Wang et al., 2020). Oxidative stress has been implicated in NAFLD progression (Chen et al., 2020; Monserrat-Mesquida et al., 2020). Whether and how 12αOH BAs alter hepatic redox signaling during the onset of steatosis remain elusive.

This study will continue previous work to explore the role and possible mechanism of 12αOH BAs in the development of hepatic steatosis. The BA profiles in the liver, gut contents, and feces in rats on the CA diet for 12 weeks were first investigated. The

differences in the hepatic, intestinal, and fecal metabolome between Ct rats and CA-induced hepatic steatosis rats were compared. Attention was also paid to the effect of CA on the Redox status of the liver. Also, the correlation network was visualized based on the differential metabolites. This study provides an additional point of view to understand the effects of 12αOH BAs on the pathophysiology of the gut–liver axis.

3.2 Materials and methods

3.2.1 Animal experiments

All animal experiments were approved by the Institutional Animal Care and Use Committee of National Corporation Hokkaido University (approval numbers: 19-0161). Animals were handled according to the Hokkaido University Manual for Implementing Animal Experimentation. Male WKAH rats aged 3 weeks were purchased from Japan SLC. Rats were housed individually in wire-bottomed cages under controlled temperature (22 ± 2°C), humidity (55 ± 5%), and light cycle (12:12 h). The body weight and food consumption of each rat were recorded every two days. After 1 week of acclimation, rats were randomly assigned to two groups and fed either a control diet (Ct, n = 9) or a CA-supplemented diet at 0.5 g CA/kg diet (n = 8) for 12 weeks. The diets were prepared based on the AIN-93G formulation (Reeves et al., 1993), as described in Table 3-1. Rats were allowed free access to food during the first 10 weeks. For the last 2 weeks, food was provided during zeitgeber time (ZT) 0 to ZT 12. Water was available throughout the experiment. At the end of the test period, rats were euthanized at ZT 3 by exsanguination. The liver, jejunum, ileum, and cecum were collected and immediately frozen in liquid nitrogen. Feces were collected for 24 h before sacrifice, lyophilized, and then ground. CA-4PJ automatic adiabatic bomb calorimeter (Shimadzu Corporation, Kyoto, Japan) was used for the measurement of fecal energy content (Maegawa et al., 2021). All the samples were stored at −80°C until analysis.

3.2.2 Biochemical parameters

The levels of TG and free fatty acid (FFA) in the liver and feces were measured by LabAssay TG (Wako; 290-63701) and LabAssay NEFA (Wako; 294-63601),

respectively.

The hepatic levels of adenosine triphosphate (ATP), nicotinamide adenine dinucleotide (NAD^+/NADH), nicotinamide adenine dinucleotide phosphate ($NADP^+$/NADPH), glucose-6-phosphate dehydrogenase (G6PD) activity, and malondialdehyde (MDA) were determined by ATP colorimetric assay kit (BioVision, San Francisco, CA; K354-100), EnzyChrom NAD^+/NADH Assay Kit (BioAssay, Hayward, CA; E2ND-100), NADP/NADPH quantification kit (Sigma-Aldrich; MAK038), G6PD assay kit (Sigma-Aldrich; MAK015), and MDA assay kit (Dojindo; M496), respectively. Briefly, liver tissues were homogenized in the kit buffers or PBS according to the instructions. An aliquot of homogenates was taken for total protein determination by a BCA assay (Takara). The rest was deproteinized by Deproteinizing sample preparation kit (BioVision; K808-200) and used for measurements. Infinite M200 was used for the measurement of the parameters, and values were normalized with the total protein concentration.

3.2.3 BA analysis

BA compositions in the liver, cecal contents, and feces were analyzed as described in Chapter 2 section 2.2.8.

3.2.4 Organic acid measurement

Organic acids in the cecal contents and feces were measured as reported (Hoshi et al., 1994). In brief, wet samples were diluted in water and mixed with crotonic acid as an internal standard, followed by the removal of hydrophobic substances with chloroform. Organic acids were analyzed using an HPLC system (Shimadzu) with two Shim-pack SCR-102H columns (300 mm × 8 mm, Shimadzu) and a CCD-6A conductivity detector (Shimadzu).

3.2.5 Extraction of metabolites

Metabolites were extracted from the liver, small intestinal mucosa, and feces as described previously with some modifications (Maddocks et al., 2013). Briefly, 50 mg of wet tissue samples or 30 mg of dry fecal samples were homogenized in 1.5 mL of ice-cold methanol/acetonitrile/H_2O (50/30/20) containing 10 μL of L-norleucine at 1 mg/mL as internal standard. Homogenates were sonicated for 10 sec followed by

incubation at –20°C for 2 h to allow protein precipitation. After centrifugation at 16000 × *g* for 10 min at 4°C, the supernatant was collected and filtered through 0.2 μm PTFE membranes (Millipore). Samples were diluted in an equal volume of acetonitrile before LC-MS analysis. An aliquot (20 μL) from each sample was pooled together as the quality control (QC) sample.

3.2.6 Untargeted metabolomics by UPLC-MS

LC-MS analysis was performed on a Dionex Ultimate 3000 UPLC combined with an Orbitrap MS. Analytes were separated by a zwitterionic SeQuant ZIC-*p*HILIC column (150 × 4.6 mm, 5 μm; Merck, Darmstadt, Germany). The mobile phase consisted of 20 mmol/L of ammonium carbonate for A and acetonitrile for B (Zhang et al., 2014). A linear gradient started from 80% to 40% B in 20 min, followed by a wash at 20% B for 5 min and re-equilibration at 80% B for 10 min with a flow rate of 300 μL/min. The injection volume was 5 μL. The column temperature was 30°C. The column was equilibrated by acetonitrile and four consecutive injections of the QC before the sample injection. The QC was also injected regularly throughout the run to monitor the stability of the platform. MS conditions were as follows: the electrospray ionization was operated in a positive/negative dual polarity mode in the analysis. Acquisition mode: MS full scan; acquisition range: 60–1000 (m/z); heater temperature: 400°C; sheath gas flow rate: 45arb; auxiliary gas flow rate: 10arb; spray voltage: 2.5 kV; capillary temperature: 250°C; resolution: 1.4e5.

3.2.7 MS Data processing

The raw MS spectra data were processed by Compound Discoverer 3.0 (Thermo Scientific) according to the manual. The parameter settings were as follows: the RT error was set to 0.5 min, the m/z error was set to 5 ppm, and the peak identification interface was set to m/z 1.5 (Tian et al., 2022). Online databases (mzCloud, ChemSpider, HMDB, etc.) were used to compare and identify various compounds. Features with no name annotations were filtered out. The names of metabolites obtained from the databases and their abbreviations used in this study are shown in Table 3-2.

3.2.8 RT-qPCR

The method for qPCR was the same as described in Chapter 2 section 2.2.10. The

sequences of primers are listed in Table 3-3.

3.2.9 Co-immunoprecipitation (Co-IP)

Briefly, the nuclear protein from liver tissues was obtained by a nuclear extraction kit (Abcam, Cambridge, UK; ab113474) followed by concentration measurement by a BCA assay. Then, 500 μg of nuclear extracts was pretreated with 15 μL of Pierce Protein A magnetic beads (Thermo Scientific; 88845), diluted in 400 μL of PBS containing protease inhibitor cocktail (Nacalai Tesque), and treated with 2 μg of anti-PPARα antibody (Abcam; ab227074) overnight at 4°C. Nonspecific IgG (Cell Signaling; 2729S) was used as the negative control. The antigen-antibody complex was then incubated with 20 μL of Pierce Protein A magnetic beads for 1 h at room temperature. The immunoprecipitates were washed with a wash buffer (25 mmol/L Tris, 500 mM NaCl, 0.05% Tween-20, pH 7.5) and suspended with 100 μL SDS-PAGE loading buffer at 100°C for 10 min. Finally, 10 μL of the samples were subjected to immunoblotting (IB). Membranes were incubated with the anti-PAR primary antibody (1:1000 dilution; Bio-Techne, Abingdon, UK; 4335-MC-100) overnight at 4°C and an anti-mouse secondary antibody (1:5000; Abcam; ab6789) for 1 h at room temperature.

3.2.10 Western blot analysis

Briefly, 50 μg of nuclear extracts from liver tissues were denatured and loaded on 7.5% or 10% gels. Separated proteins were transferred to PVDF membranes, followed by Ponceau S staining for 5 min, and blocked with Blocking One (Nacalai Tesque) for 1 h. After incubation with primary antibodies [anti-PPARα (1:1000; Abcam; ab227074), anti-PAR (1:1000; Bio-Techne; 4335-MC-100), or anti-PARP1 (1:1000; Cell Signaling; 9542)] at 4°C overnight, membranes were incubated with an anti-rabbit secondary antibody (1:5000; Cell Signaling; 7074) or anti-mouse secondary antibody (1:5000; Abcam; ab6789) for 1 h at room temperature. The signals were visualized using Chemi-Lumi One Super (Nacalai Tesque). The density of the bands was quantified using the ImageJ 1.53a software and normalized with the levels of total protein stained by Ponceau S.

3.2.11 Statistics

Statistical tests were performed using JMP Pro 16 (SAS Institute Inc.). For the

univariate statistical methods, unpaired Student's *t*-test or Mann-Whitney test with a significance level of $P < 0.05$ were used. Outliers were not excluded. Data are presented as box-and-whisker plots, with the box showing the lower, median, and upper quartile values, and the whiskers representing the minimum and maximum values. Volcano plots for differential metabolites were plotted based on the univariate analysis. For the multivariate statistical methods, the orthogonal partial least squares discriminant analysis (OPLS-DA) and heatmap cluster analysis were performed using Metaboanalyst (www.metaboanalyst.ca) (Pang et al., 2022). The variable importance in projection (VIP) scores computed from the OPLS-DA were used to identify the metabolites that made significant contributions to the intergroup differentiation. Association among the metabolites and liver TG was evaluated with multivariate correlation analysis. Pathway enrichment analysis was conducted based on the Kyoto Encyclopedia of Genes and Genomes (KEGG) database. The metabolic correlation network was visualized using the Cytoscape 3.9.1 software (Shannon et al., 2003). A centrality analysis was performed by this software to identify the influential nodes of the network based on the scores of betweenness centrality.

Table 3-1 Diet compositions.

Ingredient (g/kg diet)	Ct	CA
Corn starch [a]	397.5	397.5
Casein [b]	200	200
Dextrin [c]	132	132
Sucrose [d]	100	99.5
Soybean oil [e]	70	70
Cellulose [f]	50	50
Mineral mixture [g]	35	35
Vitamin mixture [g]	10	10
L-Cystine [h]	3	3
Choline hydrogen tartrate [h]	2.5	2.5
Cholic acid [h]	-	0.5

Ct, control diet; CA, cholic acid-supplemented diet.

[a] Amylalpha, Chuo Foods Co., Ltd., Aichi, Japam.

[b] NZMP Acid Casein, Fonterra Co-Operative Group Limited, Auckland, New Zealand.

[c] TK-16, Matsutani Chemical Industry Co., Ltd., Hyogo, Japan.

[d] Nippon Beet Sugar Manufacturing Co.,Ltd., Tokyo, Japan.

[e] J-Oil Mills, Inc., Tokyo, Japan.

[f] Crystalline cellulose, Ceolus PH-102, Asahi Kasei Corp., Tokyo, Japan.

[g] Mineral and vitamin mixtures were prepared according to the AIN-93G formulation.

[h] Fujifilm Wako Pure Chemical Corporation, Osaka, Japan.

Table 3-2 Abbreviations of differential metabolites used in this study.

Abbreviation	Full name given in the databases
Acetamide1	*N*-{3-[(4-Acetamidobutyl)amino]propyl}acetamide
Acetamide2	*N*-(4-Cyanobenzyl)-2-[(1*S*,4*S*,5*S*)-5-isopropyl-4-{[(isopropylcarbamoyl)amino]methyl}-2-methyl-2-cyclohexen-1-yl]acetamide
Diamine	*N*-Ethyl-*N*'-isopropyl-6-(methylsulfinyl)-1,3,5-triazine-2,4-diamine
Ethyl-5*c*8*c*11*c*14*c*17*c*-20:5	Ethyl eicosapentaenoic acid
Gly-Lys	Glycyllysine
GSH	Glutathione (reduced)
GSSG	Glutathione (oxidized)
Lys-Val	Lysylvaline
MG(0:0/22:1(13Z)/0:0)	1,3-Dihydroxy-2-propanyl (13*Z*)-13-docosenoate
NAD^+	Nicotinamide adenine dinucleotide
Pro-Leu	Prolylleucine
Propanamide	*N*1-[4-(aminosulfonyl)phenyl]-2,2-dimethylpropanamide
Pyrimidine-2,4,7-trione	8-methyl-1,3-diphenyl-5-piperidino-1,2,3,4,7,8-hexahydropyrido[2,3-d]pyrimidine-2,4,7-trione
Pyrimidinedione	1-(2-Deoxypentofuranosyl)-5-methyl-2,4(1*H*,3*H*)-pyrimidinedione
4-Hydroxypyrimidine	2-Dimethylamino-5,6-dimethyl-4-hydroxypyrimidine
4*c*7*c*10*c*13*c*16*c*19*c*-22:6	Docosahexaenoic acid
5*c*8*c*11*c*14*c*-20:4	Arachidonic acid
6:0 (6-oxo)	6-Oxohexanoic acid
7*c*10*c*13*c*16*c*-22:4	Adrenic acid
8*c*11*c*14*c*-20:3	Dihomo-γ-linolenic acid
9*t*11*t*-18:2	9,11-Linoleic acid
9*c*11*t*-18:2(13-OH)	13*S*-hydroxyoctadecadienoic acid
9*c*-18:1	Oleic acid
9*c*12*c*-18:2	Linoleic acid
9*t*12*t*-18:2	Linoelaidic acid
9*c*12*c*15*c*-18:3	α-Linolenic acid
9*t*12*t*15*t*-18:3	Linolenelaidic acid
9*c*-16:1	Palmitoleic acid
11*t*-20:1	11*E*-eicosenoic acid
12:0	Lauric acid
14:0	Myristic acid
15:0	Pentadecanoic acid
16:0	Palmitic acid
16:0(16-OH)	16-Hydroxypalmitic acid
17:0	Margaric acid
18:0	Stearic acid
18:0(12-OH)	12-Hydroxystearic acid

Table 3-3 qPCR primer sequences.

Gene	Forward primer (5' to 3')	Reverse primer (5' to 3')
Acadm	CCGCAGAGGCTACAAGGTCC	TCTGGCAAACTTCCGAGCAAT
Acox1	CAGCAGGAGAAATGGATGCG	TCGAAGATGAGTTCCGTGGC
Alpi	ACATCGCCACACAGCTCATT	TCCGACTATCCAGCCTGACT
Cd36	AACTCAGGACCCCAAGGACA	GCTGTTGAGCACACCTTGAA
Cpt1a	CATTCCAGGAGAGTGCCAGG	AGCCTTTGCCGAAAGAGTCA
Fatp4	GCCAACACAGAGCATCTGGA	CAGCCATTCGGTAATACCTGCT
G6pd	GAACGGTGGGATGGAGTACC	GGAAGATGTCACCTGCCACA
Gclc	CCGACCAATGGAGGTACAGT	TGTAAGACGGCATCTCGCTC
Gclm	GCCTGCGGAAAAAGTGTCC	AAACATCTGGAAACTCCCTGACC
Glud	CCAGAGTCAAAGCCAAGATCA	CACTCCTCCAGCATTCAGGT
Gpx1	ATCAGTTCGGACATCAGGAGA	TCACCATTCACCTCGCACTT
Gpx4	AATTCGCAGCCAAGGACATCG	CCAGGATTCGTAAACCACACTCG
Gstk1	CGCATTTGGTCCCGAGATGA	GCTTGCTCTTCACCAGTTCG
Idh1	CAGACTCAGTAGCCCAAGGTTA	CAGCCTCTGCTTCTACCGTC
Idh2	ACAACACCGACGAGTCCATT	AGATGTCCTTGAAACGCCCG
Il1b	TGGCAACTGTCCCTGAACTC	ACACTGCCTTCCTGAAGCTC
mNadk	GCCTGGTAAAGCGGAGAGAG	AAGTGACCTTCAGACCGTTCC
Nadk	CCTTGCTCTATGCCTCCTCAC	AACAGCAGCATTCCCCTCTATC
Nampt	AGGGGCATCTGCTCATTTGG	CACGCTGTTATGGTACTGTGC
Nnt	CAGGTTCCGAGGGTGACAAT	ACCAACTATCAGGATCTTCGCTG
Nox2	GTTCCAGTGCGTGTTGCTC	GCATTCACACACCACTCCAC
Nox4	TCCATCAAGCCAAGATTCTGAG	GGTTTCCAGTCATCCAGTAGAG
Nrf1	GACACGGTTGCTTCGGAAAC	CATTCTCCAAAGGTGCTGCG
Nrf2	TCAGAGCAAGTGACGAGATGG	CCGAAATGTTGAGTGTGGTGAG
Parp1	TATGCCAAGTCCAACAGGAGC	CAGCGGTCAATCATACCCAGT
Pgc1a	AAATCTGCGGGATGATGGAGAC	CAGGGTCAAAATCGTCTGAGT
Pgc1b	CGGTGAAGGTCGTGTGGTAT	TGCGTTTTCTCAGGGTAGCG
Ppara	CTCGGAGGGCTCTGTCATCA	TTGCCAGGGGACTCATCTGT
Sirt1	GCAAAGGAGCAGATTAGTAAGCG	GGAACTAGAGGATAAGGCGTCA
Tfam	GGGGCGTGCTAAGAACACT	TACAGATAAGGCTGACAGGCG
Tnfa	TTCTCATTCCTGCTCGTGGC	AACTGATGAGAGGGAGCCCA
Rplp0	GGCAAGAACACCATGATGCG	GTGATGCCCAAAGCTTGGAA

3.3 Results

3.3.1 CA diet altered BA profiles and induced hepatic lipid accumulation in rats

It was confirmed that hepatic steatosis was induced by CA diet for 12 weeks accompanied by altered BA profiles such as a marked increase in the levels of 12αOH BAs in liver tissues, cecal contents, and feces (Figure 3-1A-D) as shown in the previous report (Lee et al., 2020). TCA and TDCA increased significantly in liver tissues of the rats upon CA diet (Figure 3-1A). DCA predominated in cecal contents and feces (Figure 3-1B, C). The levels of non-12OH BAs increased moderately in cecal contents and feces. CA diet induced accumulation of liver TG and FFA without inflammation and tended to increase liver ATP level (Figure 3-1D). No difference was observed in final body weight, total food intake (data not shown), and fecal energy excretion between the groups (Figure 3-1E). CA diet did not alter fecal TG excretion but significantly decreased FFA excretion (Figure 3-1E).

3.3.2 Metabolic alterations in the gut–liver axis of CA-fed rats

Untargeted metabolomics was performed to investigate the gut and liver's metabolic responses to CA. There was a clear difference in OPLS-DA plot of the fecal metabolites between the rats fed Ct and CA diet (Figure 3-2A). In the feces, 153 metabolites were detected and annotated and levels of 69 metabolites were significantly different among them ($P < 0.05$, Figure 3-2B). Almost all the metabolites with VIP score >1, which indicates contributions to the group separation in the OPLS-DA model, were significantly different between the groups (Figure 3-2C). The metabolites with a significant difference were subjected to a heatmap cluster (Figure 3-2D). A clear separation was found between the groups based on the compositional difference in the metabolites. Moreover, a significant enrichment of cluster 1 metabolites in the CA-fed rats was observed. The majority of cluster 1 metabolites such as aromatic amino acids (AAAs), amines, steroids, and benzenoids, were positively associated with liver TG (Figure 3-2D, E). In contrast, levels of the metabolites in cluster 2 decreased in the CA-fed rats and correlated to liver TG negatively. The cluster 2 metabolites included fatty acids, pyrimidine derivatives, purine derivatives, and histamine metabolites (Figure 3-2D, F).

There was a clear separation in OPLS-DA plot of the hepatic metabolites between the groups (Figure 3-3A). Alteration of metabolites was found in 30 out of 162 metabolites in the CA-fed rats (Figure 3-3B). Both the number and the average fold-change magnitude of differential metabolites in the liver were less than that in their fecal counterparts (Figure 3-3C). Combined VIP scores with *P* values were used for the selection of the variable metabolites (Thévenot et al., 2015). The levels of hepatic metabolites that contributed to the group separation in the OPLS-DA model were not necessarily significantly different between the groups (Figure 3-3D). Metabolites with significant difference ($P < 0.05$) and trends of difference ($0.05 < P < 0.1$ and VIP > 1) were selected for heatmap in the cluster analysis (Figure 3-3E). These metabolites were mainly involved in several metabolic pathways, such as nicotinate and nicotinamide metabolism, glutathione metabolism, aminoacyl-tRNA biosynthesis, pantothenate and CoA biosynthesis, branched-chain amino acids (BCAAs), and histidine metabolism (Figure 3-3F). No significant differences were found in the Krebs cycle intermediates.

A subtle difference was observed in the cecal and fecal concentrations of organic acids in the CA-fed rats (Figure 3-4A, B). In addition, few metabolites changed significantly in the ileal mucosa by the CA diet intervention (Figure 3-5).

3.3.3 Alteration of NAD^+-related metabolites and poly(ADP-ribosyl)ation of PPARα in the liver of CA-fed rats

The CA diet altered the balance of NAD^+-related molecules in the liver (Figure 3-6A) and raised the hepatic levels of nicotinamide and nicotinic acid. The ratio of NADH/NAD^+ was quantified with a colorimetric assay and was decreased in the CA-fed rats. Nicotinamide is not only the main precursor of NAD^+ but also a product of deacetylation and poly(ADP-ribosyl)ation (Garten et al., 2015). The mRNA expressions of the enzymes that participate in the NAD^+-related pathways were analyzed. The CA diet did not affect the expression of *Nampt*, the rate-limiting enzyme required for NAD^+ synthesis (Figure 3-6B) (Garten et al., 2015). *Sirt1*, an NAD^+-dependent deacetylase (Garten et al., 2015), was not affected by CA diet. PARP1 is responsible for ADP-ribosylation of several target proteins (Garten et al., 2015), and the expression levels in mRNA and protein were elevated by the CA diet (Figure 3-6B,

F).

Furthermore, as identified by metabolomics, the CA diet significantly elevated the levels of two essential fatty acids including linoleic acid and α-linolenic acid (Figure 3-6C). No significant difference was detected for other fatty acids (data not shown). In the liver, the gene expression of *Cd36* which is responsible for lipid uptake (Rada et al., 2020) remained unchanged (Figure 3-6D). Decreases were observed in the hepatic expressions of the genes involved in fatty acid oxidation including *Ppara*, *Cpt1a*, and *Acox1* in the CA-fed rats (Figure 3-6D). A significant negative correlation was observed between hepatic linoleic acid and *Cpt1a* (Figure 3-6E). An increase in poly(ADP-ribosyl)ation of PPARα was detected using Co-IP in the CA diet-fed rats (Figure 3-6F). Moreover, the hepatic concentration of TDCA positively correlated with *Parp1* expression (Figure 3-6G). The concentrations of TDCA and TCA negatively correlated *Ppara* expression (Figure 3-6H).

Little change was observed in the expressions of fatty acid transporters in the small intestine, except for an increase in *Fatp4* in the ileum (Figure 3-7A, B). The levels of linoleic acid in the jejunum and ileum did not differ between the groups, while some moderate increases were observed in other fatty acids such as palmitic acid, stearic acid, and palmitoleic acid in the jejunum of the CA-fed rats (Figure 3-7C, D).

3.3.4 CA diet stimulates the pentose-phosphate pathway to produce reducing equivalents, protecting the liver against oxidative stress

It was further determined whether the CA diet affects other redox couples in the liver. The total level of NADP(H) remained unchanged, whereas both increase and decrease were observed in the oxidized form and the reduced form, respectively (Figure 3-8A). Thus, a decreased ratio of NADPH/$NADP^+$ was observed under the CA diet feeding. The pentose phosphate pathway (PPP) is involved in glucose oxidation that supplies cytosolic NADPH (Xiao et al., 2018). CA diet increased the level of sedoheptulose 7-phosphate (S-7-P), a PPP intermediate (Figure 3-8B). Consistently, the enzyme activity of G6PD, the key enzyme in the PPP (Xiao et al., 2018), increased in the CA-fed rats (Figure 3-8B). Significant changes were observed in the gene expressions of enzymes involved in the regulation of NADP(H) balance between the groups (Figure 3-8C). The

expressions of *Me3* and *Nnt* that catalyze the reduction of $NADP^+$ to NADPH in the mitochondria (Xiao et al., 2018) were decreased in the rats fed the CA diet. By contrast, the expressions of isocitrate-α-ketoglutarate shuttle-related genes that provide NADPH from the cytosol to mitochondria (Xiao et al., 2018) were increased in the CA-fed rats. Significant correlations were found among hepatic TDCA, TCA and some NADP(H)-related parameters (Figure 3-8D).

Moreover, an alteration was identified in the balance of glutathione/glutathione disulfide (GSH/GSSG) in the liver (Figure 3-8E). The reduced form increased, and the oxidized form decreased significantly in the CA-fed rats, resulting in a marked increase in the GSH/GSSG ratio. No differences were found in the key genes encoding GSH synthesis regardless of a significant decrease in the levels of some GSH precursors including serine and glycine in the CA-fed rats (Figure 3-8F, G). NADPH can be either used as a coenzyme for GSH recycling or as a substrate for NADPH oxidases (NOXs) to generate reactive oxygen species (Xiao et al., 2018). CA diet significantly increased the mRNA levels of *Nox4* without affecting *Nox2* (Figure 3-8H). The hepatic level of malondialdehyde (MDA), a marker of lipid peroxidation (Chen et al., 2020), remained unchanged (Figure 3-8H). The level of *Gpx1*, which catalyzes the clearance of reactive oxygen species using GSH as an electron donor (Xiao et al., 2018), was significantly increased in the CA-fed rats (Figure 3-8I). A similar change was found in another antioxidant enzyme *Gstk1*. No difference was found in *Gpx4*. In addition, a subtle difference was observed in gene expressions with regard to mitochondrial biogenesis (Figure 3-8J).

3.3.5 Significance of DCA and the taurine-conjugate in the liver lipid accumulation in the CA-fed rats

Multivariate correlation analysis was carried out to investigate the relationships between the fecal and hepatic differential metabolites. Negative and positive correlations were observed in the levels of 343 pairs of fecal-hepatic metabolites and that of 345 pairs, respectively (Figure 3-9A). An integrative metabolic network was visualized based on the significant correlations among the fecal metabolites, hepatic metabolites, and liver TG using the Cytoscape software. A centrality analysis of the

network was conducted and hepatic TDCA, nicotinamide, and guanidinoethyl sulfonate were identified as the most prominent metabolites in relation to liver TG (Figure 3-9B). Although TCA was highly abundant in the liver, TDCA associated with the levels of NAD^+ and nicotinamide (Figure 3-9C). Moreover, fecal DCA exhibited significant associations with many fecal metabolites (Figure 3-9D). The association between hepatic TDCA and fecal metabolites was highly consistent with that of fecal DCA and fecal metabolites.

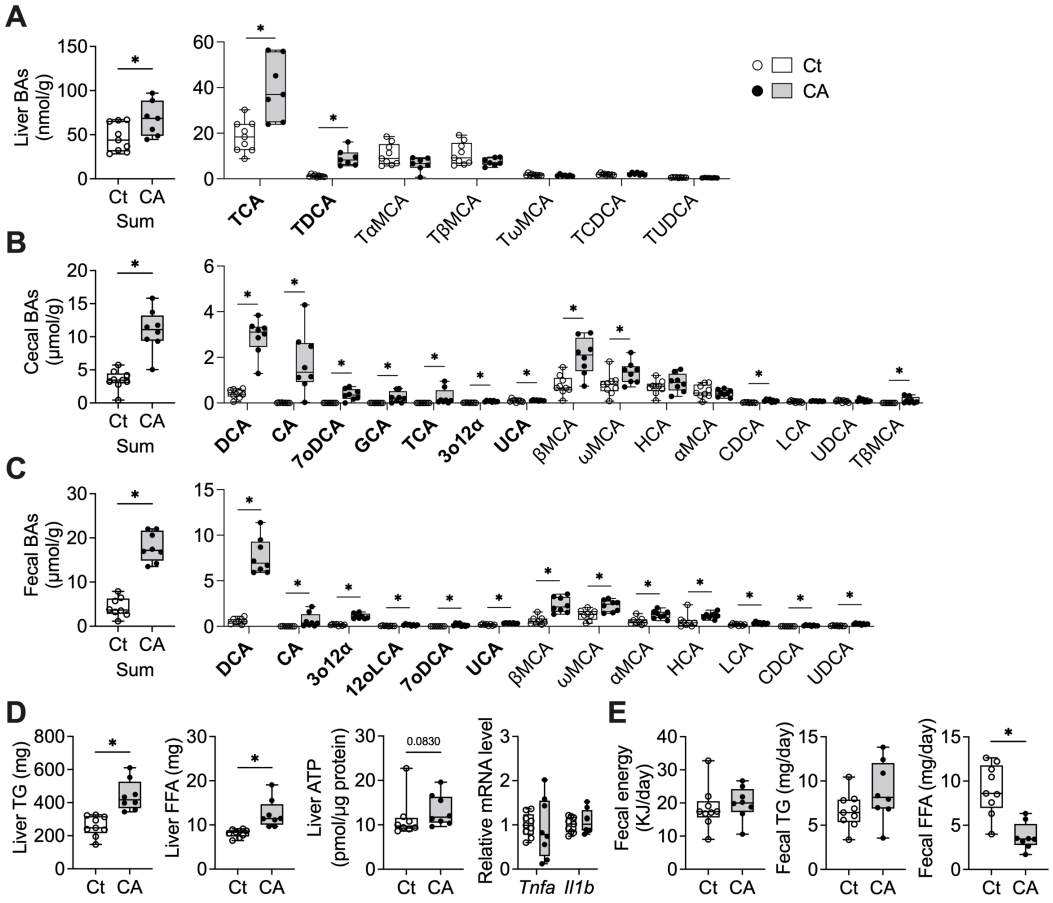

Figure 3-1 Cholic acid (CA) diet for 12 weeks altered the bile acid (BA) profiles and induced hepatic steatosis in rats. Levels of sum and individual BAs in liver tissues **(A)**, cecal contents **(B)**, and feces **(C)** in control (Ct) and the CA-fed rats. The name of the 12α-hydroxylated BAs (bold font) and non-12-hydroxylated BAs (plain font) were shown. BAs that account for less than 1% of the sum are not shown. Measured BAs were shown in Table 2-2. **(D)** Hepatic levels of triacylglycerol (TG), free fatty acid (FFA), adenosine triphosphate (ATP), and genes encoding pro-inflammatory cytokines. **(E)** Fecal excretion of energy, TG, and FFA. Asterisks indicate the significant difference between the groups ($P < 0.05$, Student's *t*-test or Mann-Whitney test).

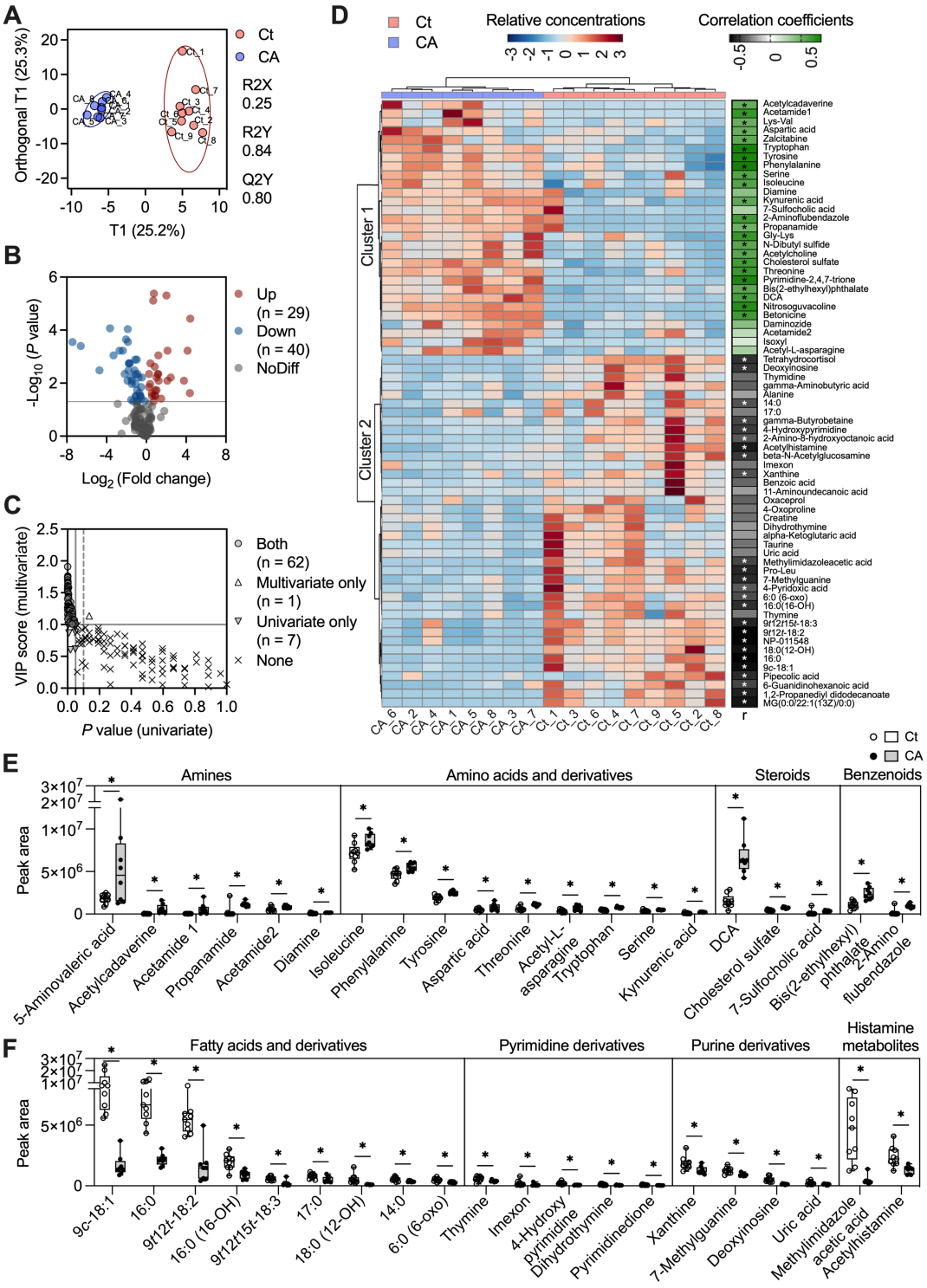

Figure 3-2 Alterations in fecal metabolome in rats fed the cholic acid (CA) or control (Ct) diet for 12 weeks. (A) The orthogonal partial least squares discriminant analysis (OPLS-DA) plot shows the overall differences in the fecal metabolome between Ct and the CA-fed rats based on all the annotated metabolites. Each symbol represents an individual sample; circles represent 95% confidence intervals. **(B)** Metabolites with a significant difference were presented in a volcano plot ($P < 0.05$, Mann−Whitney test). Colored symbols (red and blue) represent metabolites with

significant differences between the groups. The horizontal line shows the threshold (P = 0.05). **(C)** Selection of metabolites of interest based on the univariate P values and multivariate variable VIP scores. The vertical and horizontal lines indicate thresholds (P = 0.05 and VIP = 1, respectively). The dashed vertical line shows the P = 0.1 threshold. Metabolites selected using both the univariate and multivariate approaches (i.e., those in the $P < 0.05$ and VIP > 1 region) were displayed as circles. Metabolites selected by only one of the approaches were displayed as triangles. **(D)** Heatmap and cluster of the metabolites with a significant difference ($P < 0.05$). The green and grey gradient colors represent positive and negative correlations with hepatic TG levels, respectively. Asterisks show a significant correlation ($P < 0.05$, multivariate correlation analysis). **(E)** Metabolites that were enriched in the feces of the CA-fed rats. **(F)** Metabolites that were reduced in the feces of the CA-fed rats. Data are expressed using box-and-whisker plots. Asterisk indicates the significant differences between the two groups ($P < 0.05$, Mann-Whitney test). Abbreviations of the metabolites are listed in Table 3-2.

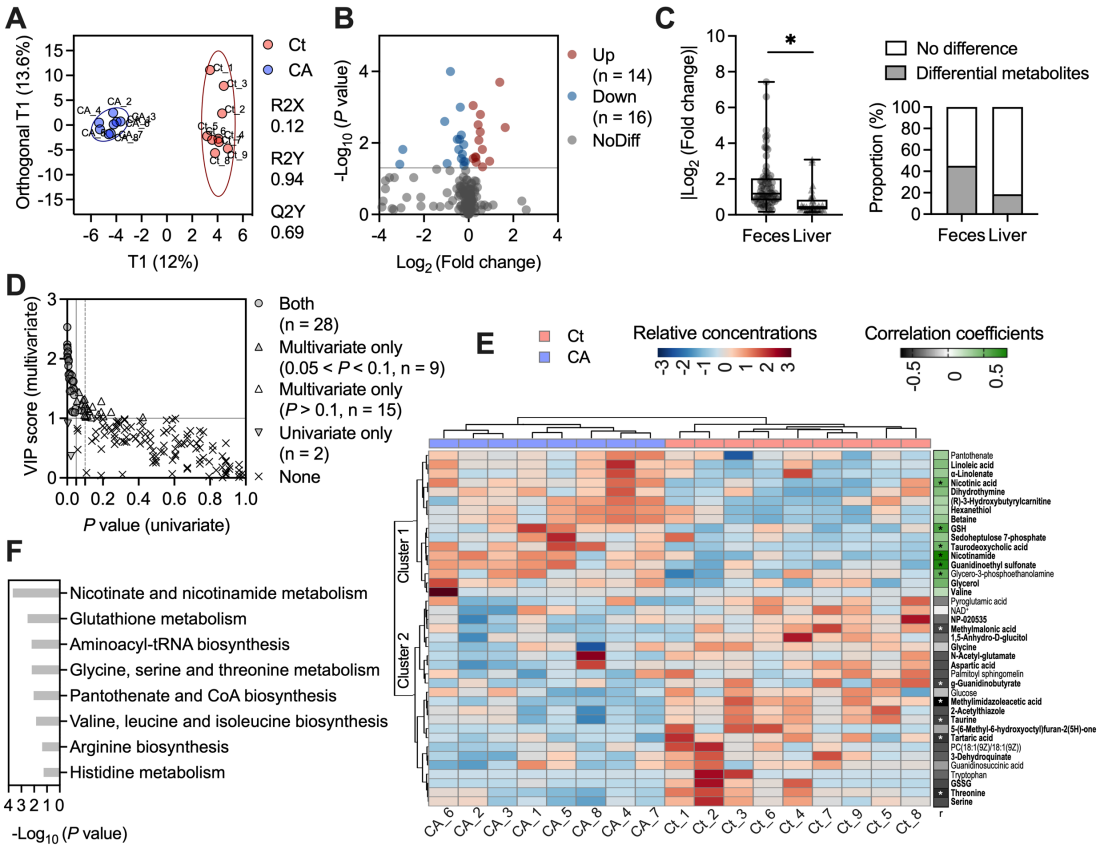

Figure 3-3 Alterations in liver metabolome in rats fed the CA or Ct diet for 12 weeks. (A) The OPLS-DA plot shows the overall differences in the liver metabolome between Ct and the CA-fed rats based on the annotated metabolites. Each symbol represents an individual sample; circles represent 95% confidence intervals. **(B)** Metabolites with a significant difference were presented in a volcano plot ($P < 0.05$, Mann−Whitney test). Colored symbols (red and blue) represent metabolites with significant differences between the groups. The horizontal line shows the threshold ($P = 0.05$). **(C)** Comparison of the proportion and fold-change of the metabolites in feces and liver. The absolute values of $\log_2$ (fold change) for the metabolites in the feces and liver. Asterisk indicates the significant differences between feces and liver ($P < 0.05$, Mann-Whitney test). The proportion of metabolites with a significant difference between the groups in feces and liver. (**D**) Selection of metabolites of interest based on the univariate *P* values and multivariate variable VIP scores. The vertical and horizontal lines indicate thresholds ($P = 0.05$ and VIP = 1, respectively). The dashed vertical line shows the $P = 0.1$ threshold. Metabolites selected using both the univariate and multivariate approaches (i.e., those in the $P < 0.05$ and VIP > 1 region) were displayed as circles. Metabolites selected by only one of the approaches were displayed as triangles. **(E)** Heatmap and cluster of the metabolites with a significant difference ($P < 0.05$). The green and grey gradient colors represent positive and negative correlations with hepatic TG levels, respectively. Asterisks show a significant correlation ($P < 0.05$, multivariate correlation analysis). **(F)** Pathway enrichment analysis of metabolites with significant differences according to the KEGG pathway. See Table 3-2 for the abbreviations used.

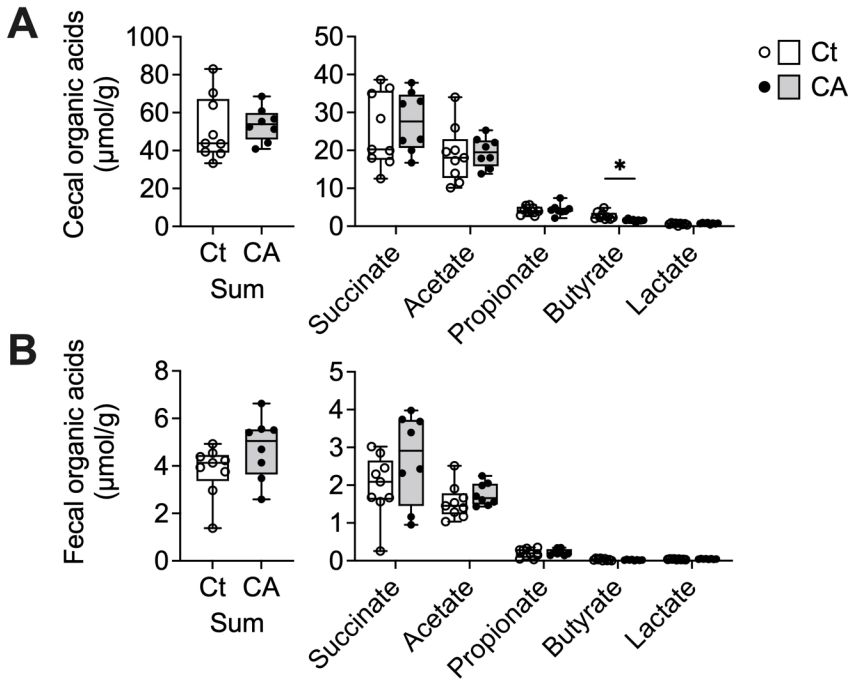

Figure 3-4 Organic acid concentrations in the cecal contents and feces in rats fed the CA or Ct diet for 12 weeks. (A) The levels of total and individual organic acids in cecal contents. **(B)** The levels of total and individual organic acids excreted in feces. Data were expressed using box-and-whisker plots. Asterisk indicates the significant differences between the groups ($P < 0.05$, Student's *t*-test).

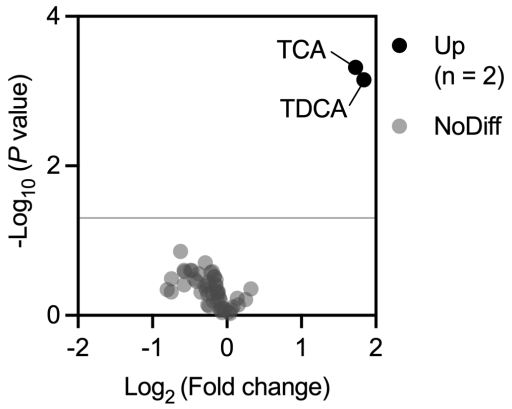

Figure 3-5 Alterations in metabolome in the ileal mucosa in rats fed the CA or Ct diet for 12 weeks. Metabolites with a significant difference were presented in a volcano plot ($P < 0.05$, Mann−Whitney test). The horizontal line shows the threshold ($P = 0.05$).

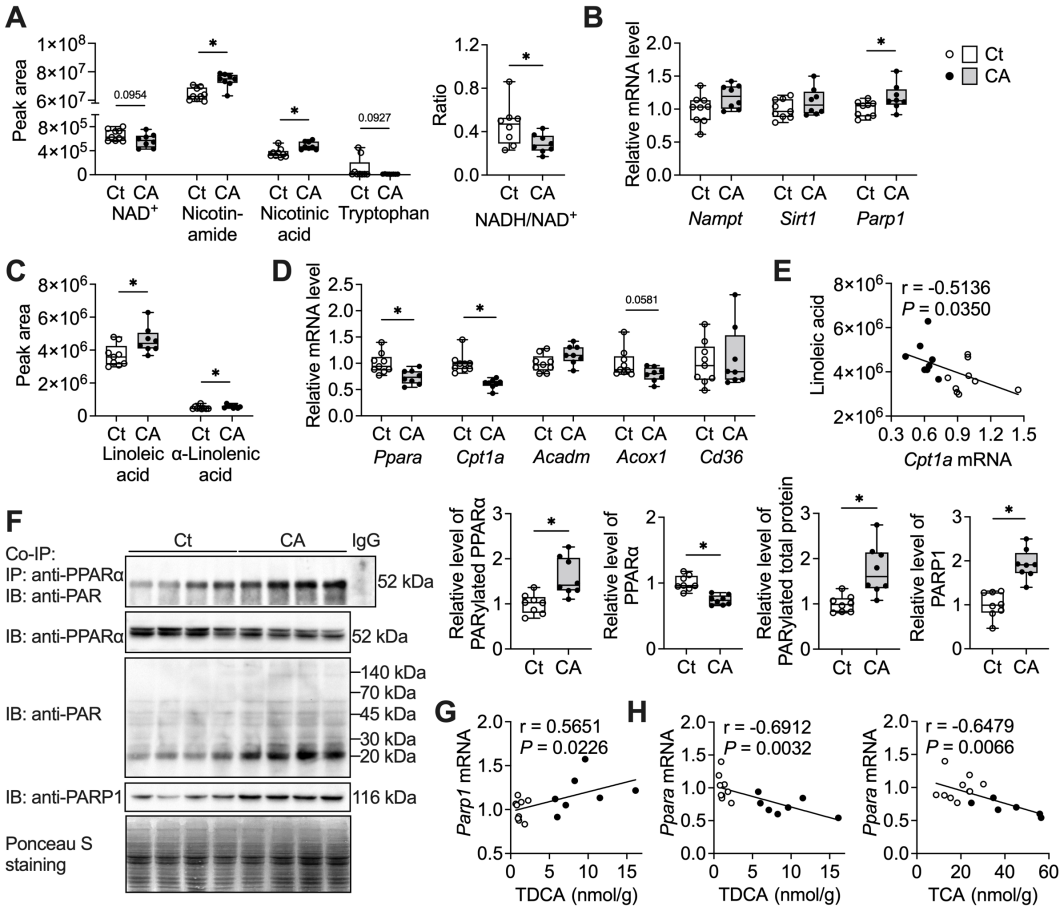

Figure 3-6 Promotion of NAD$^+$ consumption by activating PARP1 and enhancement of poly(ADP-ribosyl)ation of PPARα in the liver of the CA-fed rats. **(A)** Hepatic levels of NAD$^+$-related metabolites detected by untargeted metabolomics. The ratio of NADH/NAD$^+$ was quantified using a colorimetric assay. Asterisks indicate a significant difference between the groups ($P < 0.05$, Student's *t*-test or Mann-Whitney test). **(B)** Hepatic mRNA expression of genes involved in NAD$^+$ metabolism. **(C)** Hepatic levels of linoleic acid and α-linolenic acid detected by untargeted metabolomics. **(D)** Hepatic mRNA expression of genes encoding fatty acid oxidation and transport. **(E)** Pearson's correlation between the hepatic level of linoleic acid and *Cpt1a* expression. **(F)** Poly(ADP-ribosyl)ation level of PPARα was analyzed by co-immunoprecipitation in nuclear extracts from the liver. The levels of PPARα, PAR, and PARP1 were determined using immunoblotting. Relative quantification of the density of the bands was performed using ImageJ after normalization with Ponceau S staining. **(G)** Pearson's correlation between hepatic levels of TDCA and *Parp1*. **(H)** Pearson's correlation between hepatic BA levels and *Ppara* expression. *Acox1*, acyl-CoA oxidase 1; *Acadm*, medium-chain acyl-coenzyme A dehydrogenase; *Cd36*, cluster of differentiation 36; *Cpt1a*, carnitine palmitoyltransferase 1A; NAD(H), nicotinamide adenine dinucleotide; *Nampt*, nicotinamide phosphoribosyltransferase; PAR: ADP-ribose polymers; *Parp1*, poly(ADP-ribose) polymerase 1; *Ppara*, peroxisome proliferator-activated receptor α; *Sirt1*, sirtuin 1.

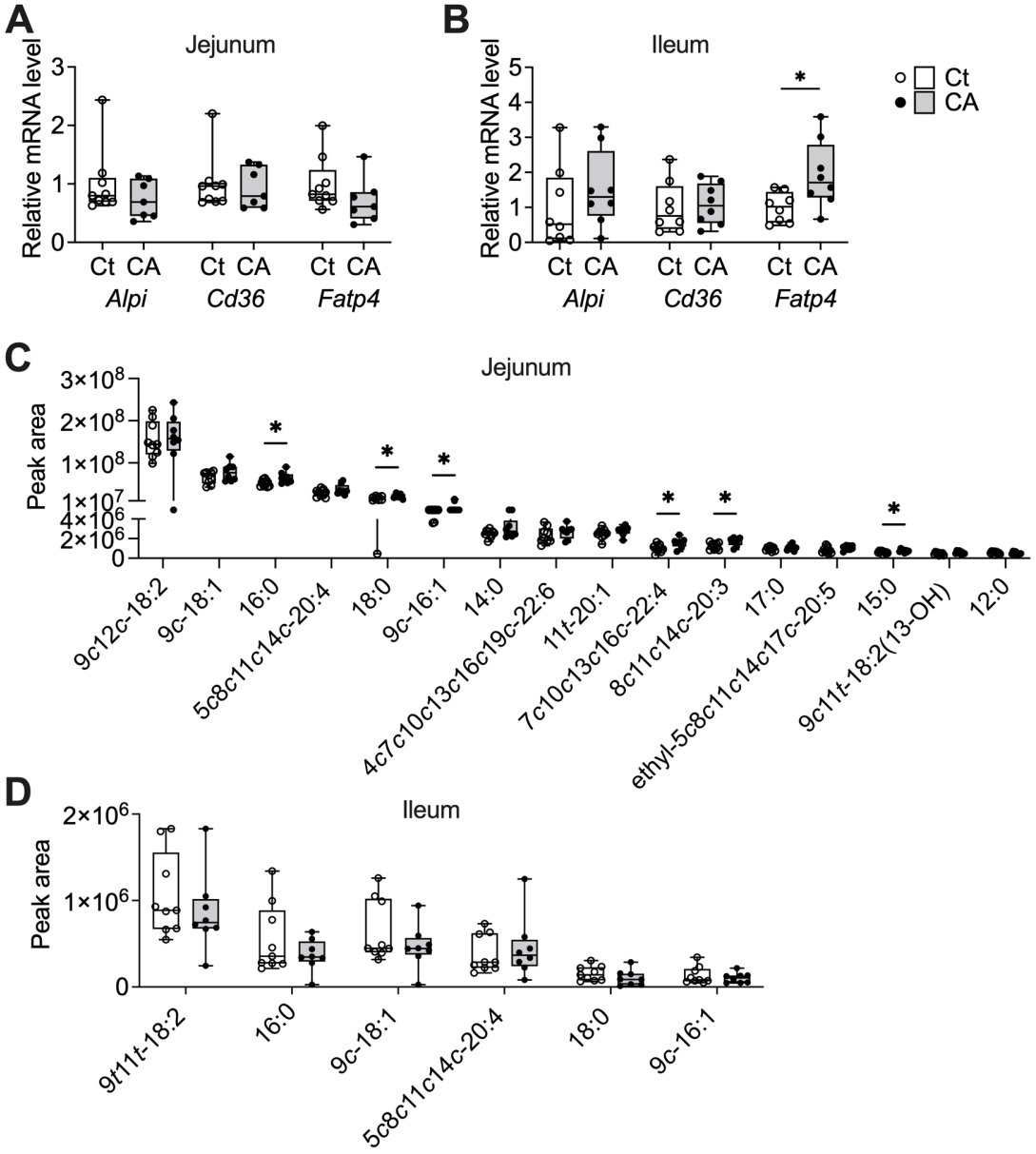

Figure 3-7 The levels of fatty acids and gene expressions in relation to fatty acid transport in the small intestinal mucosa. The mRNA expression of genes encoding fatty acid transporters in the jejunal (A) and ileal (B) mucosa. Levels of fatty acids in the jejunal (C) and ileal (D) mucosa detected by untargeted metabolomics. Data are expressed using box-and-whisker plots ($P < 0.05$, Student's t-test). Abbreviations of the metabolites are listed in Table 3-2. *Alpi*, alkaline phosphatase intestinal; *Cd36*, cluster of differentiation 36; *Fatp4*, fatty acid transport protein 4.

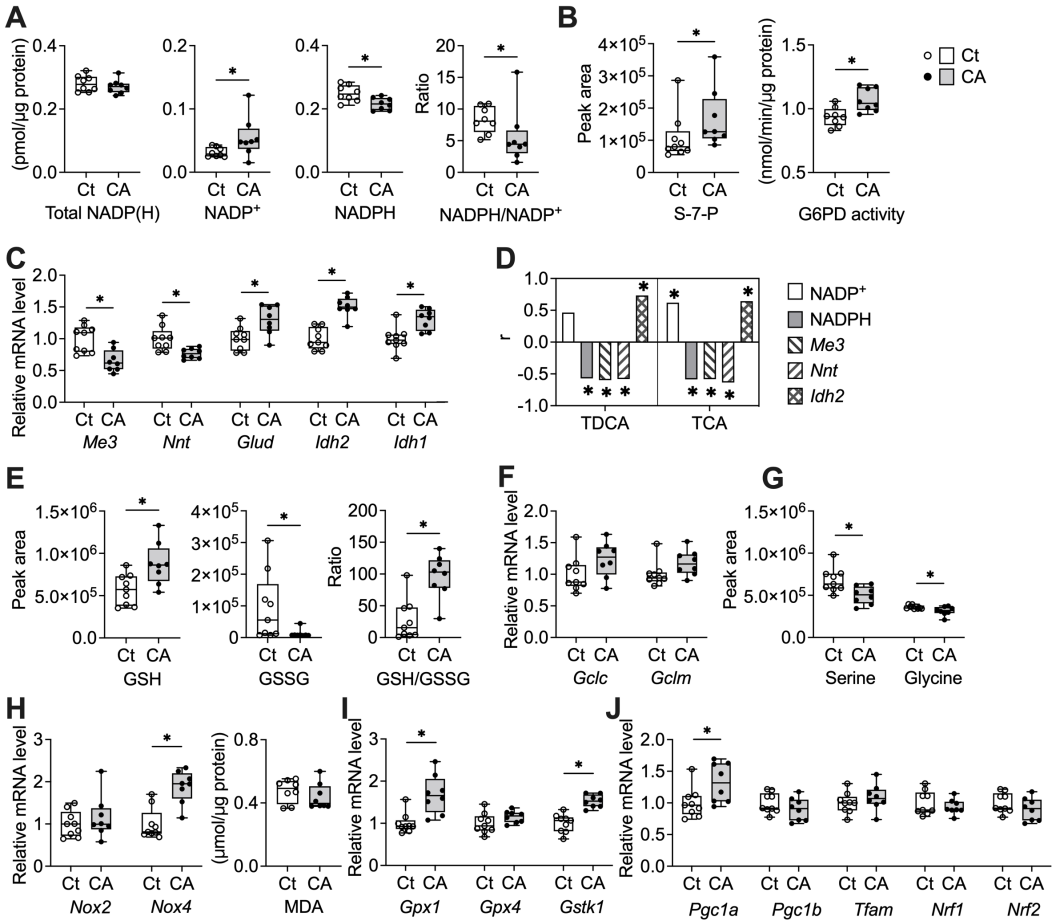

Figure 3-8 Comparison of molecules involved in NADP(H) metabolism and pentose-phosphate pathway. (A) Levels and ratios of NADP(H) in the liver. Values were quantified using a colorimetric assay. Asterisks indicate a significant difference between the groups ($P < 0.05$, Student's *t*-test or Mann-Whitney test). **(B)** The level of S-7-P detected by untargeted metabolomics. G6PD activity in the liver was quantified with a colorimetric assay. **(C)** The expression of genes involved in NADP(H) formation in the liver. **(D)** Pearson's correlation among hepatic TDCA, TCA, and some NADP(H) related parameters. **(E)** Levels and ratios of GSH and GSSG in the liver measured with untargeted metabolomics. **(F)** The expression of genes encoding the synthesis of GSH. **(G)** Levels of serine and glycine in the liver measured with untargeted metabolomics. **(H)** The expressions of NADPH oxidases and MDA levels. MDA level was determined with a fluorometric assay. **(I)** The expression of genes encoding antioxidant enzymes. **(J)** Hepatic mRNA expression of genes regulating mitochondrial biogenesis. G6PD, glucose-6-phosphate dehydrogenase; *Gclc*, glutamate-cysteine ligase catalytic subunit; *Gclm*, glutamate-cysteine ligase modifier subunit; *Glud*, glutamate dehydrogenase; *Gpx*, GSH peroxidase; GSH, glutathione; GSSG, glutathione disulfide; *Gstk1*, GSH S-transferase κ1; *Idh*, isocitrate dehydrogenase; MDA, malondialdehyde; *Nadk*, NAD^+ kinase; *mNadk*, mitochondrial *Nadk*; NADP(H), nicotinamide adenine dinucleotide phosphate; *Nnt*, nicotinamide nucleotide transhydrogenase; *Nox*, NADPH oxidase; *Nrf*, nuclear respiratory factor; *Pgc1a*, PPARγ coactivator 1α; *Pgc1b*, PPARγ coactivator 1β; S-7-P, sedoheptulose 7-phosphate; *Tfam*, mitochondria transcription factor A.

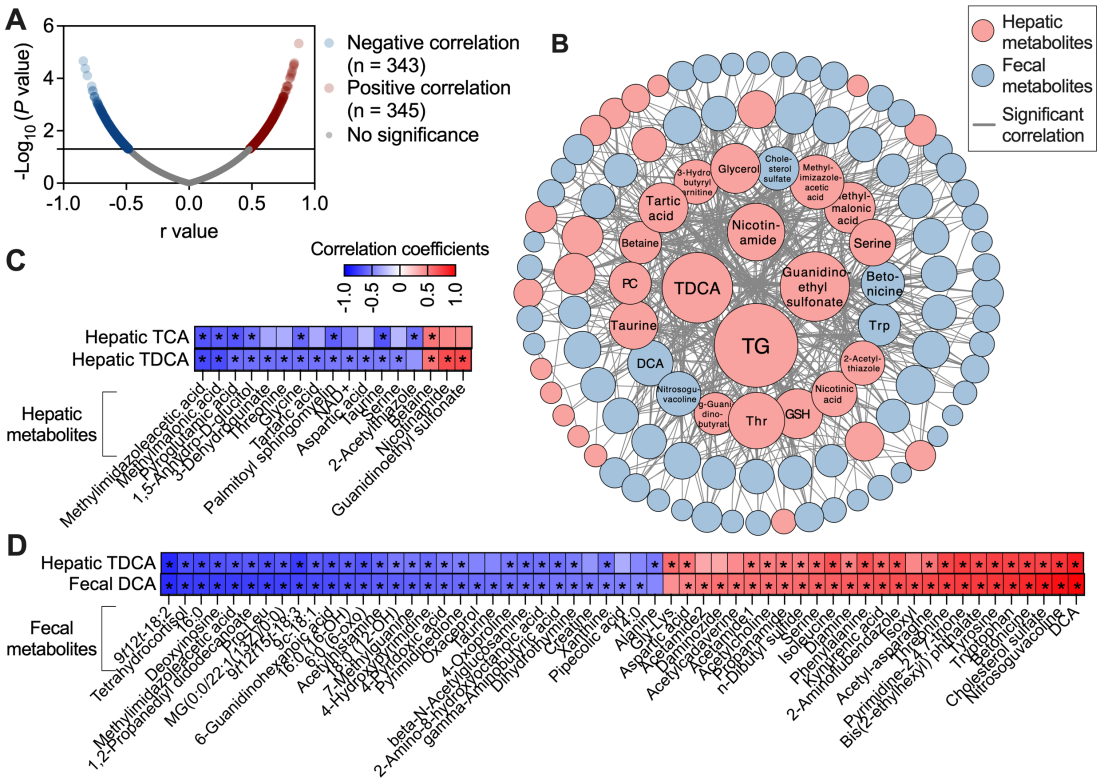

Figure 3-9 Correlation network of the fecal and hepatic metabolites in response to the CA diet. (A) Distribution of correlation coefficients between fecal and hepatic metabolites with a significant difference between the groups. Red and blue symbols represent metabolites with a significant correlation. The horizontal line shows the threshold (P = 0.05, multivariate correlation analysis). **(B)** Metabolic correlation network of TG and differential metabolites. The nodes in red and blue represent metabolites with a significant difference in the liver and feces, respectively. Significant correlation was linked with a line between the metabolites. The node size indicates proportional to the betweenness centrality. **(C)** Significant correlations between selected BAs and the hepatic metabolites. **(D)** Significant correlations between selected BAs and the fecal metabolites. Asterisks indicate a significant correlation (P = 0.05). See Table 3-2 for the abbreviations used.

3.4 Discussion

The present study focused on the gut and liver metabolic responses to 12αOH BAs and their relevance to hepatic TG accumulation. These data demonstrated changes in gut microbial metabolites, suppression of the hepatic fatty acid β-oxidation, and alteration of redox state in the liver of rats fed the CA-diet. The microbial product DCA and its liver counterpart TDCA were highlighted as central players in these metabolic alterations.

DCA migrated to the liver via the portal circulation was possibly conjugated with taurine to form TDCA (Figure 3-1). Such BA signature under the CA diet shared great similarities to the BA profiles under a high-fat diet (Hori et al., 2020; Yoshitsugu et al., 2019). The CA diet model provides evidence that 12αOH BAs play a primary role in metabolic alteration associated with hepatic lipid accumulation. An interesting finding was that the CA diet-fed rats exhibited a distinct microbial metabolome (Figure 3-2) that highly associated with DCA and its hepatic counterpart TDCA (Figure 3-9). DCA exerts a growth inhibition effect in some bacterial populations such as *Lactobacilli* and *Bifidobacterium* (Kurdi et al., 2006). In a recent study in which the rats were fed the same dose of CA for 13 weeks, an abundance of DCA was accompanied by decreased microbial diversity and an increase in the relative abundance of phyla *Firmicutes* and a proportional decrease in *Bacteroidetes* in the cecal contents (Lee et al., 2020). It is reasonable to assume that DCA drives changes in gut microbiota that is enriched with DCA-tolerant taxa.

The outcome of this DCA stress on microbial metabolome was featured as the depletion of fatty acids and enrichment in amino acids and amines (Figure 3-2). A previous study reported that some lipophilic gut bacteria such as *Alistipes* spp., *Bilophila* spp., and members of *Proteobacteria* are capable to degrade fatty acids and generate energy under anaerobic conditions (Agans et al., 2018). These gut microbes are found to increase on high-fat diets (Daniel et al., 2014; Schneeberger et al., 2015). Increased levels of various amino acids, especially AAAs and BCAAs suggested an imbalance of BCAAs and AAAs metabolism by DCA. Gut microbes synthesize amines from some amino acids such as ornithine, arginine, and lysine

through decarboxylation (Michael, 2016). Metabolites of cadaverine, a lysine derivative, increased markedly which could be attributed to an alteration of gut bacterial metabolism (Noack et al., 1998). In the present study, fatty acids and amino acids were possibly utilized by gut microbes as energy substrates to sustain growth in response to the DCA stress.

Moreover, the correlations between microbial metabolites and liver TG (Figure 3-2) suggest the associations of a change in microbial metabolism with host liver lipid metabolism. Similar microbiological signatures have been observed in people with obesity and fatty liver diseases and are associated with enhanced energy harvest from the diet (Mouzaki et al., 2013; Turnbaugh et al., 2006). Despite no apparent gain in dietary energy in the CA-fed rats, fecal metabolome suggests an alteration in microbial processing of dietary lipids and proteins. A previous study reported that conventional mice fed with a high-fat diet excrete less fecal lipids than that of the germ-free mice fed with the same diet, which contributes to a higher food efficiency and liver TG content (Rabot et al., 2010). Increased gut bacterial biosynthetic potential for AAAs and BCAAs is linked with hepatic steatosis in humans (Hoyles et al., 2018). This study highlights the contribution of DCA to a microbial metabolic phenotype featured as elevated AAAs and BCAAs metabolism that is associated with steatosis.

Notably, TDCA significantly correlated with NAD^+ and nicotinamide in the liver (Figure 3-9). This suggested that DCA taurine conjugate TDCA affects hepatic metabolism. Inverse correlations between NAD^+-consuming genes and those involved in β-oxidation have been previously found in the liver from human cohorts (Gariani et al., 2016). Hepatic depletion of NAD^+ in mice fed a western diet contributes to steatosis which is alleviated by NAD^+ repletion (Gariani et al., 2016). Considering that nicotinate and nicotinamide metabolism was the top pathway altered in the liver of the CA-fed rats (Figure 3-3), the importance was highlighted of NAD^+ and β-oxidation in hepatic steatosis. Mechanistically, PARP1 was activated under the CA diet, which resulted in NAD^+ consumption and ADP-ribosylation of PPARα that suppressed its downstream transcripts linked to fatty acid oxidation (Figure 3-6). PARPs in an inactive form in the nucleus are activated by DNA damage (Schreiber et al., 2006). PARP1 is activated both

in mice challenged with a high-fat diet and in human NAFLD (Huang et al., 2017). PARP1 activation impairs PPARα signaling, which plays an important role in oxidative stress-induced lipid accumulation in hepatocytes (Huang et al., 2017). In the present study, PARP1 was activated even in the absence of significant changes in the oxidative stress marker MDA (Figure 3-8). Considering that TDCA positively correlated with *Parp1* (Figure 3-6), constant and higher levels of DCA delivered to the liver are responsible for the PARP activation.

The incorporation of long-chain fatty acids in the mitochondria for oxidation relies on carnitine palmitoyl transferase 1a (CPT1a) (Kersten and Stienstra, 2017). The inverse correlation between linoleic acid and *Cpt1a* in the liver (Figure 3-6) suggested a link between hepatic FFA accumulation and impaired β-oxidation under the CA diet. The induction of fatty acid oxidation depends on PPARα (Kersten and Stienstra, 2017). In human NAFLD, reduction in hepatic fatty acid oxidation is accompanied by a decreased PPARα expression (Croci et al., 2013; Francque et al., 2015). Marked increases in hepatic TDCA and TCA are found in subjects with NAFLD (Lake et al., 2013). Some studies demonstrate that CA and TCA antagonize PPARα (Chen et al., 2022; Sinal et al., 2001). In this study, TDCA and TCA inversely correlated with *Ppara* (Figure 3-6), suggesting that increased levels of 12αOH BAs decreased PPARα expression. Altogether, an abundance in 12αOH BAs activates PARP1, which impairs PPARα signaling and thus may decrease fatty acid oxidation.

CA diet-induced steatosis might involve *de novo* lipogenesis. We reported an elevated expression of sterol regulatory element-binding protein 1 (*Srebp1*), a key lipogenic transcription factor, by the CA diet (Lee et al., 2020). This is supported by a decreased ratio of NADPH/$NADP^+$ under CA diet (Figure 3-8). In this condition, the ATP levels slightly increased (Figure 3-1), possibly to meet the demand for biosynthesis. As NADPH is indispensable for reductive anabolism, the underlying mechanism may involve an increased flux of metabolic fuels into PPP to produce cytosolic NADPH by CA diet in the refed condition (Figure 3-8). On the other hand, nicotinamide nucleotide transhydrogenase (NNT) is important for the production of mitochondrial NADPH because NADPH is impermeable in the mitochondrial membrane (Xiao et al., 2018). A

lower *Nnt* mRNA has been reported in the liver of NAFLD subjects, which accounts for a limited defense against oxidative stress (Mardinoglu et al., 2017). This study suggests that 12αOH BAs is possibly involved in the reduction of *Nnt* expression. It is of note that CA diet upregulated the genes involved in the isocitrate-α-ketoglutarate shuttle, suggesting that cytosolic NADPH may be replenished into mitochondria. Lipotoxicity accounts for oxidative stress and further activates pro-inflammatory pathways, which facilitates NAFLD progression (Chen et al., 2020). In this study, the promotion of PPP and isocitrate-α-ketoglutarate shuttle may play an important role in NADPH-mediated antioxidant defense, as the level of GSH increased and there were no signs of peroxidation and inflammation in CA-induced hepatic steatosis (Lee et al., 2020). Taken together, these data suggest that 12αOH BAs regulate the balance of redox couples which shifts the liver to a reduced state for antioxidant defenses.

Significant increases in two essential fatty acids including linoleic acid and α-linolenic acid were found in the liver of CA-fed rats (Figure 3-6). Since essential fatty acids are exclusively obtained from the diet and could not be endogenously produced by the liver (Spector and Kim, 2015), it is possible that 12αOH BAs could favor liver lipid accumulation by enhancing the uptake of dietary lipids. Fecal excretion of energy and lipids is high in *Cyp8b1* knockout mice, which prevents Western diet-induced hepatic steatosis (Bertaggia et al., 2017). Further, TCA treatment restored both the plasma and fecal levels of a lipid tracer in *Cyp8b1* knockout mice. These observations suggest the significance of 12αOH BAs in the intestinal absorption of dietary lipids.

Liver secretion of TG as very low-density lipoprotein (VLDL) particles to peripheral tissues is important for liver fat mobilization (Ipsen et al., 2018). An earlier study reports parallel inhibition of apolipoprotein B and VLDL secretion by TCA in human hepatocytes (Lin et al., 1996). Dietary CA supplementation suppresses VLDL secretion in KK-A^y mice that spontaneously develop hepatic steatosis (Watanabe et al., 2004). Additionally, the expression of microsomal TG transfer protein (MTTP), an enzyme critical for VLDL assembly, is positively regulated by PPARα (Améen et al., 2005). These observations suggest that a decreased TG export is possibly involved in liver TG accumulation under the CA diet.

Several studies point out DCA as a driver of NAFLD progression as follows. The fecal level of DCA increases with disease severity in the human NAFLD cohort (Smirnova et al., 2022). FXR signaling that regulates lipid and glucose metabolism is suppressed with increased DCA in patients with NASH (Jiao et al., 2018). Increased DCA stimulates a senescence-associated secretory phenotype in hepatic stellate cells that promotes disease progression toward fibrosis and liver cancer (Yoshimoto et al., 2013). The data in this study highlight the roles of DCA in manipulating microbial metabolism and its hepatic counterpart TDCA in regulating hepatic lipid metabolism. These events occurred with the onset of simple steatosis without signs of inflammation and oxidative stress.

There are some potential limitations to be discussed in the present study. As with all untargeted metabolomics studies, not every metabolite can be captured in a single assay due to the wide diversity of metabolites in terms of chemical characteristics and concentrations. It should be noted that metabolites were extracted in methanol/acetonitrile/H_2O, thus the levels of hydrophobic molecules were not analyzed by this method. Metabolites unable to be extracted could not be considered. Further, the increase in 12αOH BAs induced by dietary CA supplementation resembles the changes in BAs observed in human with metabolic disorders (Haeusler et al., 2016, 2013; Smirnova et al., 2022). It should be careful to extrapolate the present findings for humans when considering the difference in microbiota and BA metabolism between humans and rodents.

3.5 Conclusion

An increase in 12αOH BAs that does not disturb secondary BA production in the gut induced the following alterations: (1) alterations in gut microbial metabolism, characterized by depletion of fatty acids and enrichment in amino acids and amines; (2) activation of PARP1 that impairs NAD^+ homeostasis and PPARα signaling, and disturbs FFA degradation; (3) producing NADPH probably via promotion of PPP for antioxidant defense. These findings highlight the central roles of microbial metabolites DCA and TDCA in the initiation of hepatic steatosis by altering gut–liver metabolisms.

Chapter 4 General discussion

High-fat diets are strongly related to the incidence of a series of gut–liver axis diseases and metabolic diseases (Stenman et al., 2012; L. Wang et al., 2020; Westerbacka et al., 2005). Dietary fat upregulates the hepatic classical BA synthesis pathway (Hori et al., 2020), leading to increased levels of TCA in the proximal intestinal tract and DCA in the fecal output in rats (Yoshitsugu et al., 2019). Understanding the mechanisms of how these 12αOH BAs are involved in the nutritional stress-associated gut–liver axis pathophysiology may inspire researchers for potential strategies to prevent or treat these diseases. This study demonstrated that the primary and secondary 12αOH BAs impaired the barrier function in different sites of the intestine to various degrees, with the effect of ileal TCA being more apparent than that of colonic DCA both in *in vivo* and *ex vivo* models at physiological concentrations. Accumulation of TCA in the ileal mucosa led to down-expressions of claudins and antimicrobial peptides, which may be due to increased phosphorylation of MLC2 and decreased *Fxr* transcription. At the same time, TCA had a subtle effect on ileal cellular metabolism while DCA reprogrammed the fecal metabolome, characterized by enrichment in amino acids and amines, and depletion of fatty acids. In turn, DCA of microbial origin entered the circulation and changed the redox status and lipid metabolism of the liver via the activation of PARP1 and suppression of PPARα signaling. The results of gut–liver metabolomics indicated that DCA acted as a central node linking gut microbial metabolism alteration and hepatic lipid metabolism disturbance. These results shed light on the importance of 12αOH BAs in the onset of hepatic steatosis via mediating gut-liver communications.

An interesting question to peruse is whether the increased gut permeability is involved in the onset of hepatic steatosis in this CA diet model. In this study, it was found that intestinal permeability increased as early as week 2 after dietary CA intervention. This suggests that gut barrier impairment can be present already at the initial phases of hepatic steatosis. One study shows that patients with NAFLD have a significant increase in intestinal permeability compared with healthy subjects, which

may be explained by the disruption of tight junction integrity (Miele et al., 2009). The increased gut permeability is positively correlated with the degree of steatosis (Miele et al., 2009). In addition, the impaired gut barrier may result in the translocation of gut-derived microbial products or even microbes into the circulation, which may contribute to hepatic inflammation (Mouries et al., 2019). In this study, the CA-fed rats showed no signs of inflammation, neither in the intestine nor in the liver. However, CA-treated rats are more susceptible to a challenge with lipopolysaccharide (LPS), characterized by dramatically increased transaminase activities in the aortic plasma (Lee et al., 2020). This indicates that the liver under the CA diet is more responsive to stimulation that promotes the development of inflammation. It cannot be ruled out that 12αOH BAs might exacerbate an inflammatory response in other settings and later stages of the disease (Devkota et al., 2012; L. Wang et al., 2020).

In addition, BA receptors are highly expressed in the ileum due to the fact that the majority of BA reabsorption occurs in this site (Inagaki et al., 2006; Kawamata et al., 2003). Thus, the ileum is one of the sites of BA sensing. In this study, the transcriptional level of *Fxr* was impaired in the ileum under the CA diet, which may be attributed to the antagonistic effect of TCA on FXR (Tveter et al., 2020). Bile duct ligation results in increased permeability in the ileum and a deactivated FXR signaling in the small intestine, while selective FXR reactivation in the ileum enhanced gut barrier function (Verbeke et al., 2015). FXR agonism restores the damaged epithelial mucosal barrier in the dextran sulfate sodium (DSS) model (Chen et al., 2022). Those observations suggest that FXR regulates gut barrier function. Also, FXR may play an important role in lipid homeostatic regulation. Depletion of FXR results in steatosis in mice fed normal chow (Sinal et al., 2000). FXR-TGR5 dual agonism prevents the progression of western diet-induced hepatic steatosis, while the effect is still present in TGR5-null mice (Wang et al., 2022). An interesting finding is that suppression of intestinal FXR signaling is observed in NAFLD patients, resulting in a significant reduction in serum fibroblast growth factor 19 (FGF19) (Jiao et al., 2018). It can be attractive to investigate whether ileal FXR agonism protects against CA diet-induced leaky gut and the potential relevance of dysregulation of hepatic lipid metabolism.

It is speculated that an increased gut permeability may amplify the effect of BA on the gut barrier. The paracellular pathway allows the permeation of small molecules with a molecular mass < 600 Da but excludes macromolecules and microorganisms (Watson et al., 2001). Macromolecules reach the lamina propria via the transcellular pathway, are taken up by local dendritic cells, and interact with immune cells (Ménard et al., 2010). In this study, the CA diet-induced higher permeation was not only detected by a small inert probe Cr-EDTA with a molecular mass of 344 Da, but also by FD4 with a larger molecular mass of 4000 Da. Overexpression of immunoglobulin A (IgA) in the ileum is found in rats fed the CA diet for 13 weeks (Yoshitsugu et al., 2021). This implies an enhanced immune response to antigens by the ileum under abundant TCA. The increased small intestinal permeability to macromolecules, for example, dietary antigens, may contribute to food allergy by exacerbating inappropriate immune responses (Ménard et al., 2010). Increased entry of microbial antigens is related to inflammatory bowel disease (IBD). CA or TCA supplementation promotes IBD in hosts that are genetically susceptible or have impaired mucosal barrier function (Chen et al., 2022; Devkota et al., 2012). Whether the 12αOH BAs-induced leaky gut causes the excess absorption of antigens and elevates the susceptibility to digestive diseases remain to be answered. Measurement of gut permeability using adapted probes is a possible strategy.

Despite the fact that DCA is the prominent molecule linking altered gut–liver metabolites with increased liver TG levels after the CA diet for 12 weeks, short-term CA diet-induced hepatic lipid accumulation may be independent of DCA production in the gut. CA diet feeding elevates liver TG at an early period (1~2 weeks) (data not shown), even though fecal DCA content is much lower than CA at that time. Also, in the rats fed the CA diet while concomitantly being treated with VCM that abolished DCA production, gut permeability and hepatic TG level (data not shown) are still higher than in the control. These results raise a possibility that primary 12αOH BAs induce hepatic steatosis in a different metabolic pathway from conventional rats with a high level of DCA in the gut. Focusing on the mechanism of hepatic steatosis induced by primary 12αOH BAs can be interesting in future studies.

Despite the fact that rodents have distinct BA metabolism compared to humans, the implication of increased levels of 12αOH BAs in gut–liver diseases is also frequently reported in human studies as follows. The serum concentrations of CA and DCA are increased in abnormal colorectal patients (Chen et al., 2021). Both the absolute concentration and proportion of 12αOH BAs are higher in the serum of IBD patients (Chen et al., 2022). An increased level of fecal DCA drives changes in the fecal microbiome and correlates with disease severity in NAFLD patients (Smirnova et al., 2022). Although this study demonstrated that abundant 12αOH BAs impaired gut barrier function, altered fecal metabolome, and disturbed hepatic metabolism in rats, more mechanistic studies are needed to clarify their roles in gut–liver diseases and metabolic diseases, in particular, in humans.

Conclusion

In conclusion, this study provides evidence that high levels of 12αOH BAs are critical regulators of intestinal and hepatic pathophysiology in rats. Abundant TCA impairs ileal barrier function. The underlying mechanism might involve the phosphorylation of MLC2 and deficiency in *Fxr* transcriptional level. DCA plays a central role in modifying fecal and hepatic metabolome and alters gut microbial metabolism, particularly the processing of fatty acids and amino acids. The hepatic redox pathway is strongly affected by 12αOH BAs. These results provide a novel perspective on how 12αOH BAs regulate the pathophysiology of the gut–liver axis.

References

Agans, R., Gordon, A., Kramer, D.L., Perez-Burillo, S., Rufián-Henares, J.A., Paliy, O., 2018. Dietary fatty acids sustain the growth of the human gut microbiota. Appl Environ Microbiol 84, e01525-18. https://doi.org/10.1128/AEM.01525-18

Albillos, A., De Gottardi, A., Rescigno, M., 2020. The gut-liver axis in liver disease: Pathophysiological basis for therapy. J Hepatol 72, 558–577. https://doi.org/10.1016/j.jhep.2019.10.003

Améen, C., Edvardsson, U., Ljungberg, A., Asp, L., Åkerblad, P., Tuneld, A., Olofsson, S.-O., Lindén, D., Oscarsson, J., 2005. Activation of peroxisome proliferator-activated receptor α increases the expression and activity of microsomal triglyceride transfer protein in the liver. J Biol Chem 280, 1224–1229. https://doi.org/10.1074/jbc.m412107200

Angelin, B., Björkhem, I., Einarsson, K., Ewerth, S., 1982. Hepatic uptake of bile acids in man. J Clin Invest 70, 724–731. https://doi.org/10.1172/jci110668

Araki, Y., Andoh, A., Bamba, H., Yoshikawa, K., Doi, H., Komai, Y., Higuchi, A., Fujiyama, Y., 2003. The cytotoxicity of hydrophobic bile acids is ameliorated by more hydrophilic bile acids in intestinal cell lines IEC-6 and Caco-2. Oncol Rep 10, 1931–1936. https://doi.org/10.3892/or.10.6.1931

Bernstein, H., Holubec, H., Bernstein, C., Ignatenko, N., Gerner, E., Dvorak, K., Besselsen, D., Ramsey, L., Dall'Agnol, M., Blohm-Mangone, K.A., Padilla-Torres, J., Cui, H., Garewal, H., Payne, C.M., 2006. Unique dietary-related mouse model of colitis. Inflamm Bowel Dis 12, 278–293. https://doi.org/10.1097/01.MIB.0000209789.14114.63

Bertaggia, E., Jensen, K.K., Castro-Perez, J., Xu, Y., Di Paolo, G., Chan, R.B., Wang, L., Haeusler, R.A., 2017. *Cyp8b1* ablation prevents Western diet-induced weight gain and hepatic steatosis because of impaired fat absorption. Am J Physiol Endocrinol Metab 313, E121–E133. https://doi.org/10.1152/ajpendo.00409.2016

Bijvelds, M.J.C., Jorna, H., Verkade, H.J., Bot, A.G.M., Hofmann, F., Agellon, L.B., Sinaasappel, M., de Jonge, H.R., 2005. Activation of CFTR by ASBT-mediated bile salt absorption. Am J Physiol Gastrointest Liver Physiol 289, G870–G879. https://doi.org/10.1152/ajpgi.00226.2005

Binnerts, W.T., Van 't Klooster, A.T., Frens, A.M., 1968. Soluble chromium indicator measured by atomic absorption in digestion experiments. Vet Rec 82, 470.

Camilleri, M., 2019. Leaky gut: mechanisms, measurement and clinical implications in humans. Gut 68, 1516–1526. https://doi.org/10.1136/gutjnl-2019-318427

Chalasani, N., Younossi, Z., Lavine, J.E., Charlton, M., Cusi, K., Rinella, M., Harrison, S.A., Brunt, E.M., Sanyal, A.J., 2018. The diagnosis and management of nonalcoholic fatty liver disease: practice guidance from the American Association for the Study of Liver Diseases. Hepatology 67, 328–357. https://doi.org/10.1002/hep.29367

Chen, F., Dai, X., Zhou, C.-C., Li, K., Zhang, Y., Lou, X.-Y., Zhu, Y.-M., Sun, Y.-L., Peng, B.-X., Cui, W., 2021. Integrated analysis of the faecal metagenome and serum metabolome reveals the role of gut microbiome-associated metabolites in

the detection of colorectal cancer and adenoma. Gut 0, 1–11. https://doi.org/10.1136/gutjnl-2020-323476
Chen, L., Jiao, T., Liu, W., Luo, Y., Wang, Jue, Guo, X., Tong, X., Lin, Z., Sun, C., Wang, K., He, Y., Zhang, Y., Xu, H., Wang, Jiawen, Zuo, J., Ding, Q., He, S., Gonzalez, F.J., Xie, C., 2022. Hepatic cytochrome P450 8B1 and cholic acid potentiate intestinal epithelial injury in colitis by suppressing intestinal stem cell renewal. Cell Stem Cell 29, 1366–1381. https://doi.org/10.1016/j.stem.2022.08.008
Chen, M.L., Takeda, K., Sundrud, M.S., 2019. Emerging roles of bile acids in mucosal immunity and inflammation. Mucosal Immunol 12, 851–861. https://doi.org/10.1038/s41385-019-0162-4
Chen, Z., Tian, R., She, Z., Cai, J., Li, H., 2020. Role of oxidative stress in the pathogenesis of nonalcoholic fatty liver disease. Free Radic Biol Med 152, 116–141. https://doi.org/10.1016/j.freeradbiomed.2020.02.025
Chiang, J.Y.L., 2009. Bile acids: regulation of synthesis. J Lipid Res 50, 1955–1966. https://doi.org/10.1194/jlr.r900010-jlr200
Chiang, J.Y.L., Ferrell, J.M., 2018. Bile acid metabolism in liver pathobiology. Gene Expr 18, 71–87. https://doi.org/10.3727/105221618X15156018385515
Chopyk, D.M., Grakoui, A., 2020. Contribution of the intestinal microbiome and gut barrier to hepatic disorders. Gastroenterology 159, 849–863. https://doi.org/10.1053/j.gastro.2020.04.077
Clifford, B.L., Sedgeman, L.R., Williams, K.J., Morand, P., Cheng, A., Jarrett, K.E., Chan, A.P., Brearley-Sholto, M.C., Wahlström, A., Ashby, J.W., Barshop, W., Wohlschlegel, J., Calkin, A.C., Liu, Y., Thorell, A., Meikle, P.J., Drew, B.G., Mack, J.J., Marschall, H.-U., Tarling, E.J., Edwards, P.A., de Aguiar Vallim, T.Q., 2021. FXR activation protects against NAFLD via bile-acid-dependent reductions in lipid absorption. Cell Metab 33, 1–14. https://doi.org/10.1016/j.cmet.2021.06.012
Croci, I., Byrne, N.M., Choquette, S., Hills, A.P., Chachay, V.S., Clouston, A.D., O'Moore-Sullivan, T.M., Macdonald, G.A., Prins, J.B., Hickman, I.J., 2013. Whole-body substrate metabolism is associated with disease severity in patients with non-alcoholic fatty liver disease. Gut 62, 1625–1633. https://doi.org/10.1136/gutjnl-2012-302789
Daniel, H., Gholami, A.M., Berry, D., Desmarchelier, C., Hahne, H., Loh, G., Mondot, S., Lepage, P., Rothballer, M., Walker, A., Böhm, C., Wenning, M., Wagner, M., Blaut, M., Schmitt-Kopplin, P., Kuster, B., Haller, D., Clavel, T., 2014. High-fat diet alters gut microbiota physiology in mice. ISME J 8, 295–308. https://doi.org/10.1038/ismej.2013.155
de Aguiar Vallim, T.Q., Tarling, E.J., Edwards, P.A., 2013. Pleiotropic roles of bile acids in metabolism. Cell Metab 17, 657–669. https://doi.org/10.1016/j.cmet.2013.03.013
Dermadi, D., Valo, S., Ollila, S., Soliymani, R., Sipari, N., Pussila, M., Sarantaus, L., Linden, J., Baumann, M., Nyström, M., 2017. Western diet deregulates bile acid homeostasis, cell proliferation, and tumorigenesis in colon. Cancer Res 77, 3352–3363. https://doi.org/10.1158/0008-5472.CAN-16-2860

Devkota, S., Wang, Y., Musch, M.W., Leone, V., Fehlner-Peach, H., Nadimpalli, A., Antonopoulos, D.A., Jabri, B., Chang, E.B., 2012. Dietary-fat-induced taurocholic acid promotes pathobiont expansion and colitis in Il10−/− mice. Nature 487, 104–108. https://doi.org/10.1038/nature11225

Donnelly, K.L., Smith, C.I., Schwarzenberg, S.J., Jessurun, J., Boldt, M.D., Parks, E.J., 2005. Sources of fatty acids stored in liver and secreted via lipoproteins in patients with nonalcoholic fatty liver disease. J Clin Invest 115, 1343–1351. https://doi.org/10.1172/jci23621

Eggink, H.M., van Nierop, F.S., Schooneman, M.G., Boelen, A., Kalsbeek, A., Koehorst, M., ten Have, G.A.M., de Brauw, L.M., Groen, A.K., Romijn, J.A., Deutz, N.E.P., Soeters, M.R., 2018. Transhepatic bile acid kinetics in pigs and humans. Clin Nutr 37, 1406–1414. https://doi.org/10.1016/j.clnu.2017.06.015

Eslam, M., Newsome, P.N., Sarin, S.K., Anstee, Q.M., Targher, G., Romero-Gomez, M., Zelber-Sagi, S., Wai-Sun Wong, V., Dufour, J.-F., Schattenberg, J.M., Kawaguchi, T., Arrese, M., Valenti, L., Shiha, G., Tiribelli, C., Yki-Järvinen, H., Fan, J.-G., Grønbæk, H., Yilmaz, Y., Cortez-Pinto, H., Oliveira, C.P., Bedossa, P., Adams, L.A., Zheng, M.-H., Fouad, Y., Chan, W.-K., Mendez-Sanchez, N., Ahn, S.H., Castera, L., Bugianesi, E., Ratziu, V., George, J., 2020. A new definition for metabolic dysfunction-associated fatty liver disease: An international expert consensus statement. J Hepatol 73, 202–209. https://doi.org/10.1016/j.jhep.2020.03.039

Fouad, Y., Waked, I., Bollipo, S., Gomaa, A., Ajlouni, Y., Attia, D., 2020. What's in a name? Renaming 'NAFLD' to 'MAFLD.' Liver Int 40, 1254–1261. https://doi.org/10.1111/liv.14478

Francque, S., Verrijken, A., Caron, S., Prawitt, J., Paumelle, R., Derudas, B., Lefebvre, P., Taskinen, M.-R., Van Hul, W., Mertens, I., Hubens, G., Van Marck, E., Michielsen, P., Van Gaal, L., Staels, B., 2015. PPARα gene expression correlates with severity and histological treatment response in patients with non-alcoholic steatohepatitis. J Hepatol 63, 164–173. https://doi.org/10.1016/j.jhep.2015.02.019

Friedman, S.L., Neuschwander-Tetri, B.A., Rinella, M., Sanyal, A.J., 2018. Mechanisms of NAFLD development and therapeutic strategies. Nat Med 24, 908–922. https://doi.org/10.1038/s41591-018-0104-9

Fuchs, C.D., Trauner, M., 2022. Role of bile acids and their receptors in gastrointestinal and hepatic pathophysiology. Nat Rev Gastroenterol Hepatol 19, 432–450. https://doi.org/10.1038/s41575-021-00566-7

Gariani, K., Menzies, K.J., Ryu, D., Wegner, C.J., Wang, X., Ropelle, E.R., Moullan, N., Zhang, H., Perino, A., Lemos, V., Kim, B., Park, Y.-K., Piersigilli, A., Pham, T.X., Yang, Y., Ku, C.S., Koo, S.I., Fomitchova, A., Cantó, C., Schoonjans, K., Sauve, A.A., Lee, J.-Y., Auwerx, J., 2016. Eliciting the mitochondrial unfolded protein response by nicotinamide adenine dinucleotide repletion reverses fatty liver disease in mice. Hepatology 63, 1190–1204. https://doi.org/10.1002/hep.28245

Garten, A., Schuster, S., Penke, M., Gorski, T., de Giorgis, T., Kiess, W., 2015. Physiological and pathophysiological roles of NAMPT and NAD metabolism. Nat

Rev Endocrinol 11, 535–546. https://doi.org/10.1038/nrendo.2015.117
Griffiths, W.J., Sjovall, J., 2010. Bile acids: analysis in biological fluids and tissues. J Lipid Res 51, 23–41. https://doi.org/10.1194/jlr.R001941-JLR200
Gupta, B., Liu, Y., Chopyk, D.M., Rai, R.P., Desai, C., Kumar, P., Farris, A.B., Nusrat, A., Parkos, C.A., Anania, F.A., Raeman, R., 2020. Western diet-induced increase in colonic bile acids compromises epithelial barrier in nonalcoholic steatohepatitis. FASEB J 34, 7089–7102. https://doi.org/10.1096/fj.201902687R
Haeusler, R.A., Astiarraga, B., Camastra, S., Accili, D., Ferrannini, E., 2013. Human insulin resistance is associated with increased plasma levels of 12a-hydroxylated bile acids. Diabetes 62, 4184–4191.
Haeusler, R.A., Camastra, S., Nannipieri, M., Astiarraga, B., Castro-Perez, J., Xie, D., Wang, L., Chakravarthy, M., Ferrannini, E., 2016. Increased bile acid synthesis and impaired bile acid transport in human obesity. J Clin Endocrinol Metab 101, 1935–1944. https://doi.org/10.1210/jc.2015-2583
Haeusler, R.A., Pratt-Hyatt, M., Welch, C.L., Klaassen, C.D., Accili, D., 2012. Impaired generation of 12-hydroxylated bile acids links hepatic insulin signaling with dyslipidemia. Cell Metab 15, 65–74. https://doi.org/10.1016/j.cmet.2011.11.010
Hagio, M., Matsumoto, M., Fukushima, M., Hara, H., Ishizuka, S., 2009. Improved analysis of bile acids in tissues and intestinal contents of rats using LC/ESI-MS. J Lipid Res 50, 173–180. https://doi.org/10.1194/jlr.D800041-JLR200
Hagio, M., Matsumoto, M., Ishizuka, S., 2011. Bile acid analysis in various biological samples using ultra performance liquid chromatography/electrospray ionization-mass spectrometry (UPLC/ESI-MS), in: Metz, T.O. (Ed.), Metabolic Profiling, Methods in Molecular Biology. Humana Press, Totowa, NJ, pp. 119–129. https://doi.org/10.1007/978-1-61737-985-7_6
Hegyi, P., Maléth, J., Walters, J.R., Hofmann, A.F., Keely, S.J., 2018. Guts and gall: bile acids in regulation of intestinal epithelial function in health and disease. Physiol Rev 98, 1983–2023. https://doi.org/10.1152/physrev.00054.2017
Hofmann, A.F., Hagey, L.R., 2014. Key discoveries in bile acid chemistry and biology and their clinical applications: history of the last eight decades. J Lipid Res 55, 1553–1595. https://doi.org/10.1194/jlr.r049437
Hori, S., Abe, T., Lee, D.G., Fukiya, S., Yokota, A., Aso, N., Shirouchi, B., Sato, M., Ishizuka, S., 2020. Association between 12α-hydroxylated bile acids and hepatic steatosis in rats fed a high-fat diet. J Nutr Biochem 83, 108412. https://doi.org/10.1016/j.jnutbio.2020.108412
Hori, S., Satake, M., Kohmoto, O., Takagi, R., Okada, K., Fukiya, S., Yokota, A., Ishizuka, S., 2021. Primary 12α-hydroxylated bile acids lower hepatic iron concentration in rats. J Nutr 151, 523–530. https://doi.org/10.1093/jn/nxaa366
Hoshi, S., Sakata, T., Mikuni, K., Hashimoto, H., Kimura, S., 1994. Galactosylsucrose and xylosylfructoside alter digestive tract size and concentrations of cecal organic acids in rats fed diets containing cholesterol and cholic acid. J Nutr 124, 52–60. https://doi.org/10.1093/jn/124.1.52
Hoyles, L., Fernández-Real, J.-M., Federici, M., Serino, M., Abbott, J., Charpentier,

J., Heymes, C., Luque, J.L., Anthony, E., Barton, R.H., Chilloux, J., Myridakis, A., Martinez-Gili, L., Moreno-Navarrete, J.M., Benhamed, F., Azalbert, V., Blasco-Baque, V., Puig, J., Xifra, G., Ricart, W., Tomlinson, C., Woodbridge, M., Cardellini, M., Davato, F., Cardolini, I., Porzio, O., Gentileschi, P., Lopez, F., Foufelle, F., Butcher, S.A., Holmes, E., Nicholson, J.K., Postic, C., Burcelin, R., Dumas, M.-E., 2018. Molecular phenomics and metagenomics of hepatic steatosis in non-diabetic obese women. Nat Med 24, 1070–1080. https://doi.org/10.1038/s41591-018-0061-3

Huang, Kun, Du, M., Tan, X., Yang, L., Li, X., Jiang, Y., Wang, C., Zhang, F., Zhu, F., Cheng, M., Yang, Q., Yu, L., Wang, L., Huang, D., Huang, Kai, 2017. PARP1-mediated PPARα poly(ADP-ribosyl)ation suppresses fatty acid oxidation in non-alcoholic fatty liver disease. J Hepatol 66, 962–977. https://doi.org/10.1016/j.jhep.2016.11.020

Hydes, T.J., Ravi, S., Loomba, R., E. Gray, M., 2020. Evidence-based clinical advice for nutrition and dietary weight loss strategies for the management of NAFLD and NASH. Clin Mol Hepatol 26, 383–400. https://doi.org/10.3350/cmh.2020.0067

Inagaki, T., Moschetta, A., Lee, Y.-K., Peng, L., Zhao, G., Downes, M., Yu, R.T., Shelton, J.M., Richardson, J.A., Repa, J.J., Mangelsdorf, D.J., Kliewer, S.A., 2006. Regulation of antibacterial defense in the small intestine by the nuclear bile acid receptor. Proc Natl Acad Sci U S A 103, 3920–3925. https://doi.org/10.1073/pnas.0509592103

Ipsen, D.H., Lykkesfeldt, J., Tveden-Nyborg, P., 2018. Molecular mechanisms of hepatic lipid accumulation in non-alcoholic fatty liver disease. Cell Mol Life Sci 75, 3313–3327. https://doi.org/10.1007/s00018-018-2860-6

Islam, K.B.M.S., Fukiya, S., Hagio, M., Fujii, N., Ishizuka, S., Ooka, T., Ogura, Y., Hayashi, T., Yokota, A., 2011. Bile acid is a host factor that regulates the composition of the cecal microbiota in rats. Gastroenterology 141, 1773–1781. https://doi.org/10.1053/j.gastro.2011.07.046

Jia, Wei, Xie, G., Jia, Weiping, 2018. Bile acid–microbiota crosstalk in gastrointestinal inflammation and carcinogenesis. Nat Rev Gastroenterol Hepatol 15, 111–128. https://doi.org/10.1038/nrgastro.2017.119

Jiao, N., Baker, S.S., Chapa-Rodriguez, A., Liu, W., Nugent, C.A., Tsompana, M., Mastrandrea, L., Buck, M.J., Baker, R.D., Genco, R.J., Zhu, R., Zhu, L., 2018. Suppressed hepatic bile acid signalling despite elevated production of primary and secondary bile acids in NAFLD. Gut 67, 1881–1891. https://doi.org/10.1136/gutjnl-2017-314307

Jin, Y., Blikslager, A.T., 2020. The regulation of intestinal mucosal barrier by myosin light chain kinase/Rho kinases. Int J Mol Sci 21, 3550. https://doi.org/10.3390/ijms21103550

Johansson, M.E.V., Phillipson, M., Petersson, J., Velcich, A., Holm, L., Hansson, G.C., 2008. The inner of the two Muc2 mucin-dependent mucus layers in colon is devoid of bacteria. Proc Natl Acad Sci U S A 105, 15064–15069. https://doi.org/10.1073/pnas.0803124105

Kawamata, Y., Fujii, R., Hosoya, M., Harada, M., Yoshida, H., Miwa, M., Fukusumi,

S., Habata, Y., Itoh, T., Shintani, Y., Hinuma, S., Fujisawa, Y., Fujino, M., 2003. A G protein-coupled receptor responsive to bile acids. J Biol Chem 278, 9435–9440. https://doi.org/10.1074/jbc.M209706200

Kayama, H., Okumura, R., Takeda, K., 2020. Interaction between the microbiota, epithelia, and immune cells in the intestine. Annu Rev Immunol 38, 23–48. https://doi.org/10.1146/annurev-immunol-070119-115104

Kersten, S., Stienstra, R., 2017. The role and regulation of the peroxisome proliferator activated receptor alpha in human liver. Biochimie 136, 75–84. https://doi.org/10.1016/j.biochi.2016.12.019

Khan, S., Luck, H., Winer, S., Winer, D.A., 2021. Emerging concepts in intestinal immune control of obesity-related metabolic disease. Nat Commun 12, 2598. https://doi.org/10.1038/s41467-021-22727-7

Kurdi, P., Kawanishi, K., Mizutani, K., Yokota, A., 2006. Mechanism of growth inhibition by free bile acids in Lactobacilli and Bifidobacteria. J Bacteriol 188, 1979–1986. https://doi.org/10.1128/JB.188.5.1979-1986.2006

Lake, A.D., Novak, P., Shipkova, P., Aranibar, N., Robertson, D., Reily, M.D., Lu, Z., Lehman-McKeeman, L.D., Cherrington, N.J., 2013. Decreased hepatotoxic bile acid composition and altered synthesis in progressive human nonalcoholic fatty liver disease. Toxicol Appl Pharmacol 268, 132–140. https://doi.org/10.1016/j.taap.2013.01.022

Lee, D.G., Hori, S., Kohmoto, O., Kitta, S., Yoshida, R., Tanaka, Y., Shimizu, H., Takahashi, K., Nagura, T., Uchino, H., Fukiya, S., Yokota, A., Ishizuka, S., 2019. Ingestion of difructose anhydride III partially suppresses the deconjugation and 7α-dehydroxylation of bile acids in rats fed with a cholic acid-supplemented diet. Biosci Biotechnol Biochem 83, 1329–1335. https://doi.org/10.1080/09168451.2019.1597617

Lee, J.-Y., Shimizu, H., Hagio, M., Fukiya, S., Watanabe, M., Tanaka, Y., Joe, G.-H., Iwaya, H., Yoshitsugu, R., Kikuchi, K., Tsuji, M., Baba, N., Nose, T., Tada, K., Hanai, T., Hori, S., Takeuchi, A., Furukawa, Y., Shirouchi, B., Sato, M., Ooka, T., Ogura, Y., Hayashi, T., Yokota, A., Ishizuka, S., 2020. 12α-Hydroxylated bile acid induces hepatic steatosis with dysbiosis in rats. Biochim Biophys Acta Mol Cell Biol Lipids 1865, 158811. https://doi.org/10.1016/j.bbalip.2020.158811

Lee, Y., Yoshitsugu, R., Kikuchi, K., Joe, G.-H., Tsuji, M., Nose, T., Shimizu, H., Hara, H., Minamida, K., Miwa, K., Ishizuka, S., 2016. Combination of soya pulp and *Bacillus coagulans* lilac-01 improves intestinal bile acid metabolism without impairing the effects of prebiotics in rats fed a cholic acid-supplemented diet. Br J Nutr 116, 603–610. https://doi.org/10.1017/S0007114516002270

Lew, J.-L., Zhao, A., Yu, J., Huang, L., de Pedro, N., Peláez, F., Wright, S.D., Cui, J., 2004. The farnesoid X receptor controls gene expression in a ligand- and promoter-selective fashion. J Biol Chem 279, 8856–8861. https://doi.org/10.1074/jbc.M306422200

Li, M., Rajani, C., Zheng, X., Jia, W., 2022. The microbial metabolome in metabolic-associated fatty liver disease. J Gastroenterol Hepatol 37, 15–23. https://doi.org/10.1111/jgh.15746

Lin, Y., Havinga, R., Verkade, H.J., Moshage, H., Slooff, M.J.H., Vonk, R.J., Kuipers, F., 1996. Bile acids suppress the secretion of very-low-density lipoprotein by human hepatocytes in primary culture. Hepatology 23, 219–228. https://doi.org/10.1002/hep.510230204

Lindeboom, L., Nabuurs, C.I., Hesselink, M.K., Wildberger, J.E., Schrauwen, P., Schrauwen-Hinderling, V.B., 2015. Proton magnetic resonance spectroscopy reveals increased hepatic lipid content after a single high-fat meal with no additional modulation by added protein. Am J Clin Nutr 101, 65–71. https://doi.org/10.3945/ajcn.114.094730

Liu, H., Kohmoto, O., Sakaguchi, A., Hori, S., Tochigi, M., Tada, K., Lee, Y., Kikuchi, K., Ishizuka, S., 2022. Taurocholic acid, a primary 12α-hydroxylated bile acid, induces leakiness in the distal small intestine in rats. Food Chem Toxicol 165, 113136. https://doi.org/10.1016/j.fct.2022.113136

Lomonaco, R., Ortiz-Lopez, C., Orsak, B., Webb, A., Hardies, J., Darland, C., Finch, J., Gastaldelli, A., Harrison, S., Tio, F., Cusi, K., 2012. Effect of adipose tissue insulin resistance on metabolic parameters and liver histology in obese patients with nonalcoholic fatty liver disease. Hepatology 55, 1389–1397. https://doi.org/10.1002/hep.25539

Maddocks, O.D.K., Berkers, C.R., Mason, S.M., Zheng, L., Blyth, K., Gottlieb, E., Vousden, K.H., 2013. Serine starvation induces stress and p53-dependent metabolic remodelling in cancer cells. Nature 493, 542–546. https://doi.org/10.1038/nature11743

Maegawa, K., Koyama, H., Fukiya, S., Yokota, A., Ueda, K., Ishizuka, S., 2021. Dietary raffinose ameliorates hepatic lipid accumulation induced by cholic acid via modulation of enterohepatic bile acid circulation in rats. Br J Nutr 127, 1621–1630. https://doi.org/10.1017/S0007114521002610

Mardinoglu, A., Bjornson, E., Zhang, C., Klevstig, M., Söderlund, S., Ståhlman, M., Adiels, M., Hakkarainen, A., Lundbom, N., Kilicarslan, M., Hallström, B.M., Lundbom, J., Vergès, B., Barrett, P.H.R., Watts, G.F., Serlie, M.J., Nielsen, J., Uhlén, M., Smith, U., Marschall, H., Taskinen, M., Boren, J., 2017. Personal model-assisted identification of NAD $^{+}$ and glutathione metabolism as intervention target in NAFLD. Mol Syst Biol 13, 916. https://doi.org/10.15252/msb.20167422

Markov, A.G., Veshnyakova, A., Fromm, M., Amasheh, M., Amasheh, S., 2010. Segmental expression of claudin proteins correlates with tight junction barrier properties in rat intestine. J Comp Physiol B 180, 591–598. https://doi.org/10.1007/s00360-009-0440-7

Ménard, S., Cerf-Bensussan, N., Heyman, M., 2010. Multiple facets of intestinal permeability and epithelial handling of dietary antigens. Mucosal Immunol 3, 247–259. https://doi.org/10.1038/mi.2010.5

Michael, A.J., 2016. Biosynthesis of polyamines and polyamine-containing molecules. Biochem J 473, 2315–2329. https://doi.org/10.1042/BCJ20160185

Miele, L., Valenza, V., La Torre, G., Montalto, M., Cammarota, G., Ricci, R., Mascianà, R., Forgione, A., Gabrieli, M.L., Perotti, G., Vecchio, F.M., Rapaccini, G., Gasbarrini, G., Day, C.P., Grieco, A., 2009. Increased intestinal permeability

and tight junction alterations in nonalcoholic fatty liver disease. Hepatology 49, 1877–1887. https://doi.org/10.1002/hep.22848

Monserrat-Mesquida, M., Quetglas-Llabrés, M., Abbate, M., Montemayor, S., Mascaró, C.M., Casares, M., Tejada, S., Abete, I., Zulet, M.A., Tur, J.A., Martínez, J.A., Sureda, A., 2020. Oxidative stress and pro-inflammatory status in patients with non-alcoholic fatty liver disease. Antioxidants 9, 759. https://doi.org/10.3390/antiox9080759

Mouries, J., Brescia, P., Silvestri, A., Spadoni, I., Sorribas, M., Wiest, R., Mileti, E., Galbiati, M., Invernizzi, P., Adorini, L., Penna, G., Rescigno, M., 2019. Microbiota-driven gut vascular barrier disruption is a prerequisite for non-alcoholic steatohepatitis development. J Hepatol 71, 1216–1228. https://doi.org/10.1016/j.jhep.2019.08.005

Mouzaki, M., Comelli, E.M., Arendt, B.M., Bonengel, J., Fung, S.K., Fischer, S.E., Mcgilvray, I.D., Allard, J.P., 2013. Intestinal microbiota in patients with nonalcoholic fatty liver disease. Hepatology 58, 120–127. https://doi.org/10.1002/hep.26319

Mouzaki, M., Wang, A.Y., Bandsma, R., Comelli, E.M., Arendt, B.M., Zhang, L., Fung, S., Fischer, S.E., McGilvray, I.G., Allard, J.P., 2016. Bile acids and dysbiosis in non-alcoholic fatty liver disease. PLoS ONE 11, e0151829. https://doi.org/10.1371/journal.pone.0151829

Neuschwander-Tetri, B.A., 2010. Hepatic lipotoxicity and the pathogenesis of nonalcoholic steatohepatitis: The central role of nontriglyceride fatty acid metabolites. Hepatology 52, 774–788. https://doi.org/10.1002/hep.23719

Noack, J., Kleessen, B., Proll, J., Dongowski, G., Blaut, M., 1998. Dietary guar gum and pectin stimulate intestinal microbial polyamine synthesis in rats. J Nutr 128, 1385–1391. https://doi.org/10.1093/jn/128.8.1385

Otani, T., Nguyen, T.P., Tokuda, S., Sugihara, K., Sugawara, T., Furuse, K., Miura, T., Ebnet, K., Furuse, M., 2019. Claudins and JAM-A coordinately regulate tight junction formation and epithelial polarity. J Cell Biol 218, 3372–3396. https://doi.org/10.1083/jcb.201812157

Pang, Z., Zhou, G., Ewald, J., Chang, L., Hacariz, O., Basu, N., Xia, J., 2022. Using MetaboAnalyst 5.0 for LC–HRMS spectra processing, multi-omics integration and covariate adjustment of global metabolomics data. Nat Protoc 17, 1735–1761. https://doi.org/10.1038/s41596-022-00710-w

Powell, E.E., Wong, V.W.-S., Rinella, M., 2021. Non-alcoholic fatty liver disease. The Lancet 397, 2212–2224. https://doi.org/10.1016/S0140-6736(20)32511-3

Quini, C.C., Américo, M.F., Corá, L.A., Calabresi, M.F., Alvarez, M., Oliveira, R.B., Miranda, J.A., 2012. Employment of a noninvasive magnetic method for evaluation of gastrointestinal transit in rats. J Biol Eng 6, 6. https://doi.org/10.1186/1754-1611-6-6

Rabot, S., Membrez, M., Bruneau, A., Gérard, P., Harach, T., Moser, M., Raymond, F., Mansourian, R., Chou, C.J., 2010. Germ-free C57BL/6J mice are resistant to high-fat-diet-induced insulin resistance and have altered cholesterol metabolism. FASEB J 24, 4948–4959. https://doi.org/10.1096/fj.10.164921

Rada, P., González-Rodríguez, Á., García-Monzón, C., Valverde, Á.M., 2020. Understanding lipotoxicity in NAFLD pathogenesis: is CD36 a key driver? Cell Death Dis 11, 802. https://doi.org/10.1038/s41419-020-03003-w

Raimondi, F., Santoro, P., Barone, M.V., Pappacoda, S., Barretta, M.L., Nanayakkara, M., Apicella, C., Capasso, L., Paludetto, R., 2008. Bile acids modulate tight junction structure and barrier function of Caco-2 monolayers via EGFR activation. Am J Physiol Gastrointest Liver Physiol 294, G906–G913. https://doi.org/10.1152/ajpgi.00043.2007

Reeves, P.G., Nielsen, F.H., Fahey, G.C., 1993. AIN-93 purified diets for laboratory rodents: final report of the American Institute of Nutrition Ad Hoc Writing Committee on the reformulation of the AIN-76A rodent diet. J Nutr 123, 1939–1951. https://doi.org/10.1093/jn/123.11.1939

Ridlon, J.M., Kang, D.-J., Hylemon, P.B., 2006. Bile salt biotransformations by human intestinal bacteria. J Lipid Res 47, 241–259. https://doi.org/10.1194/jlr.R500013-JLR200

Rohr, M.W., Narasimhulu, C.A., Rudeski-Rohr, T.A., Parthasarathy, S., 2020. Negative effects of a high-fat diet on intestinal permeability: A review. Adv Nutr 11, 77–91. https://doi.org/10.1093/advances/nmz061

Sang, C., Wang, X., Zhou, K., Sun, T., Bian, H., Gao, X., Wang, Y., Zhang, H., Jia, W., Liu, P., Xie, G., Chen, T., 2021. Bile acid profiles are distinct among patients with different etiologies of chronic liver disease. J Proteome Res 20, 2340–2351. https://doi.org/10.1021/acs.jproteome.0c00852

Sayin, S.I., Wahlström, A., Felin, J., Jäntti, S., Marschall, H.-U., Bamberg, K., Angelin, B., Hyötyläinen, T., Orešič, M., Bäckhed, F., 2013. Gut microbiota regulates bile acid metabolism by reducing the levels of tauro-beta-muricholic acid, a naturally occurring FXR antagonist. Cell Metab 17, 225–235. https://doi.org/10.1016/j.cmet.2013.01.003

Schlegel, N., Meir, M., Spindler, V., Germer, C.-T., Waschke, J., 2011. Differential role of Rho GTPases in intestinal epithelial barrier regulation in vitro. J Cell Physiol 226, 1196–1203. https://doi.org/10.1002/jcp.22446

Schneeberger, M., Everard, A., Gómez-Valadés, A.G., Matamoros, S., Ramírez, S., Delzenne, N.M., Gomis, R., Claret, M., Cani, P.D., 2015. Akkermansia muciniphila inversely correlates with the onset of inflammation, altered adipose tissue metabolism and metabolic disorders during obesity in mice. Sci Rep 5, 16643. https://doi.org/10.1038/srep16643

Schreiber, V., Dantzer, F., Ame, J.-C., de Murcia, G., 2006. Poly(ADP-ribose): novel functions for an old molecule. Nat Rev Mol Cell Biol 7, 517–528. https://doi.org/10.1038/nrm1963

Shannon, P., Markiel, A., Ozier, O., Baliga, N.S., Wang, J.T., Ramage, D., Amin, N., Schwikowski, B., Ideker, T., 2003. Cytoscape: a software environment for integrated models of biomolecular interaction networks. Genome Res 13, 2498–2504. https://doi.org/10.1101/gr.1239303

Sinal, C.J., Tohkin, M., Miyata, M., Ward, J.M., Lambert, G., Gonzalez, F.J., 2000. Targeted disruption of the nuclear receptor FXR/BAR impairs bile acid and lipid

homeostasis. Cell 102, 731–744. https://doi.org/10.1016/s0092-8674(00)00062-3
Sinal, C.J., Yoon, M., Gonzalez, F.J., 2001. Antagonism of the actions of peroxisome proliferator-activated aeceptor-α by bile acids. J Biol Chem 276, 47154–47162. https://doi.org/10.1074/jbc.m107000200
Smirnova, E., Muthiah, M.D., Narayan, N., Siddiqui, M.S., Puri, P., Luketic, V.A., Contos, M.J., Idowu, M., Chuang, J., Billin, A.N., Huss, R.S., Myers, R.P., Boyett, S., Seneshaw, M., Min, H., Mirshahi, F., Sanyal, A.J., 2022. Metabolic reprogramming of the intestinal microbiome with functional bile acid changes underlie the development of NAFLD. Hepatology 0, 1–14. https://doi.org/10.1002/hep.32568
Sokol, R.J., Winklhofer-Roob, B.M., Devereaux, M.W., Mckim, J.M., 1995. Generation of hydroperoxides in isolated rat hepatocytes and hepatic mitochondria exposed to hydrophobic bile acids. Gastroenterology 109, 1249–1256. https://doi.org/10.1016/0016-5085(95)90585-5
Spadoni, I., Zagato, E., Bertocchi, A., Paolinelli, R., Hot, E., Sabatino, A.D., Caprioli, F., Bottiglieri, L., Oldani, A., Viale, G., Penna, G., Dejana, E., Rescigno, M., 2015. A gut-vascular barrier controls the systemic dissemination of bacteria. Science 350, 830–834. https://doi.org/10.1126/science.aad0135
Spector, A.A., Kim, H.-Y., 2015. Discovery of essential fatty acids. J Lipid Res 56, 11–21. https://doi.org/10.1194/jlr.r055095
Stenman, L.K., Holma, R., Eggert, A., Korpela, R., 2013. A novel mechanism for gut barrier dysfunction by dietary fat: epithelial disruption by hydrophobic bile acids. Am J Physiol Gastrointest Liver Physiol 304, G227–G234. https://doi.org/10.1152/ajpgi.00267.2012
Stenman, L.K., Holma, R., Korpela, R., 2012. High-fat-induced intestinal permeability dysfunction associated with altered fecal bile acids. World J Gastroenterol 18, 923–929. https://doi.org/10.3748/wjg.v18.i9.923
Suzuki, T., Hara, H., 2010. Dietary fat and bile juice, but not obesity, are responsible for the increase in small intestinal permeability induced through the suppression of tight junction protein expression in LETO and OLETF rats. Nutr Metab 7, 19. https://doi.org/10.1186/1743-7075-7-19
Takahashi, S., Fukami, T., Masuo, Y., Brocker, C.N., Xie, C., Krausz, K.W., Wolf, C.R., Henderson, C.J., Gonzalez, F.J., 2016. Cyp2c70 is responsible for the species difference in bile acid metabolism between mice and humans. J Lipid Res 57, 2130–2137. https://doi.org/10.1194/jlr.m071183
Thaiss, C.A., Levy, M., Grosheva, I., Zheng, D., Soffer, E., Blacher, E., Braverman, S., Tengeler, A.C., Barak, O., Elazar, M., Ben-Zeev, R., Lehavi-Regev, D., Katz, M.N., Pevsner-Fischer, M., Gertler, A., Halpern, Z., Harmelin, A., Aamar, S., Serradas, P., Grosfeld, A., Shapiro, H., Geiger, B., Elinav, E., 2018. Hyperglycemia drives intestinal barrier dysfunction and risk for enteric infection. Science 359, 9. https://doi.org/10.1126/science.aar3318
Thévenot, E.A., Roux, A., Xu, Y., Ezan, E., Junot, C., 2015. Analysis of the human adult urinary metabolome variations with age, body mass index, and gender by implementing a comprehensive workflow for univariate and OPLS statistical

analyses. J Proteome Res 14, 3322–3335. https://doi.org/10.1021/acs.jproteome.5b00354
Tian, J., Wu, W., Liu, S., Ling-hu, T., Zhao, Y., Gao, Y., Qin, X., 2022. Stable isotope-resolved metabolomics studies on corticosteroid-induced PC12 cells: a strategy for evaluating glucose catabolism in an in vitro model of depression. J Proteome Res 21, 788–797. https://doi.org/10.1021/acs.jproteome.1c00516
Ticho, A.L., Malhotra, P., Dudeja, P.K., Gill, R.K., Alrefai, W.A., 2019. Intestinal absorption of bile acids in health and disease. Compr Physiol 10, 21–56. https://doi.org/10.1002/cphy.c190007
Turnbaugh, P.J., Ley, R.E., Mahowald, M.A., Magrini, V., Mardis, E.R., Gordon, J.I., 2006. An obesity-associated gut microbiome with increased capacity for energy harvest. Nature 444, 1027–1031. https://doi.org/10.1038/nature05414
Tveter, K.M., Villa-Rodriguez, J.A., Cabales, A.J., Zhang, L., Bawagan, F.G., Duran, R.M., Roopchand, D.E., 2020. Polyphenol-induced improvements in glucose metabolism are associated with bile acid signaling to intestinal farnesoid X receptor. BMJ Open Diab Res Care 8, e001386. https://doi.org/10.1136/bmjdrc-2020-001386
Vancamelbeke, M., Vermeire, S., 2017. The intestinal barrier: a fundamental role in health and disease. Expert Rev Gastroenterol Hepatol 11, 821–834. https://doi.org/10.1080/17474124.2017.1343143
Verbeke, L., Farre, R., Verbinnen, B., Covens, K., Vanuytsel, T., Verhaegen, J., Komuta, M., Roskams, T., Chatterjee, S., Annaert, P., Elst, I.V., Windmolders, P., Trebicka, J., Nevens, F., Laleman, W., 2015. The FXR agonist obeticholic acid prevents gut barrier dysfunction and bacterial translocation in cholestatic rats. Am J Pathol 185, 409–419. https://doi.org/10.1016/j.ajpath.2014.10.009
Vrieze, A., Out, C., Fuentes, S., Jonker, L., Reuling, I., Kootte, R.S., van Nood, E., Holleman, F., Knaapen, M., Romijn, J.A., Soeters, M.R., Blaak, E.E., Dallinga-Thie, G.M., Reijnders, D., Ackermans, M.T., Serlie, M.J., Knop, F.K., Holst, J.J., van der Ley, C., Kema, I.P., Zoetendal, E.G., de Vos, W.M., Hoekstra, J.B.L., Stroes, E.S., Groen, A.K., Nieuwdorp, M., 2014. Impact of oral vancomycin on gut microbiota, bile acid metabolism, and insulin sensitivity. J Hepatol 60, 824–831. https://doi.org/10.1016/j.jhep.2013.11.034
Wang, L., Gong, Z., Zhang, X., Zhu, F., Liu, Y., Jin, C., Du, X., Xu, C., Chen, Y., Cai, W., Tian, C., Wu, J., 2020. Gut microbial bile acid metabolite skews macrophage polarization and contributes to high-fat diet-induced colonic inflammation. Gut Microbes 12, 1819155. https://doi.org/10.1080/19490976.2020.1819155
Wang, X.X., Xie, C., Libby, A.E., Ranjit, S., Levi, J., Myakala, K., Bhasin, K., Jones, B.A., Orlicky, D.J., Takahashi, S., Dvornikov, A., Kleiner, D.E., Hewitt, S.M., Adorini, L., Kopp, J.B., Krausz, K.W., Rosenberg, A., Mcmanaman, J.L., Robertson, C.E., Ir, D., Frank, D.N., Luo, Y., Gonzalez, F.J., Gratton, E., Levi, M., 2022. The role of FXR and TGR5 in reversing and preventing progression of Western diet–induced hepatic steatosis, inflammation, and fibrosis in mice. J Biol Chem 298, 102530. https://doi.org/10.1016/j.jbc.2022.102530

Wang, Z., Litterio, M.C., Müller, M., Vauzour, D., Oteiza, P.I., 2020. (-)-Epicatechin and NADPH oxidase inhibitors prevent bile acid-induced Caco-2 monolayer permeabilization through ERK1/2 modulation. Redox Biol 28, 101360. https://doi.org/10.1016/j.redox.2019.101360

Watanabe, M., Houten, S.M., Wang, L., Moschetta, A., Mangelsdorf, D.J., Heyman, R.A., Moore, D.D., Auwerx, J., 2004. Bile acids lower triglyceride levels via a pathway involving FXR, SHP, and SREBP-1c. J Clin Invest 113, 1408–1418. https://doi.org/10.1172/jci21025

Watson, C.J., Rowland, M., Warhurst, G., 2001. Functional modeling of tight junctions in intestinal cell monolayers using polyethylene glycol oligomers. Am J Physiol Cell Physiol 281, C388–C397. https://doi.org/10.1152/ajpcell.2001.281.2.C388

Wei, M., Huang, F., Zhao, L., Zhang, Y., Yang, W., Wang, S., Li, M., Han, X., Ge, K., Qu, C., Rajani, C., Xie, G., Zheng, X., Zhao, A., Bian, Z., Jia, W., 2020. A dysregulated bile acid-gut microbiota axis contributes to obesity susceptibility. EBioMedicine 55, 102766. https://doi.org/10.1016/j.ebiom.2020.102766

Westerbacka, J., Lammi, K., Häkkinen, A.-M., Rissanen, A., Salminen, I., Aro, A., Yki-Järvinen, H., 2005. Dietary fat content modifies liver fat in overweight nondiabetic subjects. J Clin Endocrinol Metab 90, 2804–2809. https://doi.org/10.1210/jc.2004-1983

Xiao, W., Wang, R.-S., Handy, D.E., Loscalzo, J., 2018. NAD(H) and NADP(H) redox couples and cellular energy metabolism. Antioxid Redox Signal 28, 251–272. https://doi.org/10.1089/ars.2017.7216

Yoshimoto, S., Loo, T.M., Atarashi, K., Kanda, H., Sato, S., Oyadomari, S., Iwakura, Y., Oshima, K., Morita, H., Hattori, M., Honda, K., Ishikawa, Y., Hara, E., Ohtani, N., 2013. Obesity-induced gut microbial metabolite promotes liver cancer through senescence secretome. Nature 499, 97–101. https://doi.org/10.1038/nature12347

Yoshitsugu, R., Kikuchi, K., Iwaya, H., Fujii, N., Hori, S., Lee, D.G., Ishizuka, S., 2019. Alteration of bile acid metabolism by a high-fat diet is associated with plasma transaminase activities and glucose intolerance in rats. J Nutr Sci Vitaminol 65, 45–51. https://doi.org/10.3177/jnsv.65.45

Yoshitsugu, R., Liu, H., Kamo, Y., Takeuchi, A., Joe, G.-H., Tada, K., Kikuchi, K., Fujii, N., Kitta, S., Hori, S., Takatsuki, M., Iwaya, H., Tanaka, Y., Shimizu, H., Ishizuka, S., 2021. 12α-Hydroxylated bile acid enhances accumulation of adiponectin and immunoglobulin A in the rat ileum. Sci Rep 11, 12939. https://doi.org/10.1038/s41598-021-92302-z

Younossi, Z.M., Koenig, A.B., Abdelatif, D., Fazel, Y., Henry, L., Wymer, M., 2016. Global epidemiology of nonalcoholic fatty liver disease-Meta-analytic assessment of prevalence, incidence, and outcomes. Hepatology 64, 73–84. https://doi.org/10.1002/hep.28431

Zhang, R., Watson, D.G., Wang, L., Westrop, G.D., Coombs, G.H., Zhang, T., 2014. Evaluation of mobile phase characteristics on three zwitterionic columns in hydrophilic interaction liquid chromatography mode for liquid chromatography-high resolution mass spectrometry based untargeted metabolite profiling of

Leishmania parasites. J Chromatogr A 1362, 168–179. https://doi.org/10.1016/j.chroma.2014.08.039

Zhao, S., Jang, C., Liu, J., Uehara, K., Gilbert, M., Izzo, L., Zeng, X., Trefely, S., Fernandez, S., Carrer, A., Miller, K.D., Schug, Z.T., Snyder, N.W., Gade, T.P., Titchenell, P.M., Rabinowitz, J.D., Wellen, K.E., 2020. Dietary fructose feeds hepatic lipogenesis via microbiota-derived acetate. Nature 579, 586–591. https://doi.org/10.1038/s41586-020-2101-7

Publications and academic conferences

Publications as first author:

1. **Liu H.**, Kohmoto O., Sakaguchi A., Hori S., Tochigi M., Tada K., Lee Y., Kikuchi K., Ishizuka S., 2022. Taurocholic acid, a primary 12α-hydroxylated bile acid, induces leakiness in the distal small intestine in rats. Food Chem Toxicol 165, 113136. https://doi.org/10.1016/j.fct.2022.113136

2. **Liu H.**, Yokoyama F., Ishizuka S., Alterations in the liver and fecal metabolome in cholic acid-induced hepatic steatosis in rats. (Under submission)

Academic conferences:

1. Small intestinal hyperpermeability is associated with increased primary 12α-hydroxylated bile acids in the enterohepatic circulation. 24th Annual Meeting of intestinal Microbiology. 2020.

2. Gut barrier impairment by primary 12α-hydroxylated bile acids. Meeting of JSBBA Hokkaido Branch 2020 and 50th JSNFS Hokkaido Branch. 2020.

3. Taurocholic acid, a primary 12α-hydroxylated bile acid, induces leakiness in the distal small intestine in rats. 22nd International congress of nutrition. 2022.

Acknowledgements

Upon the completion of this dissertation, I am grateful to those who have offered me encouragement and support during my doctoral study at Hokkaido University.

First of all, I extend my deepest gratitude to my supervisor Professor Satoshi Ishizuka. He has offered me the opportunity for studying at the Laboratory of Nutritional Biochemistry, Hokkaido University, and always offered me valuable suggestions for academic studies. This dissertation could not be finished without his patient guidance and support.

I deeply appreciate Associate Professor Tohru Hira for reviewing my dissertation and for his encouragement and valuable suggestions during my study at Hokkaido University. I sincerely appreciate Professor Kei Sonoyama for reviewing the dissertation and for his valuable comments.

I am grateful to my supervisor Professor Xuanri Shen at Hainan University, during my master's course. Without his support, I would not have completed my master's degree or proceeded to doctoral study.

Particular thanks go to every member of the Laboratory of Nutritional Biochemistry, Hokkaido University for their kind help and encouragement.

I would like to thank the Chinese Scholarship Council and Japanese Government Scholarship for giving me this valuable opportunity to study abroad and for the financial support.

I finally express my gratitude to my beloved family who have always been supporting me without a word of complaint.